A CONTINENTAL MARGIN RECORD OF LITTLE ICE AGE TO DECADAL CLIMATE-INDUCED CHANGES IN SEDIMENT TRANSPORT AND DELIVERY IN THE GULF OF ALASKA

By

WILLIAM F. VIENNE

A THESIS PRESENTED TO THE GRADUATE SCHOOL
OF THE UNIVERSITY OF FLORIDA IN PARTIAL FULFILLMENT
OF THE REQUIREMENTS FOR THE DEGREE OF
MASTER OF SCIENCE

UNIVERSITY OF FLORIDA

2005

Copyright 2005

by

William F. Vienne

ACKNOWLEDGMENTS

Funding for this research was provided by the U.S. Science Support Program, Joint Oceanographic Institutions (JOI), Inc. Shiptime aboard the R/V Alpha Helix was provided by the U.S. Global Ocean Ecosystem Dynamics (GLOBEC) Program. I gratefully acknowledge Dr. John Jaeger for his support and advice on this project and throughout my studies at the University of Florida. I thank all the researchers who have assisted me in collection and analysis of the cores used in this study, including Dr. Bruce Finney, Dr. Tom Weingartner, Dr. Jim Channell, Helen Evans, the crew of the R/V Alpha Helix, Kevin Hartl, William Kenney, and Dr. Jason Curtis.

TABLE OF CONTENTS

LIST OF TABLES

LIST OF FIGURES

Abstract of Thesis Presented to the Graduate School
of the University of Florida in Partial Fulfillment of the
Requirements for the Degree of Master of Science

A CONTINENTAL MARGIN RECORD OF LITTLE ICE AGE TO DECADAL CLIMATE-INDUCED CHANGES IN SEDIMENT TRANSPORT AND DELIVERY IN THE GULF OF ALASKA

By

William F. Vienne

August 2005

Chair: John Jaeger
Major Department: Geological Sciences

The Gulf of Alaska (GOA) margin is one of the few locations on Earth where orogenic processes, glacial climate, and continental margin sedimentation can be studied and quantitatively modeled in unison. Climatic changes control glacial dynamics, erosion, and sediment fluxes to the ocean, and GOA margin strata appear to preserve a strong record of terrestrial climate (i.e., temperature and precipitation) as well as paleoceanographic signals on seasonal to tectonic time scales. In collaboration with the GOA-NEP GLOBEC program, gravity cores were collected at key sampling sites along the sediment dispersal path of the Copper River, a major source of terrigenous material to the GOA shelf. Chronologies for the past 400 years were established using ^{210}Pb and ^{137}Cs, coupled with paleo-and-environmental magnetism analyzed from u-channel samples at 1 cm intervals. The sedimentary paleomagnetic record was correlated to the Sitka geomagnetic observatory record for the last century and extended using the Jackson

400-year global field model. Analyses of texture, bulk density, magnetic susceptibility, chemical composition, and sediment fabric were performed on each core. Proximal to the Copper River, high (> 3 cm y^{-1}) sediment accumulation rates permitted the measurement of high-resolution records extending back to ~1930. Variability in bulk density, magnetic susceptibility, and mass percent silt of a core collected inside Prince William Sound--a depocenter for Copper River sediment--appears to be influenced by sub-decadal to inter-decadal variability in freshwater discharge, precipitation, and bottom currents. An overall increasing trend in spring river discharge over the past ~50 years is coupled with an overall increase in sediment bulk density, magnetic susceptibility, and mass percent silt over the same time period in this core. The sediment record of a core collected from a more distal location with respect to the Copper River reveals longer term trends in strata formation on the shelf. The region where the core was collected undergoes a lower sediment accumulation rate (< 1 cm y^{-1}) than the region of the more proximal cores, producing a lower resolution but longer temporal (~400 years) sediment record. Time-series of grain size, bulk density, and magnetic susceptibility from this more distal core positively correlated with the Glacial Expansion Index developed for the region, suggesting that glacial activity--closely related to precipitation--influences the character of sediment deposited on the shelf. Comparisons in this study of sediment properties on the GOA shelf with time-series of climate data have led to the conclusion that decadal to centennial climate change plays a significant role in the development of continental shelf strata along the GOA margin.

CHAPTER 1
INTRODUCTION

A major goal of sedimentologic and stratigraphic research in the 21st century is to understand and predict processes influencing sediment production, transport, accumulation, and preservation on continental margins over instantaneous to tectonic time scales (MARGINS-NSF Source-to-Sink Science Plan 2000). The goal of this research project is to quantitatively interpret stratigraphy in order to better understand the record of environmental change on continental margins.

Margin deposits often accumulate at high rates (> 1 m ka^{-1}) and contain high temporal-resolution records of land-ocean-atmosphere processes, yet they have not been frequently examined for this purpose due to the impression that non-steady sedimentation (i.e., turbidites and mass movements) and bioturbation create a sediment record with less fidelity than deep sea sediments (Wheatcroft and Drake 2003). However, within the ocean, the continental shelf and upper slope are the best environments to examine nearshore oceanographic, atmospheric, and terrestrial processes because signals of these processes become dampened in deep sea environments. As greater emphasis is placed on evaluating higher frequency climate changes such as El Niño-Southern Oscillation (ENSO), Pacific Decadal Oscillation (PDO), and North Atlantic Oscillation (NAO), higher resolution sedimentary records are needed to examine their influence on strata formation. Comparison of high-resolution sediment properties with instrumental records of climate change is pivotal in quantifying the response of sediment dispersal systems to short-term (< 100 yr) climate variability.

The Gulf of Alaska (GOA) margin is a prime location to study and quantitatively model glacial climate and continental margin sedimentation. High sediment yields on the GOA margin result from extensive orogenic uplift and high precipitation rates, which combine to yield the highest erosion rates in the world (Hallet *et al*. 1996; Jaeger 2002). Atmospheric conditions in this region control glacial dynamics, erosion, sediment and hydrologic fluxes to the ocean, as well as oceanographic processes such as waves and currents (Mayo 1990; Calkin *et al.* 2001; Meigs and Sauber 2000; Hallet *et al.* 1996; Jaeger and Nittrouer 1998; Stabeno *et al.* 2004). Sediment on the GOA continental shelf is subjected to a highly energetic and dynamic oceanographic regime with large waves (annual maximum wave heights > 10 m), strong tides (max tidal velocities > 20 m s^{-1}), a persistant westward flowing coastal current, and strong downwelling currents (Gilhousen *et al*. 1983; Stabeno *et al*. 2004; Royer 1981). Decadal-scale sediment records on the GOA margin likely reflect these high energy conditions, and may allow for the construction of a model of coupled oceanographic processes and strata formation. Furthermore, if decadal-scale climate-induced changes are detectable in the sediment record, then changes due to long-term climate trends should also be recognizable. Longer centennial-scale climate trends have been tied to significant glacial activity during the Little Ice Age (Calkin *et al.* 2002), and may be reflected in the GOA sediment record.

The influence of centennial to decadal climate change on strata formation is examined in this research project by comparing high-resolution shelf sedimentary records with records of glacial activity over the past 400 years and with instrumental records of atmospheric and oceanographic variability over the past century. Similar studies

examining the effect of climate change on sediment properties include work relating to fluvial sediment delivery (Somerfield *et al.* 2002) and sediment transport (Bulfinch and Ledbetter 1984; Driscoll *et al.* 1985; Ledbetter and Klaus 1987; Robinson and McCave 1994; McCave *et al.* 1995).

This study examines variability in physical, magnetic, and chemical properties of sediments in three gravity cores taken on the continental shelf of southern Alaska. There are two specific objectives. The first objective is to examine lithostratigraphy by high-resolution analyses of sediment texture, sediment composition, fabric, and magnetic susceptibility in each of the cores. The second goal of this study is to relate instrumental atmospheric and oceanographic records with core lithostratigraphies in order to develop a proxy record of fluvial sediment delivery and continental shelf sediment transport. Also, records of Little Ice Age glacial activity (~1650 – 1900 A.D.) will be compared to the lithostratigraphic record in order to examine the influence of centennial-scale climate variability on strata formation.

Based on previous studies examining production and delivery of glaciomarine sediment (Hallet *et al.* 1996; Humphrey and Raymond 1994), oceanographic controls on sediment texture (McCave 1995), and characteristic sediment properties, transport, and accumulation on the GOA margin (Feely *et al.* 1978; Sharma 1979; Royer 1981; Molnia and Hein 1982; Jaeger 1998; Stabeno *et al*. 2004), the following hypotheses will be tested in this study:

- Periods of increased precipitation and runoff should result in faster flow in the buoyant Alaska Coastal Current, leading to more widespread dispersal of coarser sediment on the GOA continental shelf.

- Periods of higher waves and increased alongshore wind stress should result in increased resuspension of bottom sediment and stronger downwelling currents, leading to more widespread dispersal of coarser sediment.

- Large-scale glacial activity during the Little Ice Age likely was associated with significant changes in precipitation and runoff, thus affecting sediment yields and sediment texture on the GOA margin over a centennial timescale.

CHAPTER 2
BACKGROUND INFORMATION

Study Area

Southern Alaska features the highest coastal mountain ranges in the world with elevations exceeding 5000 m commonly within 18 km of the coast (Figure 2-1). The coastal mountain ranges prevent inland movement of frequent (generally every 3 – 5 days in winter) Pacific storms, resulting in precipitation rates of 2 - 3 m y^{-1} (Wilson and Overland 1986). Heavy precipitation rates support the extensive valley and piedmont glaciers of Southern Alaska, which generate extremely high sediment yields of 10^5 tons/km^2 y (Hallet *et al*. 1996).

Shelf Bathymetry

Bathymetry of the northern Gulf of Alaska (GOA) shelf is shaped by numerous embankments, ridges, and troughs created by extensive subsidence, uplift, and Pleistocene glaciation (Figure 2-2). Prominent geological features on the shelf influence the physical oceanography and sediment distribution in the region (Feely *et al.* 1978; Royer 1981; Jaeger 1998).

Water depths are generally shallow (< 100 m) between the Copper River Delta (Figure 2-1) and Hinchinbrook Island, and increase towards the entrance to Prince William Sound (PWS) (Figure 2-2). PWS is a semi-enclosed basin connected to the northern GOA by Hinchinbrook Entrance (HE). HE is 11 km wide, 15 km long, and deepens from a water depth of approximately 180 m on its southern end to ~400 m on its northern end (Figure 2-2).

U-shaped valleys on the shelf are lined with poorly sorted diamictons, and are presumed to have been formed during the last glacial maximum (Carlson and Karl 1982). Hinchinbrook Sea Valley is one such valley that extends southward from HE with water depths of 200 – 250 m. It is paralleled on its western flank by Montague Island and Montague Shoals, and on its eastern flank by Tarr Bank. Tarr Bank is a tectonically uplifted region with water depths generally less than 100 m out to Middleton Island.

Montague Shoals, Bainbridge Trough, Junken Bank and Resurrection Canyon lie southwest of Montague Island. Montague Shoals is a bathymetric high with water depths generally less than 100 m. Bainbridge Trough and Resurrection Canyon have water depths of 200 – 250 m and are separated by Junken Bank, which shoals at 75 m.

Sediment Distribution on the Continental Shelf

Jaeger and Nittrouer (1998) surveyed the Holocene sediment accumulation record of the northern GOA shelf using ^{210}Pb-derived sediment accumulation rates from over 80 sites and seismic reflection profiles. They observed a thick (~ 350 m) Holocene sediment package at the Copper River Delta that thinned westward (Figure 2-3). Steady-state sediment accumulation was common over much of the shelf, including in distal depocenters of the Copper River, such as PWS. Non-steady state sediment accumulation dominated the Copper River Delta as a result of frequent mass sediment movements.

The work by Feely *et al.* (1978) is the only study in the GOA of seasonal distributions in suspended particulate matter (October-November 1975, April 1976, and July 1976). They observed surface and bottom sediment plumes extending westward from the Copper River to Hinchinbrook Island during all three cruises. Images of the surface plume have been captured in subsequent satellite images (Figure 2-6). High sediment concentrations were measured by Feely *et al.* (1978) on the eastern side of

Montague Island and along the western side of Hinchinbrook Island. Water column samples collected from the Copper River-PWS region revealed sediment concentrations in the surface plume generally between 1 – 2 mg L^{-1}, with a maximum in July of 6.7 mg L^{-1} (Feely *et al.* 1978). Sediment concentrations 5 m from the seafloor varied between 1.1 and 10.4 mg L^{-1}.

Molnia and Hein (1982) examined the clay mineralogy of 110 surface samples covering the continental shelf from Yakutat Bay to PWS. Deposits from southern PWS, east of Montague Island, and south of the Copper River all possessed low percentages of kaolinite + chlorite and high percentages of illite relative to the rest of the shelf, suggesting transport of sediment westward from the Copper River to PWS.

Regional Geology

Southern Alaska is a tectonically complex and highly active region composed of several arcuate terranes accreted into their present positions in the late Mesozoic and Cenozoic Eras (Figure 2-4) (Plafker 1987; Plafker *et al.* 1994) . Intense tectonic activity caused by the subduction of the Pacific Plate beneath the North American plate and the partial subduction of the Yakutat Terrane results in frequent seismic activity, faulting, and rapid uplift. Numerous large earthquakes have occurred over the past century including the second strongest earthquake ever recorded, the Good Friday Earthquake of 1964 (M_w 9.2; moment magnitude), which was centered in northwesten PWS.

The Copper River

The Copper River is the largest single source of sediment to the Gulf of Alaska's continental shelf. Its annual sediment load is among the top 20 largest in the world at approximately 70 x 10^6 tons y^{-1} (Milliman and Meade 1983). The Copper River drainage basin is the sixth largest in Alaska at 63,000 km^2, but the river has the second highest

discharge (~ 1600 $m^3 s^{-1}$) in the state (Brabets 1997). The Upper Copper River Basin--north of the Chugach Mountains--is bounded to the north by the Alaska Range, to the east by the Wrangell-St. Elias Mountains, and to the west by the Talkeetna Mountains. The Chugach Range is bisected by the Copper River as the river flows southward. The Chugach Range effectively divides the Copper River Basin into two regions based on precipitation. The region north of the Chugach Mountains receives generally less than 1 m of total annual precipitation and in some areas less than 15 cm (Pewe 1975). In contrast, the maritime region south of the Chugach Mountains receives well over 1 m of precipitation annually. Also, annual precipitation north of the Chugach Mountains is composed of a high percentage of snow relative to rain (~ 50%). The percentage of snow relative to rain decreases southward from ~ 40 % near the Chugach Mountains to ~ 10 % at the coast.

The Copper River is a braided system that supports a large inlet-barrier island complex. The delta is composed of the river-mouth estuary, the delta front (< 60 m water depth), and the prodelta (> 60 m water depth). The sub-aerial delta plain is composed of marshes with organic mud, sand, and gravel. The delta front is dominanted by sand facies, while the prodelta is mainly clayey silt to silty clay (Ruby and Hayes 1994).

Oceanographic and Atmospheric Conditions

Annual variability in precipitation and winds in Southern Alaska is a function of the Siberian High Pressure System, the East Pacific High Pressure System, and the Aleutian Low Pressure System (Wilson and Overland 1986; Weingartner *et al.* 2002). Cold air masses of the Siberian High intensify from October through April over northeastern Siberia while the East Pacific High is centered off the coast of southern California. During this period the Siberian High pushes the Aleutian Low over the

northeast Pacific Ocean and the Gulf of Alaska, bringing strong storms to the region. From May through September the Siberian High weakens and the East Pacific High moves into the northern Pacific Ocean. The Aleutian Low becomes weaker and migrates northward to the Bering Sea and the Arctic Ocean during these months.

Easterly along-shelf winds dominate the northern Gulf of Alaska for most of the year resulting in onshore Ekman transport and downwelling. The Pacific Fisheries Environmental Laboratory (PFEL) has developed an upwelling index based on Ekman mass transport with indices computed from monthly mean pressure fields at 26 positions along the eastern Pacific coast, including a location between the Copper River Delta and PWS (60 ^{o}N 146 ^{o}W). Downwelling (i.e., negative upwelling) currents on the Gulf of Alaska shelf are strongest during the winter months (peaking in January) when the Aleutian Low and easterly winds along the coast are strongest (Figure 2-5). During summer months both weak upwelling and downwelling currents are common.

The dominant circulation feature on southern Alaska's inner continental shelf is the Alaska Coastal Current (ACC) (Figure 2-4). The ACC is characterized as a low salinity (< 31 $^{o}/_{oo}$) current with persistent westward movement year round (Figure 2-4) (Royer 1981). It forms near British Columbia and runs parallel along the coastline to the Bering Sea (Weingartner *et al.* 2002). Generally, the ACC is confined to within 35 km of the coastline, is shallow (< 50 m), and ranges in velocity from 20 – 180 cm s^{-1} (Royer 1981; Weingartner *et al.* 2002). The ACC bifurcates at Hinchinbrook Entrance with a portion of the current moving into PWS and another portion moving along the east coast of Montague Island (Figure 2-4) (Royer *et al.* 1979). Transport in the ACC is controlled by baroclinic forcing driven by freshwater discharge and winds (Royer 1981; Royer 1982,

1989; Stabeno 2004). Freshwater discharge to the GOA is high in the summer and fall with a peak in October due to a combination of rainfall and meltwater. Peak discharge of the Copper River is earlier--generally in August (Figure 2-5). Winds influence transport in the ACC by forcing coastal convergence of offshore waters, which affects coastal sea level slopes (Royer *et al.* 1989).

Southern Alaska has a mixed energy coastline with strong influence from both waves and tides. Waves in the northern Gulf of Alaska are largest in the winter months with maximum significant wave heights (i.e., average of the highest 1/3 of waves) of 8 – 9 m (Figure 2-5) (Gilhousen *et al.* 1983). Monthly means for the rest of the year are 3.5 m with summer waves averaging 1.5 m. Tides along the coast average 3 - 4 m and are composed primarily of a lunar semidiurnal tide (M_2) with secondary contribution from a lunisolar diurnal tide (Weingartner *et al.* 2002). Velocities of the M_2 tidal currents to the west of Kayak Island average 17 cm s^{-1} near the shore and 10 cm s^{-1} near the shelf break (Stabeno 2004).

Regional Glaciology

Calkin *et al.* (2001) have summarized the history of glacial advances and retreats in the Holocene for numerous land- and fjord-terminating glaciers in the region through tree ring and lichen dating of end moraines and tree ring dating of glacially overridden forests. Of particular interest to this study is the glacial expansion history related to the Little Ice Age, which began locally around A.D. 1200 and continued into the 19th century (Porter 1986). During this period, most glaciers along the GOA margin reached their Holocene maxima. Tree ring chronologies of overrun forests in the PWS region provide the most precise timing for glacial expansions. These data along with chronologies of end moraines suggest that major glacial advances occurred in the 13th century, the 17th

century, and the last half of the 18th century, a pattern similar to glacial fluctuations observed throughout Alaska (Calkin 1988) and the Canadian Cordillera (Luckman 1986, 1995; Barclay 1998).

Currently, glaciers cover ~ 20 percent of the watershed draining into the Gulf of Alaska as a result of the wet maritime climate and distribution of extremely high coastal mountain ranges (Pewe 1975; Royer 1982). Glacial activity and the position of the equilibrium line altitudes (ELA) in southern Alaska is mainly a function of elevation and precipitation (Pewe 1975; Meigs and Sauber 2000). The ELA is lowest (~700 – 1200 m) south of the Chugach and St. Elias Mountains where precipitation rates are highest (> 1 m y^{-1}) (Pewe 1975). It increases to altitudes of ~1600 – 2000 m north of these mountain ranges where precipitation rates are lower. Temperature appears to have little effect on lowering the ELA, which is evident in that temperatures north of the Chugach and St. Elias Mountains are generally up to 8 ^{o}C colder than temperatures to the south (Pewe 1975). This is further supported by studies of Wolverine Glacier, located on the Kenai Peninsula. Mayo and March. (1990) showed that Wolverine Glacier has grown since the 1970's as a result of increased precipitation and despite increased temperatures. Because glacial sediment production is predominantly a function of the velocity at which glacier ice slides along the substrate (Humphrey and Raymond 1994; Alley *et al.* 2003), glacial activity in southern Alaska is likely to have an effect on sediment yields and sediment compositions to the Gulf of Alaska continental shelf.

Decadal-Scale Climate Variability in the Gulf of Alaska

Pacific Decadal Variability is a term used to describe a group of spatial climate patterns affecting the Pacific region over decadal time scales. El Niño-Southern Oscillation (ENSO) has long been recognized as a major influence on inter-annual

climate variations in the Pacific with events persisting 6 – 18 months and periodicities of 3 – 8 years (Rasmussen and Wallace, 1983). A 1976 - 1977 shift to lower sea level pressures in the central North Pacific led to the discovery of a pattern of climate variability termed the Pacific Decadal Oscillation (PDO) (Nitta and Yamada 1989; Treberth 1990). The PDO is characterized by warm and cool regimes centered over the North Pacific that persist for 15 – 30 and 50 – 70 year periods (Hare 1996; Zhang *et al.* 1997). During positive PDO phases sea surface temperatures (SST) over the central and western North Pacific tend to be cooler than average, while temperatures along the west coast of the Americas, including Alaska, are warmer than average (Mantua and Hare 2002). Sea level pressure anomalies indicate lower sea level pressures and stronger cyclonic winds over the North Pacific during positive phases of the PDO.

Stabeno *et al.* (2004) have reviewed data from meteorological stations along the coast of southeastern Alaska at Yakutat, Seward, and Ketchikan and have determined that correlation between the PDO and coastal GOA temperature, precipitation, and wind stress is weak. However, ENSO does appear to have a pronounced effect on coastal winter time temperature and precipitation, but does not historically show a relationship with wind stresses.

Temperature and salinity measurements have been made at the head of Ressurection Canyon (Figure 2-2) on hourly to monthly time intervals since 1970. All ENSO events during this period except the 1972 event have been recognized in the 250 m (i.e., bottom layer) temperature anomaly data from this station (Royer and Weingartner 1999). An increase of one standard deviation in the temperature anomaly record has been used to indicate an ENSO event. The 1997 – 1998 El Niño was particularly well defined

with a temperature anomaly exceeding 3 standard deviations. Extensive sampling was performed along the Seward Line (extending southeast along the eastern side of Resurrection Canyon) during the 1997 – 1998 El Niño and 1998 – 1999 La Niña events. Comparing April 1998 El Niño data to April 1999 La Niña data revealed higher temperatures (by 1.5 ^{o}C) and lower salinities (by 0.4 psu) during April 1998 (Weingartner *et al.* in prep.). The April 1998 freshening along the Seward line was accompanied by increased wind stresses east of the study area, greater precipitation, and greater amounts of freshwater discharge during the summer and fall of 1997 and the early months of 1998. Increased transport within the ACC was also recognized along the Seward Line, as transport during the April 1998 El Niño was nearly double the amount calculated for the April 1999 La Niña.

Previous Studies Using Sediment Transport Proxy Records

Grain sorting of sediment occurs primarily during bottom benthic layer (BBL) resuspension and redeposition, which are controlled by the amount of stress acting on a particle and the particle's settling velocity (McCave *et al.* 1995). Bottom shear stresses due to waves and currents act to prevent deposition of suspended matter and to remobilize material on the substrate. This material may be transported significant distances by prevailing bottom currents from a region where critical shear stresses are exceeded and the material is mobilized to a region where critical shear stresses are infrequently exceeded and deposition occurs (Wheatcroft *et al.* in prep.). Sediments with diameters > 10 μm behave in a non-cohesive manner and undergo sorting dependant on the primary particle size (McCave *et al.* 1995). Therefore, sediment > 10 μm (i.e., sortable silt) is ideal for studies of processes that affect grain sorting.

McCave *et al.* (1995) reviewed several studies (Bulfinch and Ledbetter 1984; Driscoll *et al.* 1985; Ledbetter and Klaus 1987) that have examined how modern ocean currents affect fine sediment (< 63 μm) grain size distributions. These studies on the continental margins of the eastern United States, Nova Scotia rise, and Argentine Basin all showed a positive correlation between current strength and a coarsening in non-carbonate sortable silt (10 – 63 μm).

A few studies have attempted to describe the characteristic grain size distribution of sediments eroded by glaciers (Fillon and Full 1984; Andrews and Principato 2002). Andrews and Principato (2002) examined grain size data for surface samples from the Ross Sea and East Greenland in order to determine whether a characteristic grain size distribution in glacially eroded sediments and ice rafted debris (IRD) existed. The dominant sediment mode in both cases was in the < 1 μm size fraction, with a secondary mode at 10 – 30 μm. The 10 – 30 μm size fraction coincides with the sortable silt fraction presented by McCave *et al.*(1995), which suggests that glacially eroded sediments are ideal for studying processes affecting sediment sorting along continental margins.

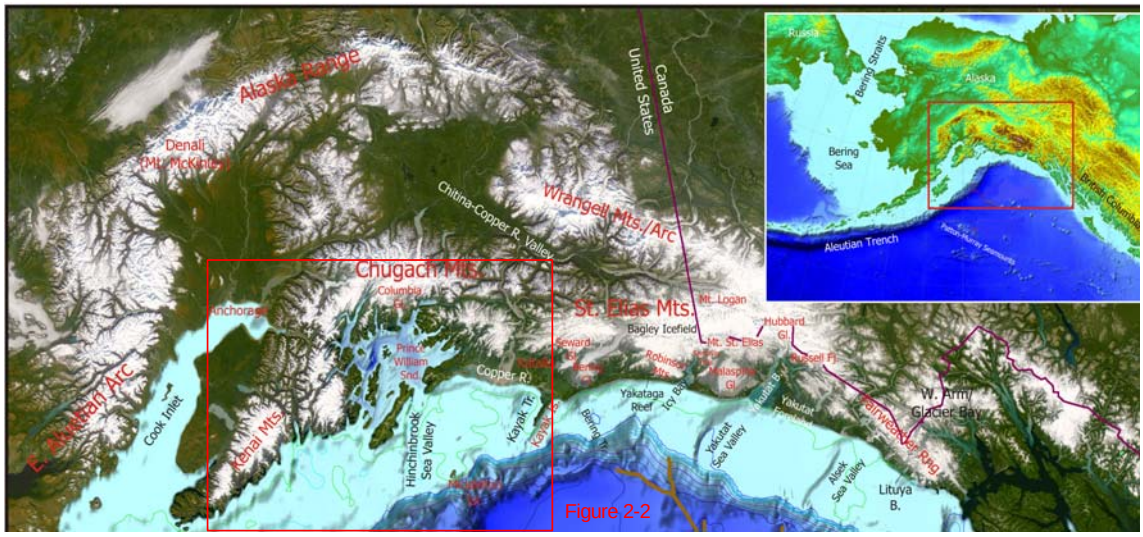

Figure 2-1. Map of southeastern Alaska.

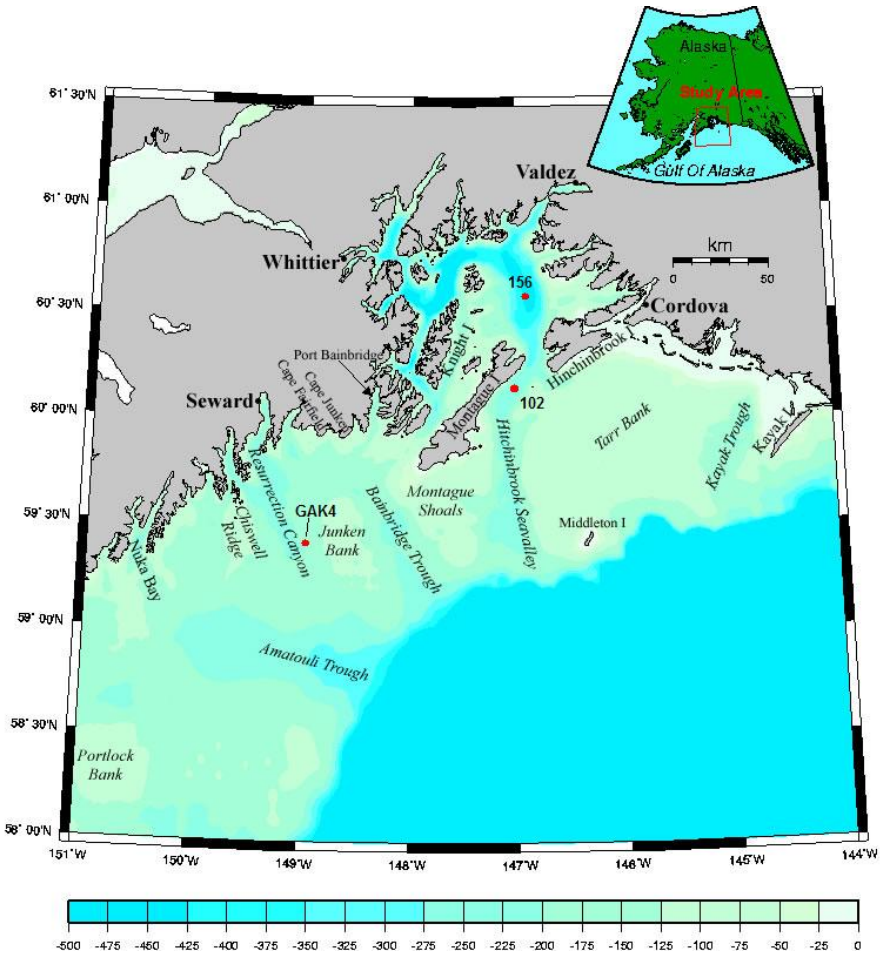

Figure 2-2. Bathymetry of the study area.

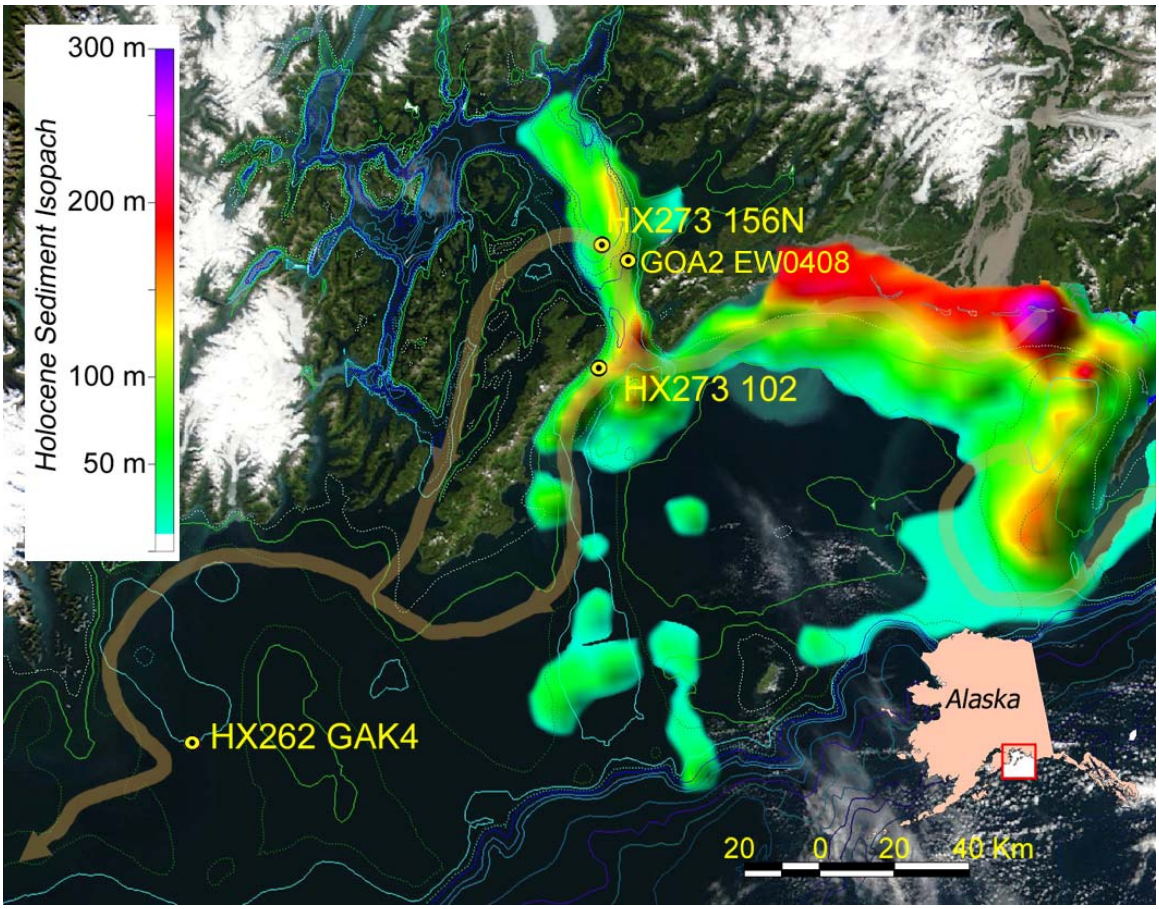

Figure 2-3. Northern Gulf of Alaska Holocene sediment thickness. The path of the Alaska Coastal Current is shown in brown.

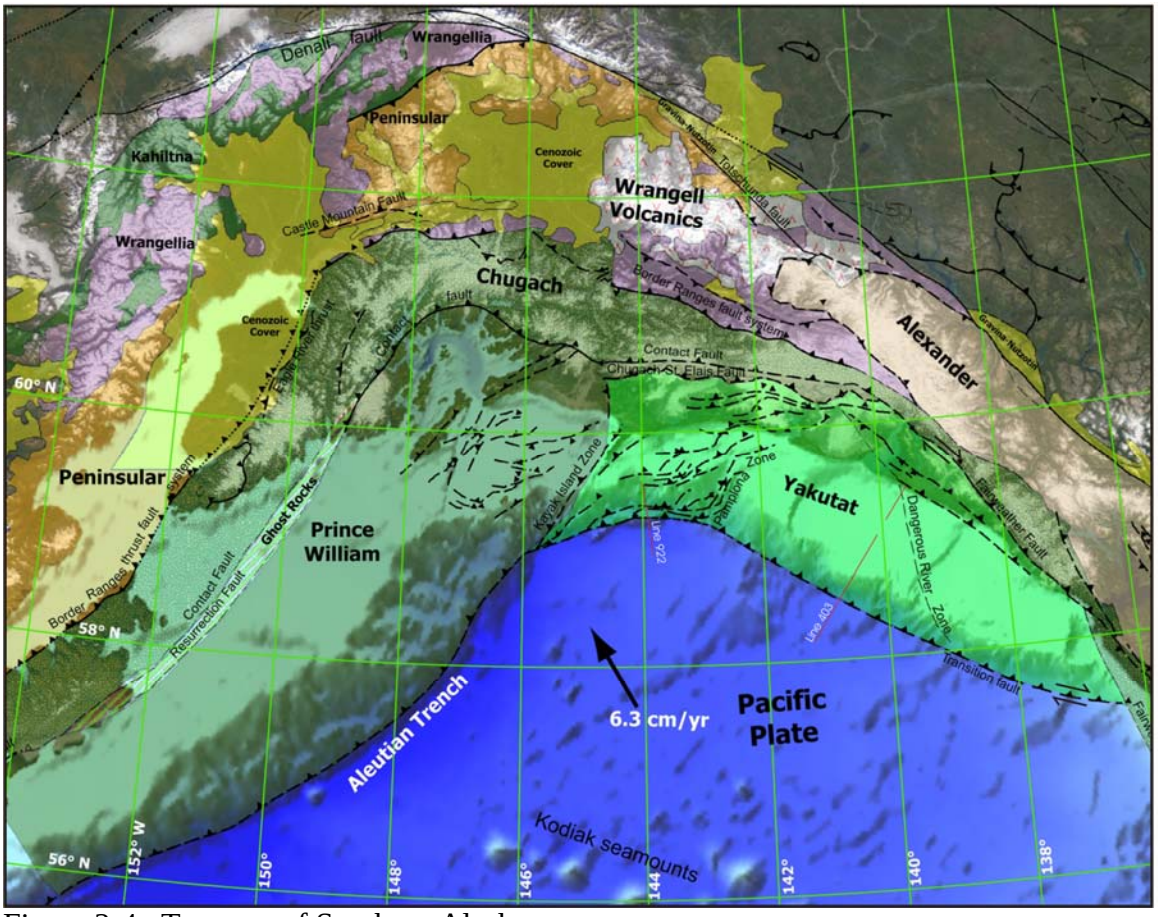

Figure 2-4. Terranes of Southern Alaska.

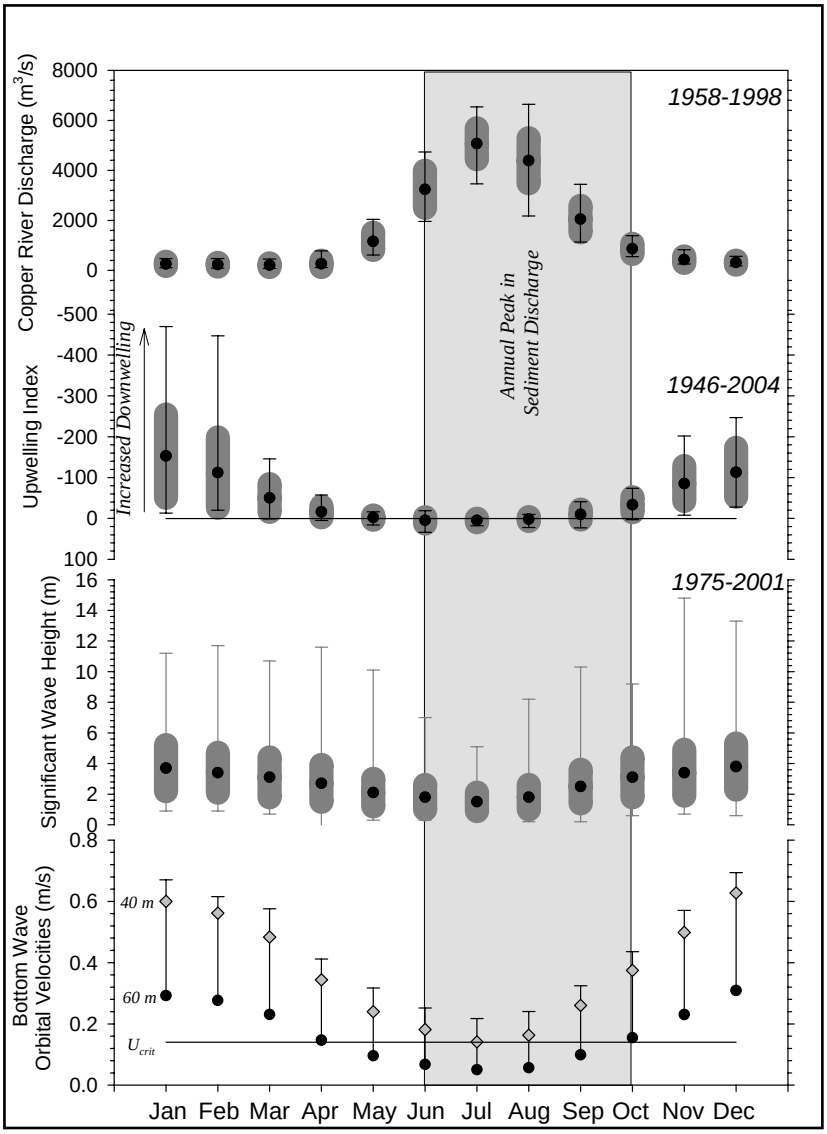

Figure 2-5. Seasonality of oceanographic and atmospheric processes. The figure displays the variability in mean monthly Copper River discharge, PFEL upwelling index, significant wave heights, and wave orbital velocities at 40 and 60 m water depth on the northern GOA shelf. Peak sediment discharge (June – October) corresponds within one month to high downwelling indices and bottom wave orbital velocities that exceed the critical resuspension value (0.14 m/s; Wiberg et al., 2002) indicating that sediment is likely quickly remobilized following the annual peak in sediment deposition.

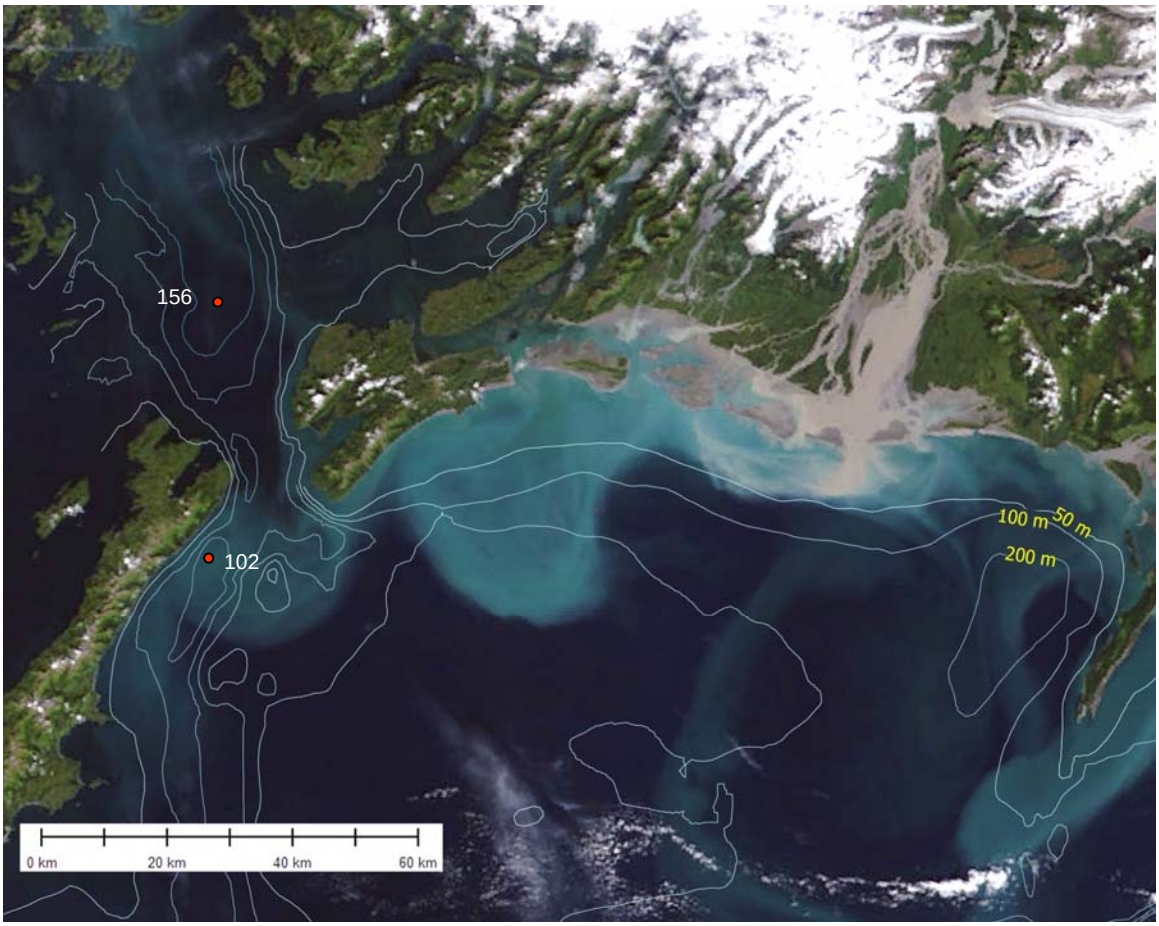

Figure 2-6. Satellite image of the study area. Terra/MODIS Satellite Image (8/22/2003) showing the Copper River Delta and PWS. Material from the Copper River moves west parallel to the shore entering PWS on the western side of Hinchinbrook Island.

CHAPTER 3
METHODS

In collaboration with the GOA-NEP GLOBEC program, three gravity cores were collected along the GOA margin at Sites 156 (60° 27.12' N, 146° 57.98' W), 102 (60° 12.60' N, 146° 57.98' W), and GAK4 (59° 24.5' N, 149° 2.9' W) (Figure 2-2). GC156 and GC102, collected in 2003, measured 3 cm in diameter and approximately 2.5 m in length. Site 156 is located in the central basin of PWS at a water depth of 415 m (Figures 3-1 and 3-2), while Site 102 lies east of Montague Island at a water depth of 250 m. The two sites were chosen because they are distal depocenters for Copper River sediment, because they lie along the path of the ACC (Figure 2-4), and because cores collected previously near these locations have shown steady state-sediment accumulation (Feely *et al.* 1978; Molnia and Hein 1982; Jaeger 1998).

GCGAK4, measuring 1.6 m in length and 2 cm in diameter, was collected in 2001 from site GAK4 by Bruce Finney. GAK4 is a site in 195 m of water located on the western side of Junken Bank (Figure 3-3) that contains a thinner package of Holocene strata than Sites 156 and 102. Site GAK4 was chosen for this study because it lies along the path of the ACC (Figure 2-4) near a location where extensive water column sampling has been carried out since 1970 (Royer and Weingartner 1999). Also, because the site contained less Holocene sediment cover, the sediment accumulation rate at the site was likely lower than at the other two sites, providing a temporally longer sediment record.

Coring sites were not chosen closer to the Copper River sediment source because of the extensive slumping and turbidity flows that occur on and near the delta (Jaeger *et al.*

1998). A swath bathymetry survey performed in 2004 by John Jaeger revealed that Site 156 lies in a relatively flat basin that gradually slopes upward to the south and more sharply to the southeast (Figure 3-1). A CHIRP seismic profile through Site 156 revealed laterally continuous reflectors, indicating a lack of slumping. However, it is important to note that the low vertical resolution of the profile makes it difficult to examine strata on the scale of GC156's length. A swath bathymetry survey of GAK4 shows that there is very little elevation change around the site (Figure 3-3).

The gravity cores were kept vertical after retrieval until they could be plugged with neoprene and capped. Once at the University of Florida, the cores were stored at 4 ^{o}C. GCGAK4 was sampled by inserting an ODP-style u-channel lengthwise in the gravity core by Bruce Finney at the University of Alaska-Fairbanks and sent to the University of Florida. GC156 and GC102 were brought whole back to the University of Florida, were split, then sampled with u-channels for magnetic susceptibility analysis. Additional analyses were run on the material remaining in the core barrels after extracting the u-channels.

Bulk Density

Gamma-ray attenuation (GRA) bulk density analysis is a non-destructive technique for examining changes in a core's physical properties. Changes in GRA bulk density often reflect variations in sediment lithology (Weber *et al*. 1997). GRA bulk density measurements were made on a Geotek Multi-sensor Core Logger (MSCL) at 0.5 cm intervals. Whole-core wet bulk density measurements were made on GC156 and GC102 before they were split. Wet bulk density measurements were also made on the GCGAK4 u-channel. Accuracy of the measurements was determined from two aluminum density calibration standards (i.e., one for the whole-core and one for the u-channel) by plotting

the product of density and thickness of the aluminum versus gamma counts per second (Weber et al. 1997). Regression analysis of a polynomial fit through the resulting points indicated the accuracy of the MSCL data. Error due to accuracy for the whole-core measurements was ± 0.18 g cm^{-3}. A precision error for the GC156 and GC102 was determined by running the aluminum standard three times and taking the average of the standard deviations for each depth interval. The error due to precision for the whole-cores was ± 0.01 g cm^{-3}. The accuracy error for the u-channel standard was ± 0.01 g cm^{-3}. A precision error for the GCGAK4 u-channel was found by running it 3 times, then taking the average of the standard deviations for each interval. The precision error for GCGAK4 was ± 0.01 g cm^{-3}. Total error is calculated using equation 3-1:

$$\text{Total Error} = \text{sqrt}(\text{Accuracy}^2 + \text{Precision}^2) \qquad \text{(Equation 3-1)}$$

The total error for GC156 and GC102 GRA bulk density was ± 0.18 g cm^{-3}, while that for GCGAK4 was ± 0.01g cm^{-3}.

Magnetic Susceptibility

Magnetic suceptibility of sediments is a useful parameter for interpreting the source of sediments, and is often influenced by the same processes affecting grain size and bulk density variability (Weber *et al.* 1997). U-channels of GCGAK4, GC156, and GC102 were analyzed at the University of Florida on a custom low-field magnetic susceptibility track utilizing a Sapphire Instruments SI2B magnetic susceptibility meter (Thomas et al. 2003).

X-Radiographs

The halves of GC156 and GC102 not sampled with u-channels were x-radiographed at the University of Florida at 58 KeV and 1.0 mA to examine the sediment fabric (i.e., internal structures, density changes) and the extent of bioturbation.

Textural Measurements

Grain size measurements were performed at the University of Florida in order to recognize relationships between texture and GRA bulk density, magnetic susceptibility, and sediment fabric. Also, grain size distributions can be related to sediment transport and deposition processes, which are of utmost relevance to this study (Inman 1949; McCave *et al.* 1995). Samples weighing approximately 2.5 g wet were taken from sediment cores at 1 cm intervals. GCGAK4 was sampled every 1 cm, while GC156 and GC102 were sampled every 5 cm. Later, more samples were extracted from GC156 and GC102 in order to develop a higher resolution record of grain size. These latter samples were extracted from depths corresponding to high and low points of magnetic susceptibility. In order to disaggregate flocculated clay particles, the mud fraction was soaked in 0.05 % $Na(PO_4)_5$ overnight and placed in a sonic bath for a minimum of 10 minutes prior to being analyzed on a Sedigraph 5100. A Micromeritics particle size reference material was analyzed to identify accuracy of the Sedigraph 5100. The standard deviation of the cumulative mass percent finer than a specified grain diameter equaled ± 0.7 %. A precision error was found by calculating the standard deviation for identical size fractions from 3 Sedigraph runs of each sample from GC156. The average standard deviation for all of the samples was ± 0.01%. Total error for the cumulative mass finer

measurement was ± 0.7 %, or ± 0.007 if expressed as a fraction, which is often the case in this paper.

Prior to running samples on the Sedigraph, sand and mud fractions were separated using a 63 μm sieve. The sand fraction was dried in an oven at 60 ^{o}C and weighed. The amount of sand present was calculated from equation 3-2:

$$\text{Fraction as sand} = \frac{\text{Dry Sand Weight}}{(1 - \text{Water Content}) * \text{Total Sample Wet Weight (g)}]} \quad \text{(Equation 3-2)}$$

Geochronolgy

^{210}Pb and ^{137}Cs were used to develop core chronologies and to distinguish event bedding (Jaeger and Nittrouer 1998). ^{210}Pb is a member of the ^{238}U decay series. It forms when ^{226}Ra in rocks and soils decays to the gas ^{222}Rn, which decays to ^{210}Pb through a series of short-lived radionuclides.

Radionuclide activities were measured on a planar-type low-energy germanium gamma spectrometer at the University of Florida. Errors in activities were calculated using an efficiency calibration and by dividing the uncertainty of each peak by the peak area.

GC156 and GC102 were sampled at 5 cm intervals from their half-rounds. GCGAK4 half-round samples were taken at approximately 10 cm intervals at the University of Alaska-Fairbanks and sent to the University of Florida. Approximately 10 - 20 g of dried sediment was crushed and packed into plastic jars. The samples were stored for 3 weeks before being counted so that ^{222}Rn (half-life = 3.8 days) and ^{226}Ra (half-life = 1600 years) could reach secular equilibrium. Excess ^{210}Pb was determined by subtracting the total ^{210}Pb activity (46 KeV peak; half-life = 22.26 years) by the activity supported by

the decay of ^{226}Ra. ^{226}Ra activity was calculated by taking the weighted average of ^{214}Pb (351 KeV peak), ^{214}Bi (609 KeV peak), and ^{214}Pb (295 KeV peak) activities.

^{210}Pb sediment accumulation rates were derived using the constant initial concentration model, which assumes that the initial concentration of ^{210}Pb in bottom surface sediments is constant through time (Nittrouer *et al.* 1979; Carpenter *et al.* 1982). Mass sediment accumulation rates were calculated from ^{210}Pb activity and cumulative mass profiles using a steady-state transport-reaction equation (Benninger *et al.* 1979):

$$\frac{\delta A}{\delta t} = D_b \frac{\delta^2 A}{\delta z^2} - S \frac{\delta A}{\delta z} - \lambda A \qquad \text{(Equation 3-3)}$$

where A = the ^{210}Pb activity at depth z, t = time, z = depth in sediment, λ = the first order decay constant of the tracer, D_b = the sediment mixing coefficient (assuming mixing is a diffusional process), and S = the sediment accumulation rate. For a region of exponentially decreasing activity, Eq. 3-3 can be solved assuming: steady state and a negligible deep biological mixing contribution, (i.e., $D_b = 0$, $\delta A/\delta t = 0$; and $\delta t = 0$)

$$A = A_o \exp[-(\lambda/S)\, z] \quad \text{(Equation 3-4)} \qquad \text{and} \qquad S = -\lambda/m \quad \text{(Equation 3-5)}$$

where A = the ^{210}Pb activity at depth z, A_o = the initial ^{210}Pb activity, λ = ^{210}Pb decay constant = 0.031 y^{-1}, and m = the slope of the regression line fit to the natural log of excess ^{210}Pb activity versus cumulative mass. Errors for the sediment accumulation rate, and subsequent age-depth relationships, were determined by altering the slope of the regression line in accordance to the regression line's confidence intervals, so that maximum and minimum values for the sediment accumulation rate could be calculated. These minimum and maximum sediment accumulation rates were then used to calculate an age-depth relationship, which included age errors.

First appearance of ^{137}Cs was assumed to coincide with the onset of atmospheric nuclear weapons testing in 1954, while the peak ^{137}Cs was assumed to coincide with the peak in nuclear weapons testing in 1964 (Smith and Comans 1996). Sediment accumulation rates were calculated from:

$$S = \frac{z}{^{137}\text{Cs age}} \qquad \text{(Equation 3-6)}$$

Biogenic Silica

Diatom tests constitute the primary biogenic component of sediments in the northern GOA, except in high energy areas such as Tarr Bank that contain gravel sized calcium carbonate skeletal fragments and very little fine-grained sediment (Sharma 1979). Because diatomaceous material in fine sediments may significantly influence bulk density values, the amount of biogenic silica in each core was examined. GC156 and GC102 were analyzed at the University of Florida. They were sampled at 1 cm intervals for 5 consecutive centimeters every 20 cm, then digested in 5N NaOH for 30 minutes at 218 ^{o}C in an Autoclave. They were analyzed on a Bran Luebbe Autoanalyzer to determine the biogenic SiO_2 concentration dissolved in solution. Duplicates of every tenth sample were run in order to determine the precision error. The average standard deviation of the duplicates was $\pm$ 0.47 %. Biogenic silica analyses for GCGAK 4 were performed at 1 cm intervals at the University of Alaska-Fairbanks on a Spectronic D+ spectrophotometer at 812 nm. Total error for the GCGAK4 samples averaged $\pm$ 5 %.

Organic Carbon and Nitrogen

Total organic carbon concentrations and organic carbon to nitrogen ratios (OC:N) can be useful in determining the amount of terrestrial versus marine organic mater in sediments (Meyers 1997). Sub-samples of material previously run on the gamma

spectrometer were soaked in a 1 N solution of hydrochloric acid overnight in order to dissolve any carbonate present. Then, 3 - 5 mg of washed and dried sub-sample was analyzed using a Carlo-Erba Elemental Analyzer to determine total organic carbon and nitrogen concentrations. GC102 and GCGAK4 were analyzed every 10 centimeters, while GC156 was analyzed at 5 cm intervals. The standard deviation of duplicate samples was $\pm$ 0.08 % for total organic carbon and $\pm$ 0.01 % for total nitrogen.

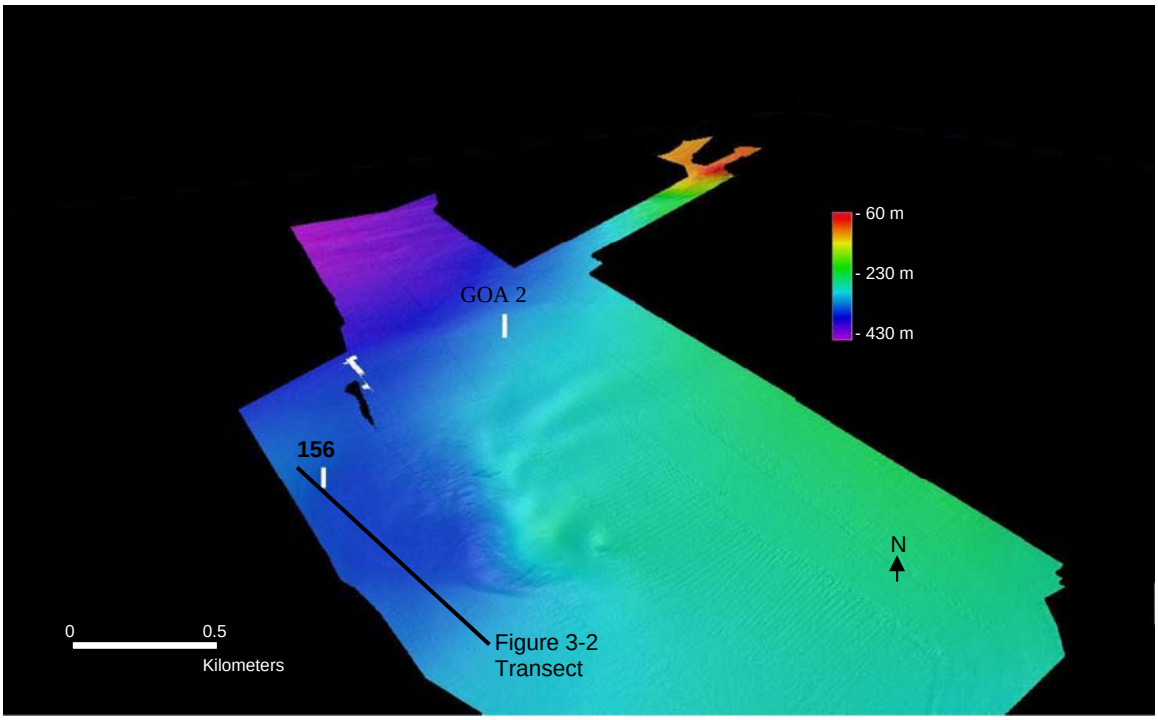

Figure 3-1. GC156 bathymetry. Map showing bathymetry at sites 156 and GOA 2 just north of the Hinchinbrook Entrance to Prince William Sound. See figure 2-2 for location. The swath survey was performed in September 2004. GC156 was collected in May 2003. JCGOA2 is a jumbo piston core collected in September 2004 by Jaeger.

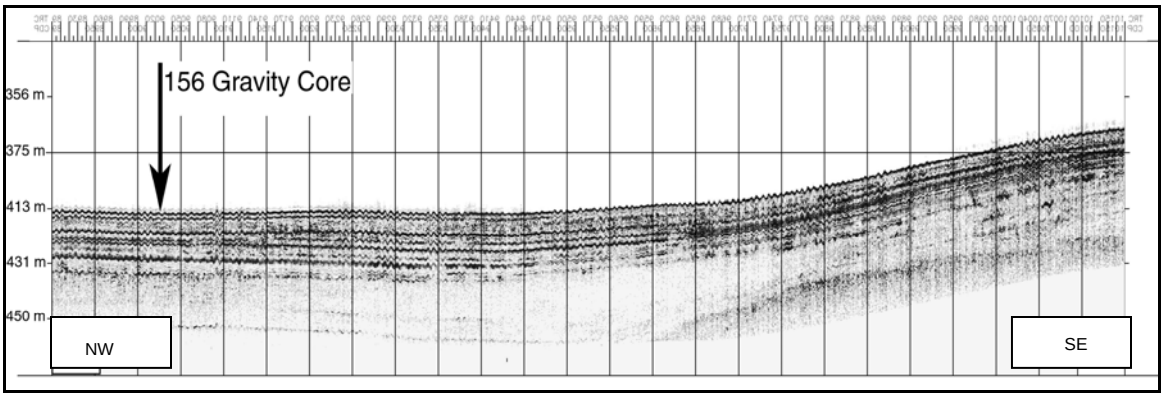

Figure 3-2. CHIRP seismic profile of region at site 156. Reflectors show no evidence of slumping and are lateral continuous, suggesting that particle settling from the water column dominates sediment emplacement. The 156 gravity core was taken in May 2003.

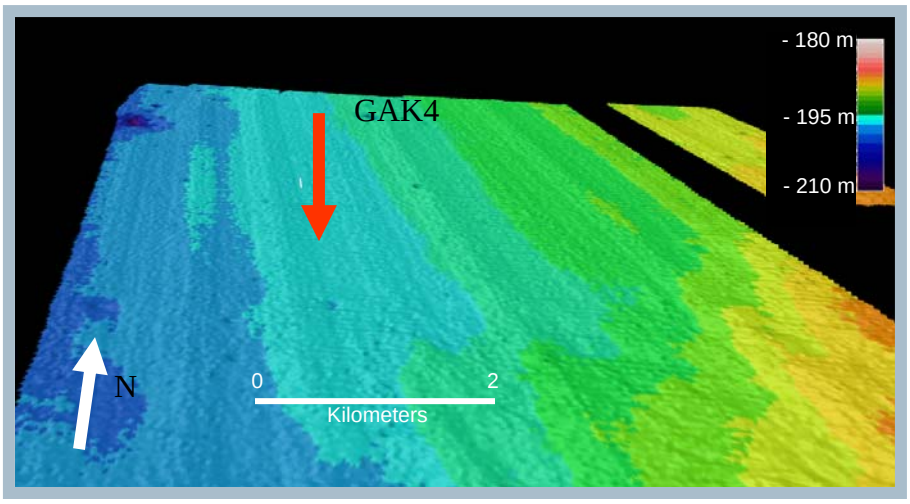

Figure 3-3. Swath bathymetry survey of the area around GAK4. Junken Bank can be seen in the lower right corner of the figure.

CHAPTER 4
RESULTS

GC156

Geochronology

A peak in GC156 ^{137}Cs activity occurs at 142 cm downcore (Figure 4-1). For the detector used, the minimum detectable activity (MDA) is 0.1 dpm g^{-1}, therefore the MDA for ^{137}Cs is first reached at 172 cm.

The ^{210}Pb profile of GC156 shows an exponential decrease in excess activity downcore, with maximum values at the surface of approximately 4 – 5 dpm g^{-1} (Figure 4-2). Low activities at the 130 – 140 cm interval correspond to coarser sediment over the same interval (Figure 4-3). Applying the technique of Benninger *et al.* (1979), the Pb^{210}-derived sediment accumulation rate is 3.2 ± 0.3 cm y^{-1} (Figure 4-2).

Physical Properties

GC156 averages 57% clay, 41% silt, and 2% sand. Mass percent silt, GRA bulk density, and magnetic susceptibility show an overall decrease downcore below 30 cm, and are positively correlated to each other (Figure 4-3; Table 4-1). Maximum values for mass percent silt, GRA bulk density, and magnetic susceptibility occur over a distinctively large peak at 122 – 142 cm (Figure 4-3). The depth of this peak corresponds to the depth of the 1964 peak in ^{137}Cs.

Maxima in mass percent silt, GRA bulk density, and magnetic susceptibility also correspond to the depth of distinct laminae in the GC156 x-radiograph (Figure 4-4). Beginning around 127 cm faint laminae appear, and at 133 cm the laminae become more

distinct with alternating light and dark bands, which reflect higher and lower densities, respectively. This interval contains the most defined laminae in the core. However, highly diffusive laminae are recognized throughout the core, indicating that bioturbation is minimal.

Burrows are evident but are not common in GC156. They appear as dark (i.e., low density) circular features or vertically oriented tubes (Figure 4-4). The most distinct burrow is an approximately 10 – 15 cm long, vertically oriented tube at 75 cm downcore.

Mass percent silt, mean silt grain size, and variability in modal grain size were compared to examine the relationship between variability in the total silt fraction and variability in specific modal ranges. Percent silt and mean silt grain size are positively correlated (Figure 4-5). Figure 4-6 displays two typical distributions of grain size modes in the 1 – 54 μm size range measured on the Sedigraph. The 178 – 179 cm interval represents a peak in mass percent silt, GRA bulk density, and magnetic susceptibility, and the 182 – 183 cm interval represents a neighboring trough (Figure 4-3). The contribution from the larger silt modes is greater in the 178 -179 cm interval than in the 182 – 183 cm interval, which is reflected in the higher overall silt content in the 178 – 179 cm interval.

Organic Carbon, Nitrogen, and Biogenic Silica

GC156 OC:TN varies from approximately 5 to greater than 10 with a mean of 7.3 (Figure 4-7). OC varies from around 0.3 % to 0.8 %.

Values of mass percent opal vary from approximately 2 – 2.5 % in GC156. There appears to be no correlation between GC156 bulk density and biogenic opal (Figure 4-7). It is important to note that error associated with GC156 opal values is high ($\pm$ 0.47 %).

GCGAK4

Geochronology

Peak ^{137}Cs activity occurs at the surface of GCGAK4 (Figure 4-8). First appearance of ^{137}Cs occurs at 13 – 15cm. Activities fall below the MDA between the peak in ^{137}Cs and its first appearance.

The ^{210}Pb profile of GCGAK4 reveals an exponential decrease in excess activity downcore, with maximum values at the surface of approximately 20 dpm g^{-1} (Figure 4-9). Applying the technique of Benninger *et al.* (1979), the sediment accumulation rate is 0.29 ± 0.05 cm y^{-1} (Figure 4-9). A 100-year sediment accumulation rate of 0.29 – 0.36 cm y^{-1} was derived by dividing the depth where ^{210}Pb goes to supported values by 100 years, which is the period of 4 - 5 ^{210}Pb half-lives.

Additionally, GCGAK4 has been dated using paleosecular variations in natural remnant magnetism (Figure 4-10) (Jaeger *et al.* 2004). Declination and inclination of GCGAK4 has been correlated with the Jackson *et al.* (2000) global field model, the Sitka, AK observatory record, and the ^{210}Pb age model. Ages given for GCGAK4 are based on a model derived from mainly a correlation with declination.

Physical Properties

GCGAK4 is composed of more fine-grained material than GC156, averaging 77% clay, 23% silt, and < 1% sand. There is a positive correlation between GCGAK4 mass percent silt, GRA bulk density, and magnetic susceptibility (Figure 4-11; Table 4-1). The most distinctive feature in the profile of percent silt, bulk density, and magnetic susceptibility is a broad peak around 70 cm, which corresponds to an approximate age of 1825 A.D.

Organic Carbon, Nitrogen, and Biogenic Silica

Values of OC:TN in GCGAK4 are generally lower than in GC156. GCGAK4 OC:TN ranges from around 5 to 9.5 with a mean of 6.7 (Figure 4-12). OC ranges from less than 1 % to around 2 %. This is an order of magnitude greater than OC values in GC156. Like GC156, OC:TN and OC are both negatively correlated with bulk density.

GCGAK4 was sampled for percent biogenic silica at a much higher resolution (every 1 cm) than GC156. Opal in GCGAK4 ranges from less than 6 % to nearly 15 %, which are much higher values than in GC156 (Figure 4-12). Like in GC156, there appears to be no correlation between GCGAK4 bulk density and percent biogenic silica, although some of the inflection points in percent opal do match the inflection points in GRA bulk density (Figure 4-14).

GC102

Geochronology

Peak ^{137}Cs activity occurs at 200 cm, while the first appearance occurs at 230 cm downcore (Figure 4-13). Activities range from 0 – 0.45 dpm g^{-1}. At 90 – 170 cm ^{137}Cs activities decrease to around 0 dpm g^{-1}.

Excess ^{210}Pb activity for GC102 ranges from approximately 0 – 3.5 dpm g^{-1}. A homogenous activity profile occurs at 60 – 80 cm and again at 90 – 170 cm, which correspond to depths where laminae are present in the x-radiograph (Figures 4-14 and 4-16). Excess ^{210}Pb activities at the 90 – 170 cm interval are very low (generally 0 dpm g^{-1}). At 180 cm activities increase to 0.8 dpm g^{-1} then decrease exponentially.

Physical Properties

Of the three gravity cores used in this project, GC102 is composed of the coarsest material with 42% clay, 37% silt, and 21% sand. There is a positive correlation between

GC102 mass percent silt, GRA bulk density, and magnetic susceptibility, but these records do not correlate as well as in the other two cores (Figure 4-15; Table 4-1). The x-radiograph of GC102 reveals extensive diffuse light and dark (dense and less dense) laminae throughout the core (Figure 4-16).

Organic Carbon, Nitrogen, and Biogenic Silica

Values for OC:TN vary from around 6 to 19 with a mean of 10.19, the highest of the three cores (Figure 4-17). OC varies from less than 0.3 % to around 0.9 %. OC:TN and OC appear to be negatively correlated with bulk density for the upper half of GC102 and positively correlated for the bottom half.

The range of biogenic silica in GC102 is approximately 1.2 % – 2.0 % (Figure 4-17). Biogenic silica and GRA bulk density appear to be negatively correlated, but it is important to note that sampling resolution is low (every 20 cm) and error is high at $\pm$ 0.47 %.

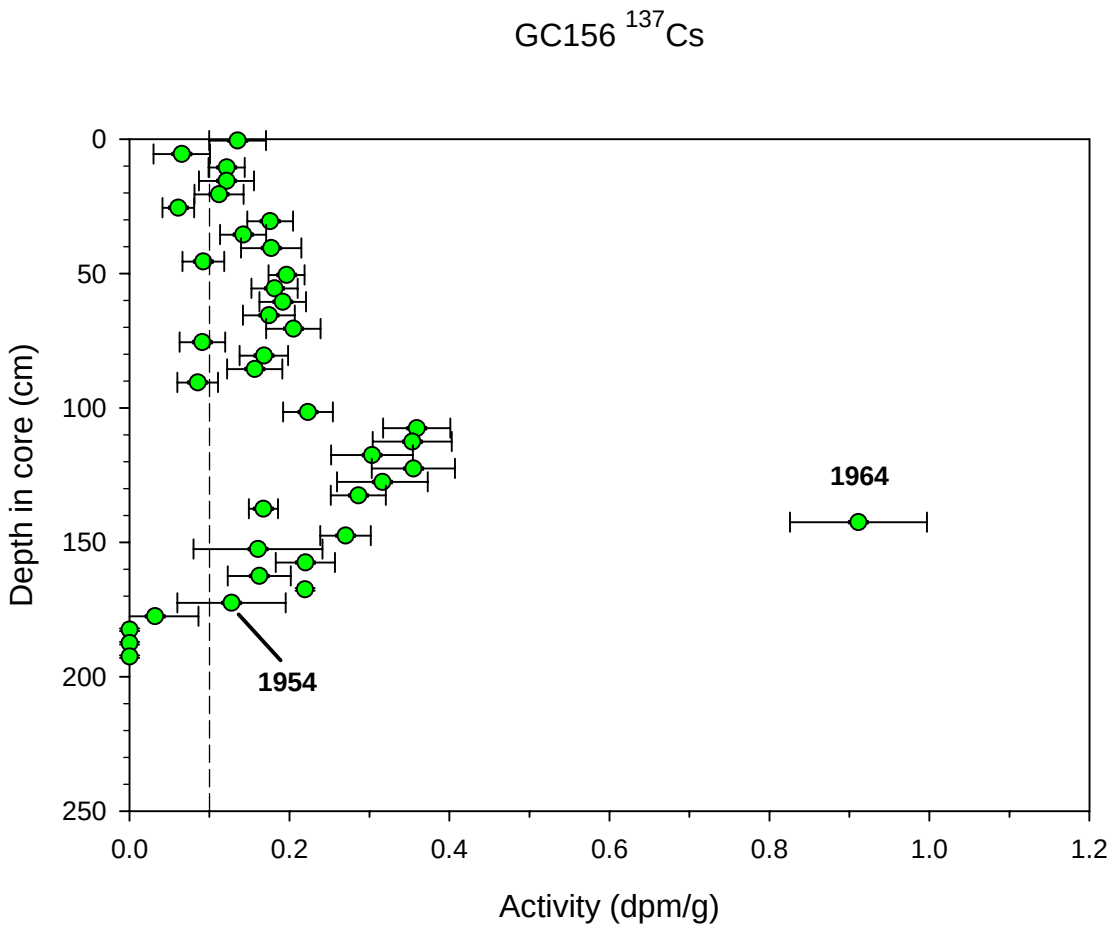

Figure 4-1. ^{137}Cs profile of GC156. A peak at 142.5 cm corresponds to the year 1964, the peak in nuclear weapons testing. First appearance of 137Cs, which corresponds to the onset of nuclear weapons testing in 1954, occurs at 170 cm. For the detector used, the MDA for 137Cs is shown at 0.1 dpm/g as a dashed line.

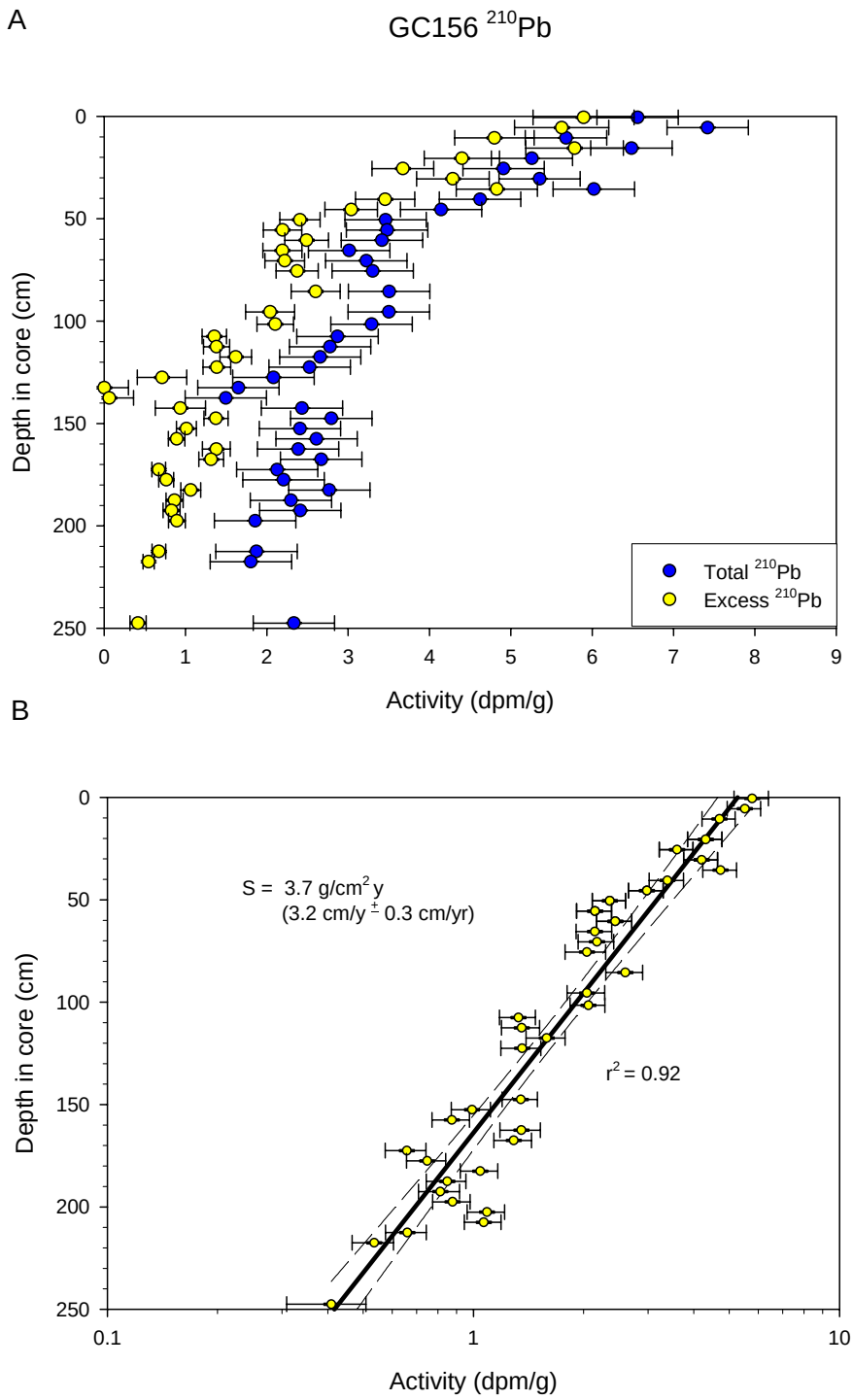

Figure 4-2. GC156 ^{210}Pb profile. 4-2A displays the profile of total and excess ^{210}Pb for GC156. 4-2B displays the profile of excess ^{210}Pb plotted on a logarithmic scale and the sediment accumulation rate (S) derived from the slope of the regression line. The 95 % confidence interval of the regression is shown as dashed lines.

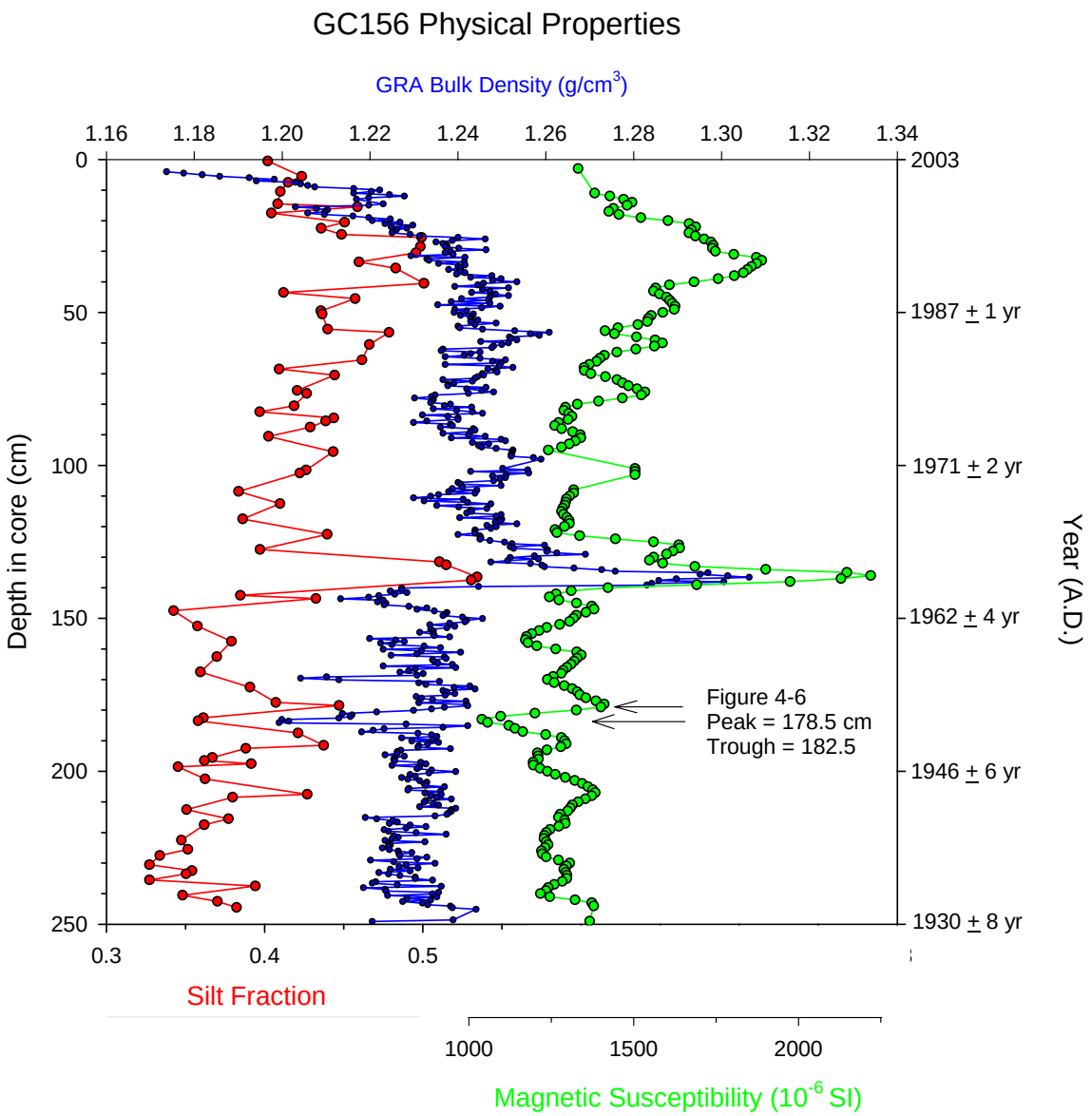

Figure 4-3. Physical properties of GC156. Ages are based on a ^{137}Cs and ^{210}Pb sedimentation rate of 3.2 cm y^{-1}.

Table 4-1. R square values between records of physical properties in each core. For the number of samples analyzed, an $r^2 = 0.1$ is statistically significant.

Core	GC156	GCGAK4	GC102
% Silt--Bulk Density	0.4	0.2	0.1
% Silt--Mag. Susc.	0.6	0.3	0.2
Bulk Den.--Mag. Susc.	0.4	0.4	0.0
% Opal--Bulk Density	--	0.0	--

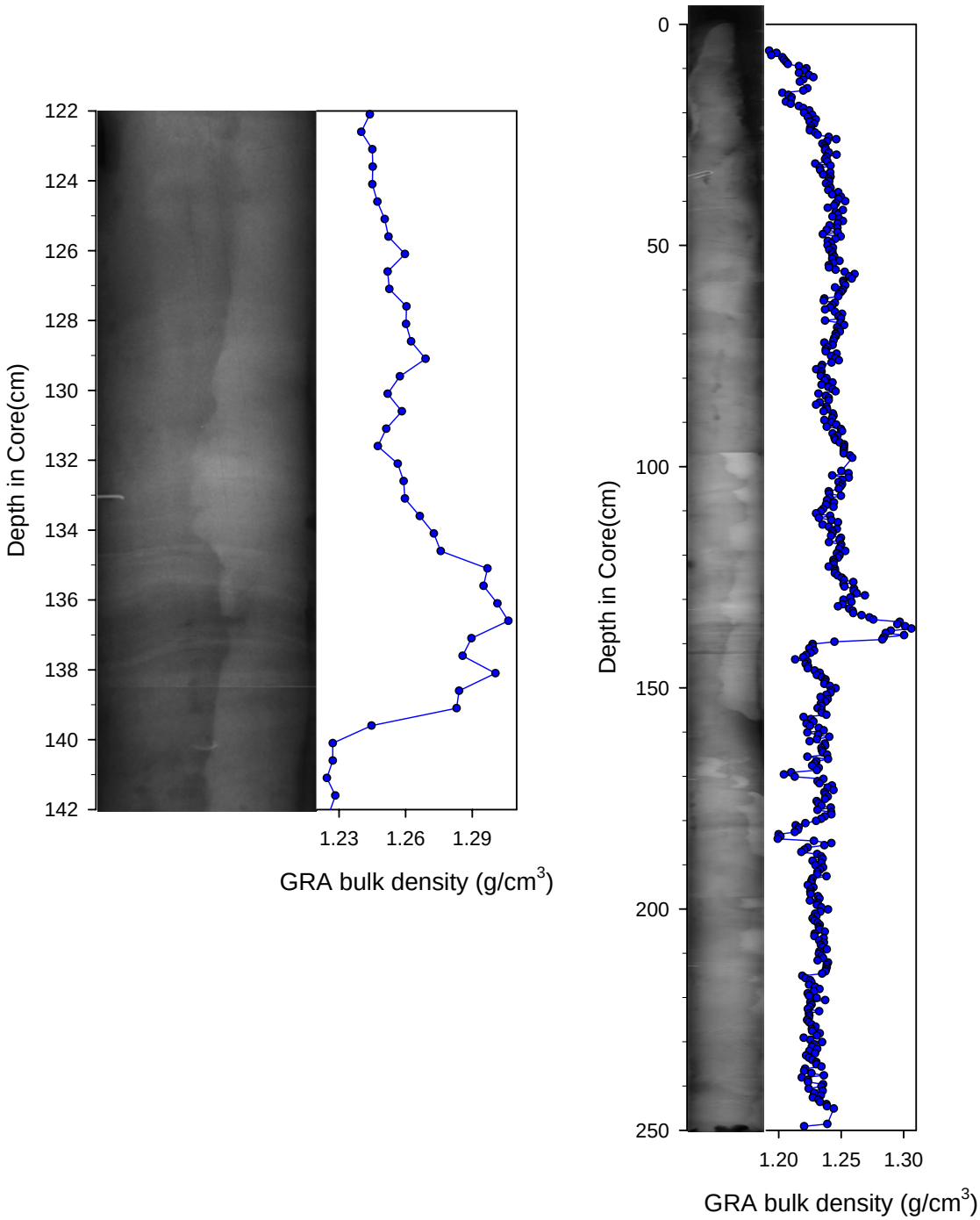

Figure 4-4. GC156 x-radiograph. The large peak in bulk density shows up in the x-radiograph as alternating light and dark laminae. Abundant depositional laminae preserved in the core indicate that bioturbation is minimal.

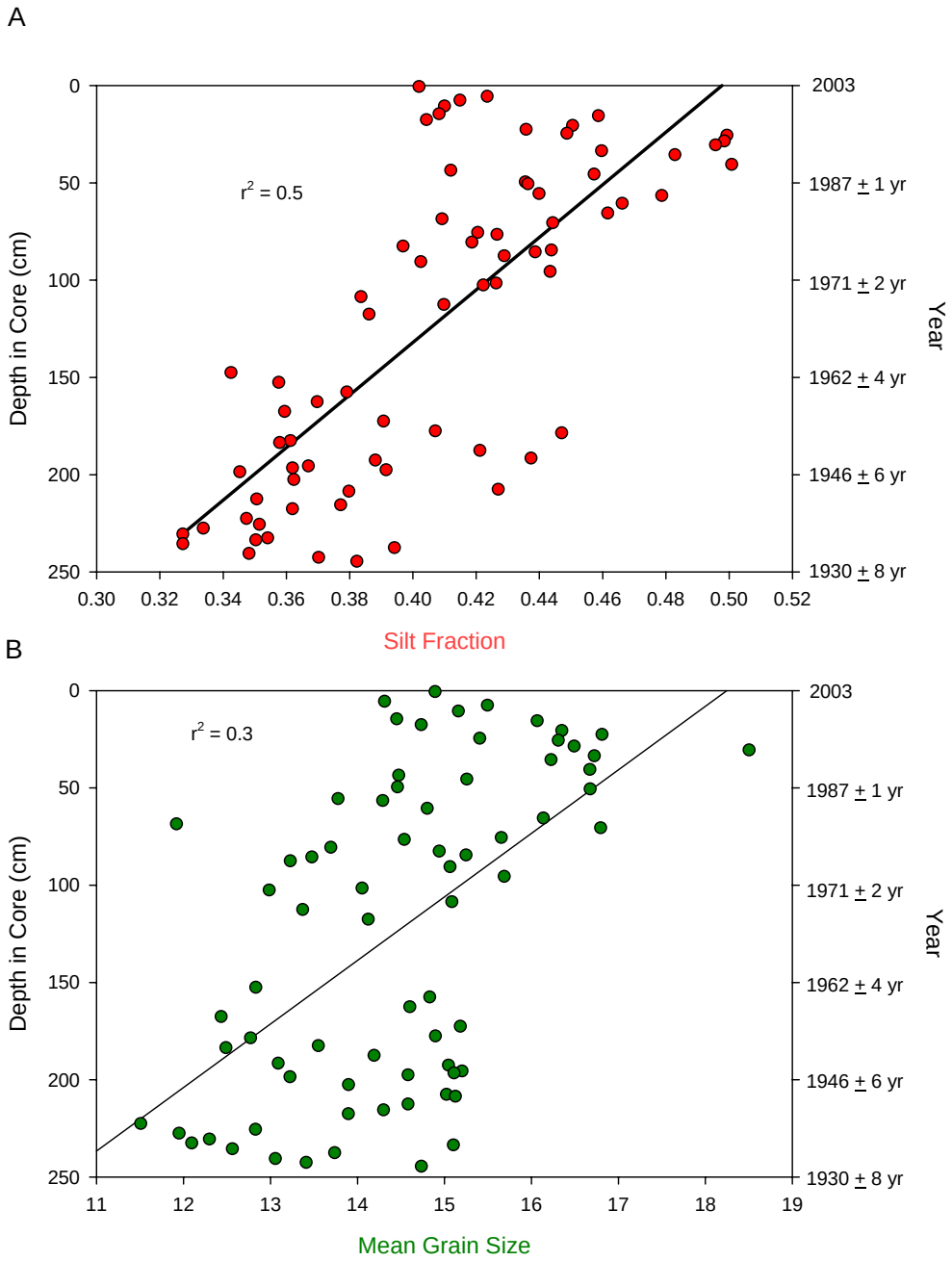

Figure 4-5. Profile of silt fraction (A) and mean silt grain size (B) for GC156. A linear regression has been fit through each plot. The large peak at ~130 cm have been removed. Both regression lines reveal an overall increasing upwards trend.

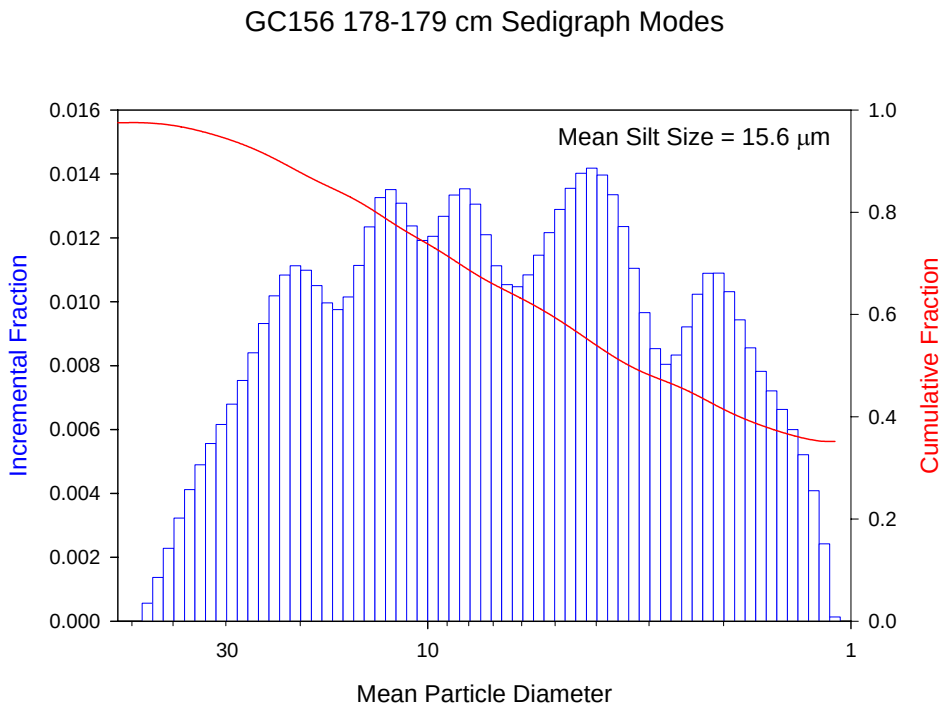

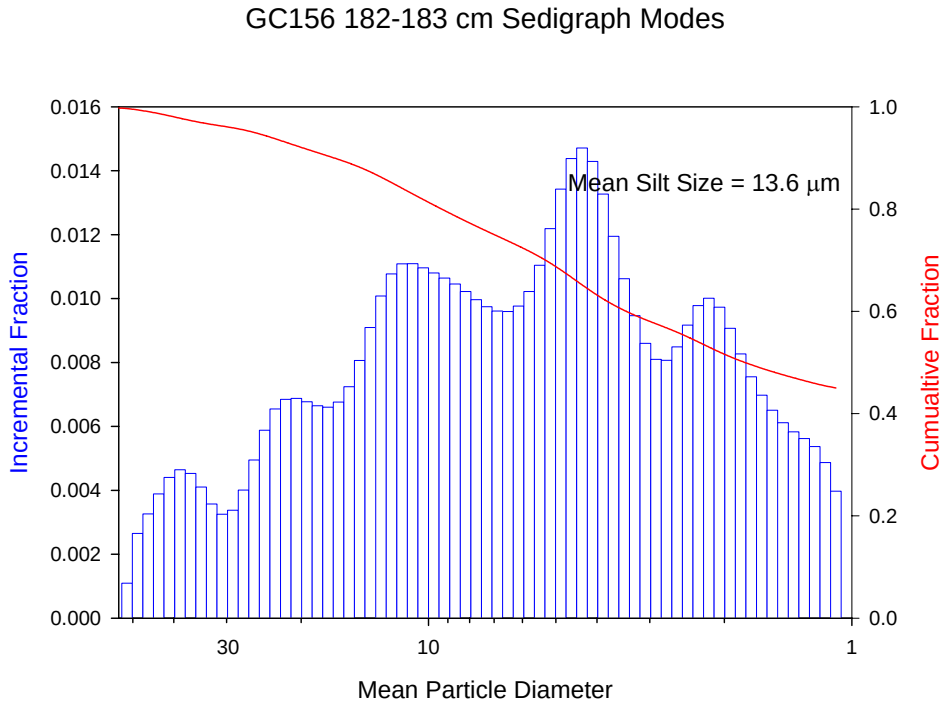

Figure 4-6. Silt Modes. Sedigraph-derived grain size modes and the cumulative finer mass fraction for 178 -179 cm and 182 – 183 cm depth intervals in GC156. They respectively represent a peak and a trough in mass percent silt, GRA bulk density, and magnetic susceptibility. These intervals are identified in Figure 4-3.

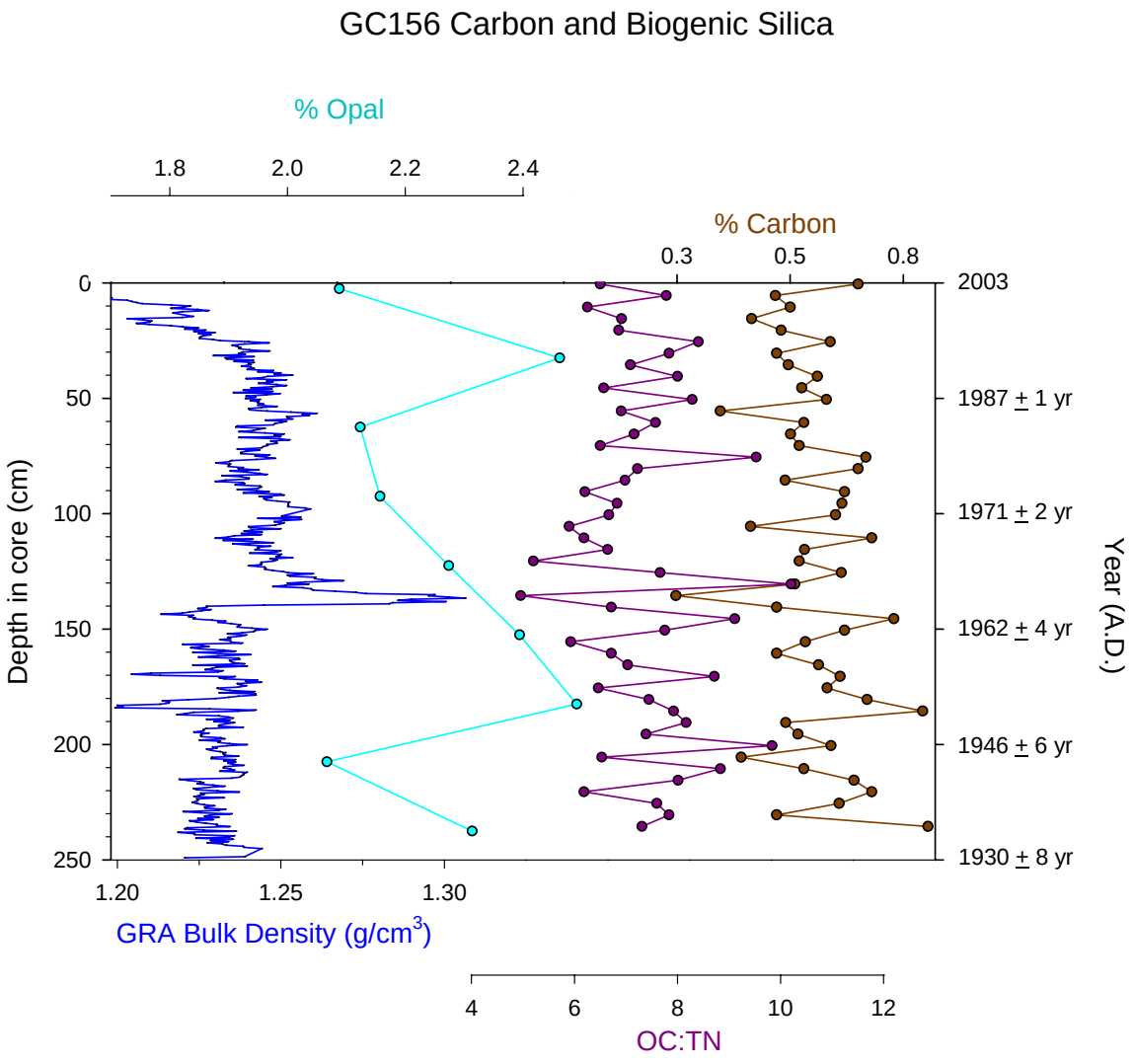

Figure 4-7. GC156 GRA bulk density, % biogenic silica, OC:TN, and % carbon.

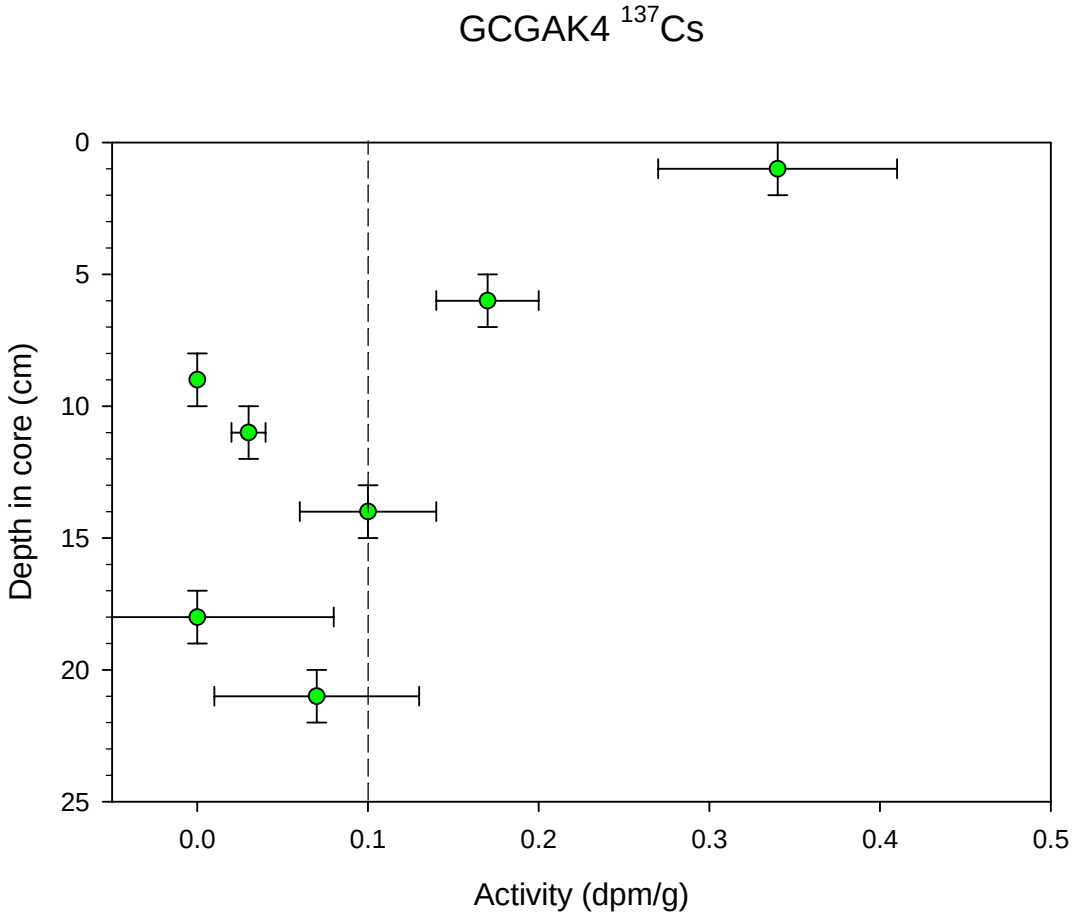

Figure 4-8. ^{137}Cs profile of GCGAK4. For the detector used, the MDA for ^{137}C is shown at 0.1 dpm/g.

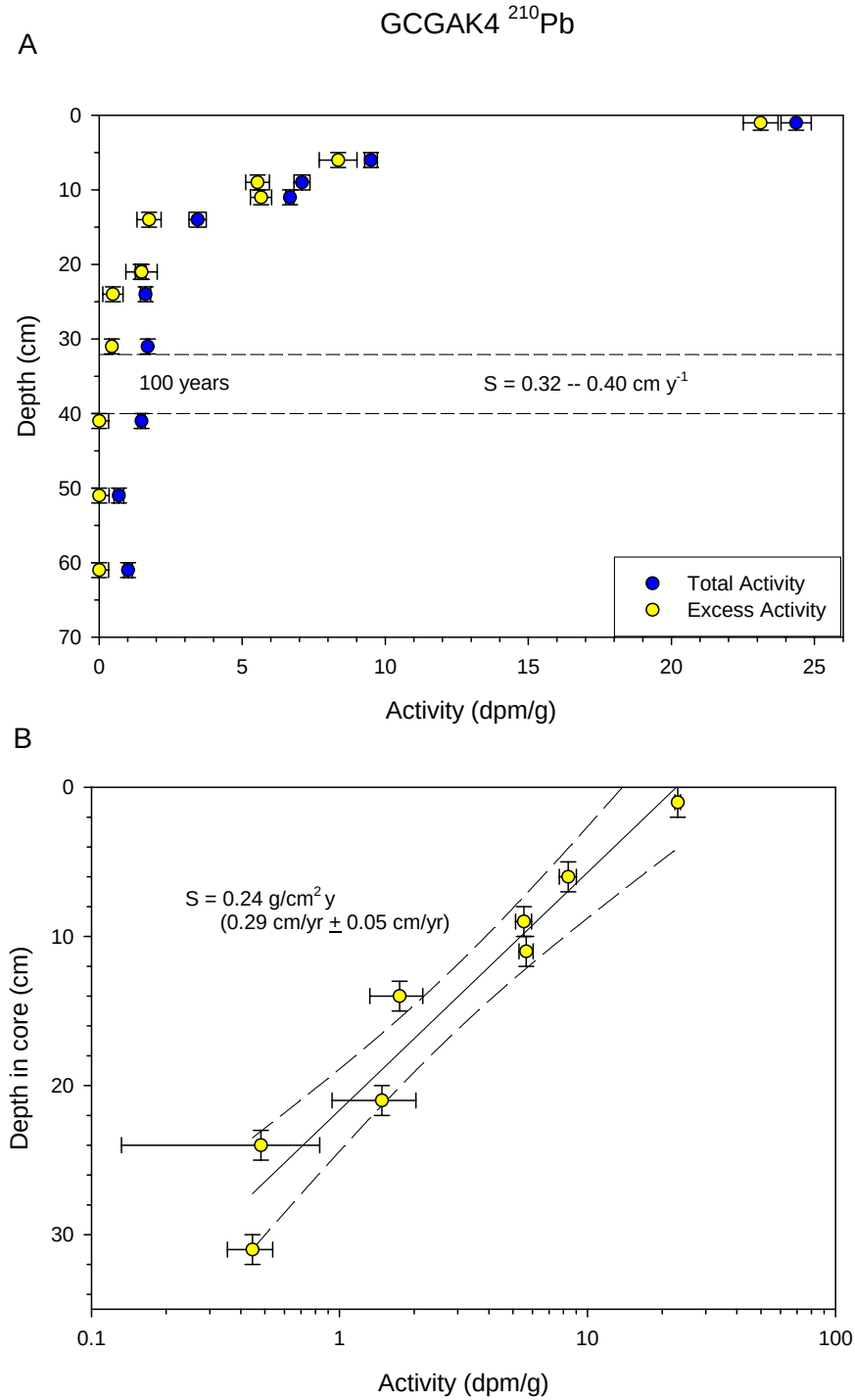

Figure 4-9. GCGAK4 ^{210}Pb profiles. 4-10A displays the profile of total and excess ^{210}Pb for GCGAK4. The interval where excess ^{210}Pb goes to background is highlighted by dashed lines. The ^{210}Pb sediment accumulation rate is calculated using the technique of Benninger *et al.* in 4-10B. A linear regression has been fit through the excess ^{210}Pb data with the 95 % confidence interval of the regression shown as dashed lines.

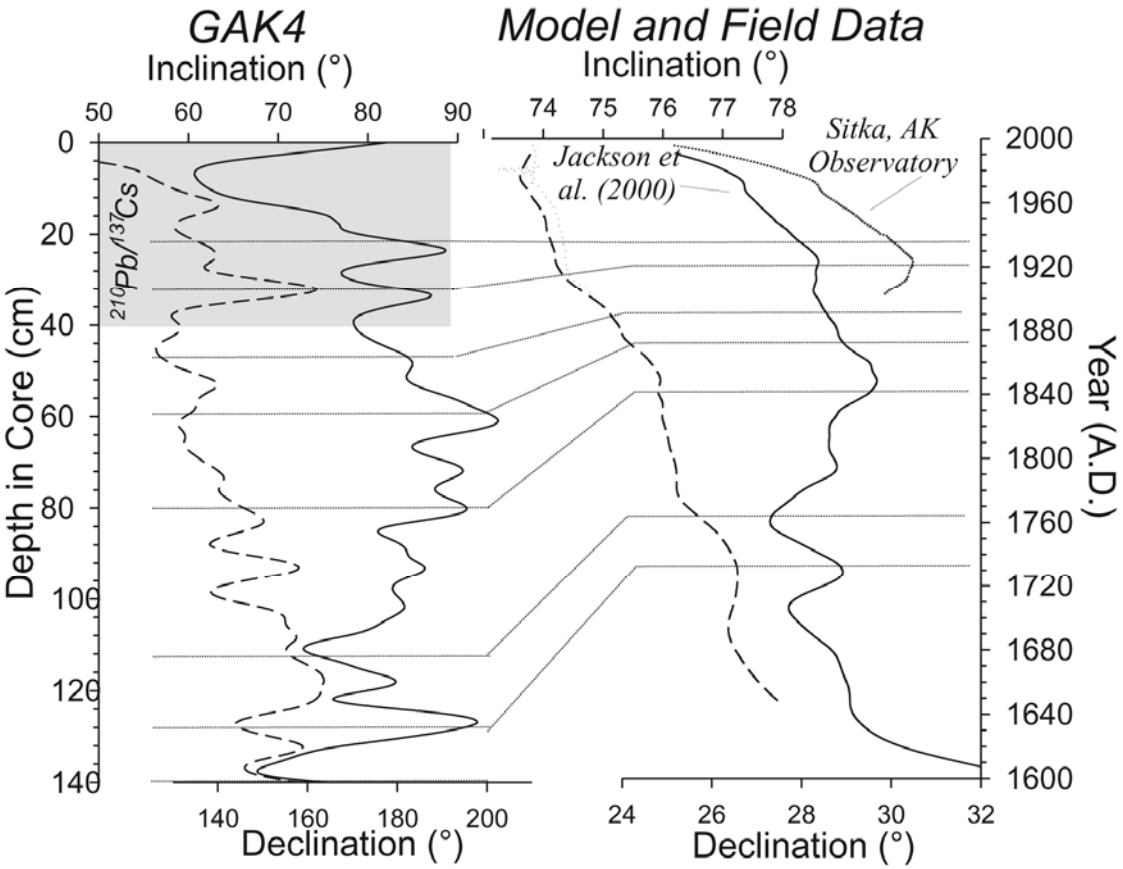

Figure 4-10. GCGAK4 paleosecular declination and inclination age model. The age model was developed for the past 400 years by comparison with modeled field data from Jackson et al. (2000) and observed data from Sitka, AK.

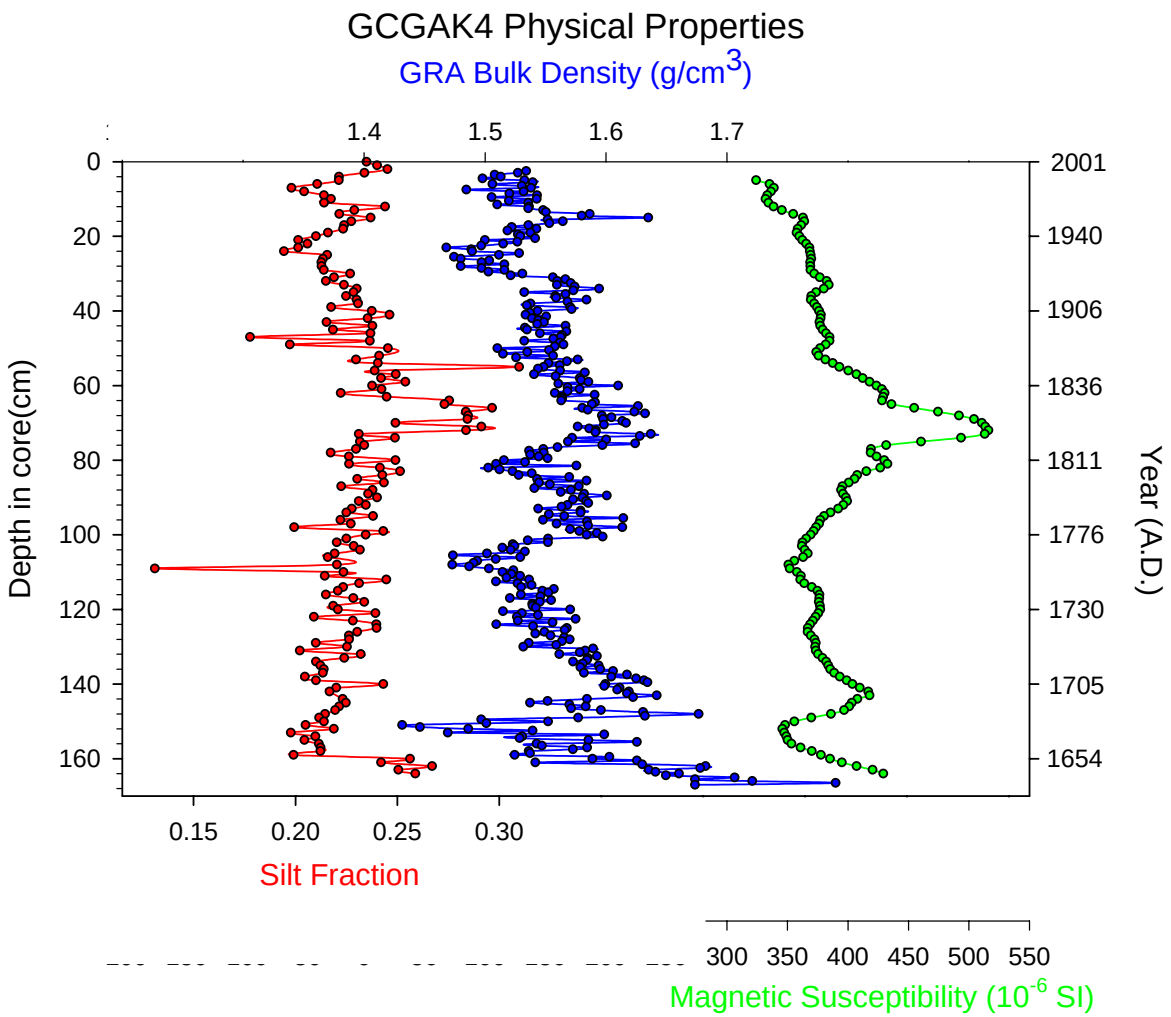

Figure 4-11. Physical properties of GCGAK4. Ages are based on the model developed from Jackson et al. (2000) and observed data from Sitka, AK.

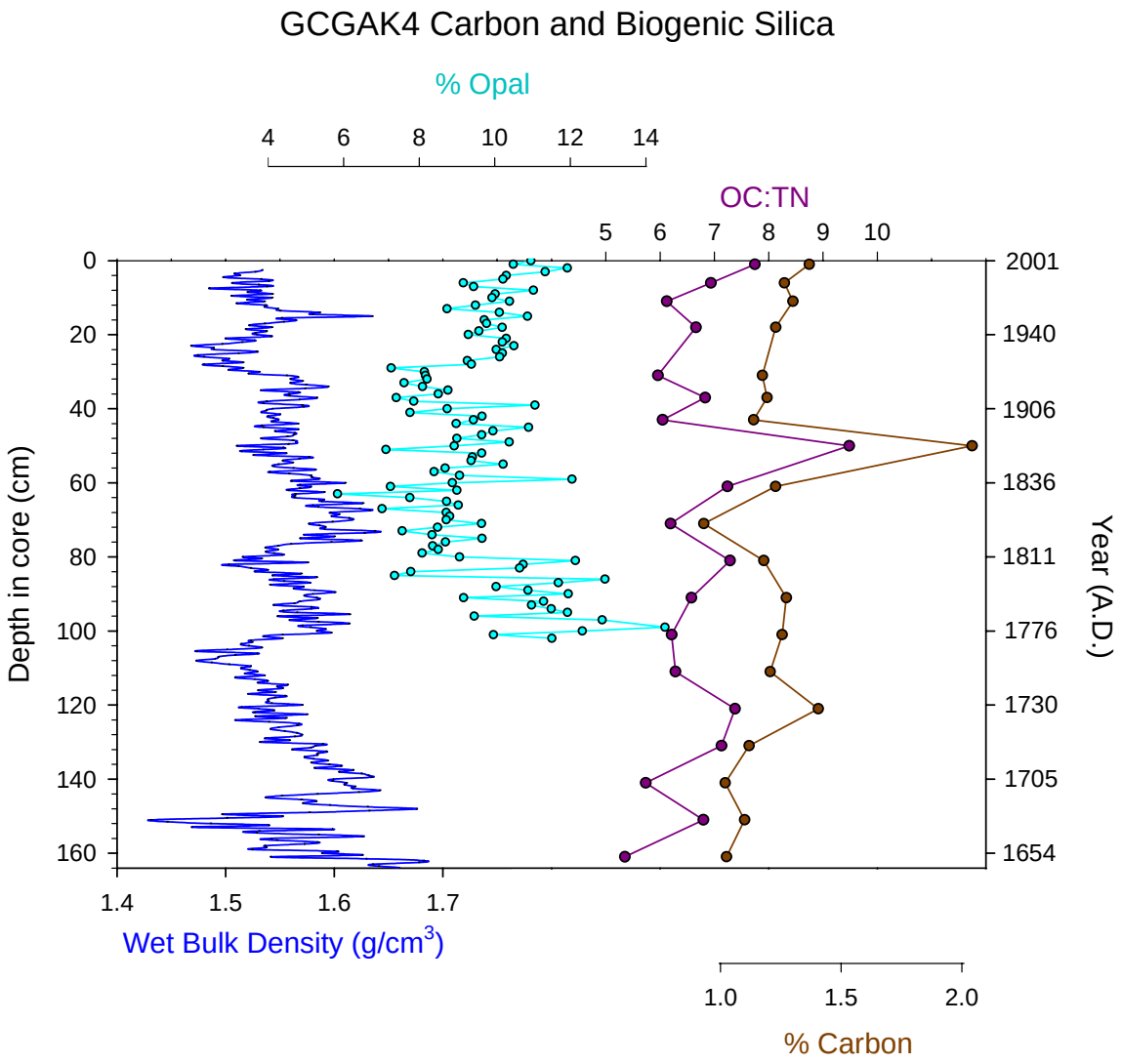

Figure 4-12. GCGAK4 OC:TN, % carbon, % biogenic silica.

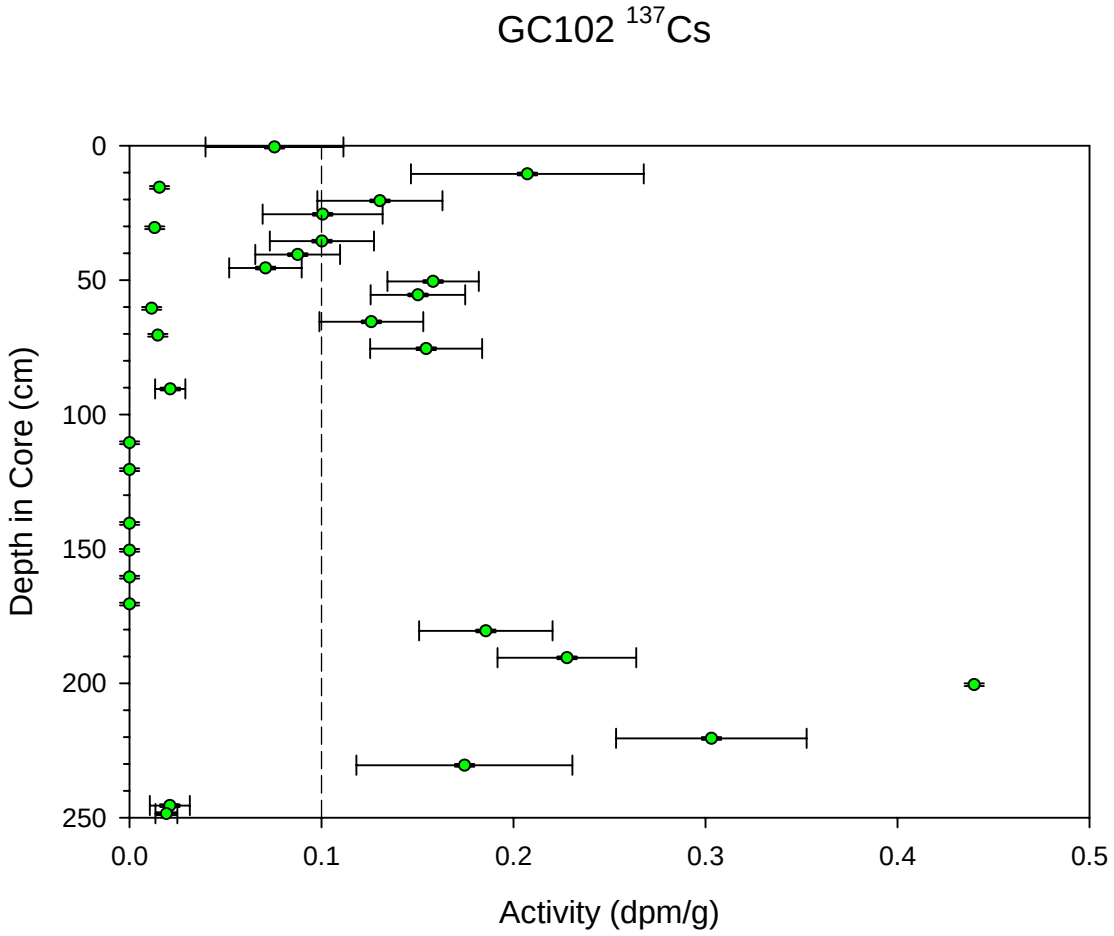

Figure 4-13. Profile of ^{137}Cs in GC102. A peak at 200 cm corresponds to the year 1964, the peak in nuclear weapons testing. First appearance of ^{137}Cs, which corresponds to the onset of nuclear weapons testing in 1954, occurs at 220 cm. For the detector used, the MDA for ^{137}Cs is shown at 0.1 dpm/g.

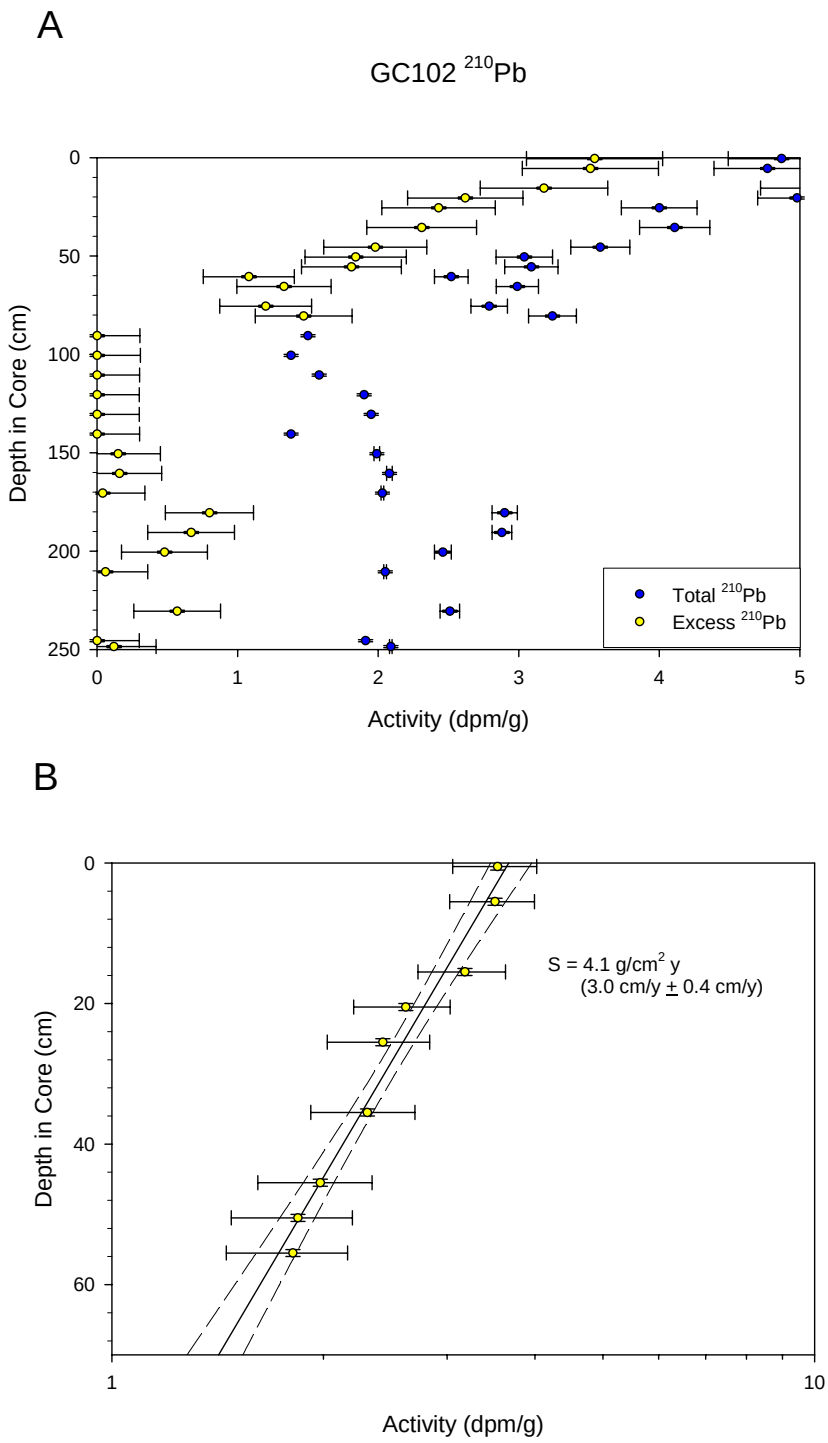

Figure 4-14. GC102 ^{210}Pb profiles. Figure 4-15A shows the downcore profile of total and excess ^{210}Pb for GC102. Figure 4-15B shows the profile of excess ^{210}Pb plotted on a logarithmic scale for the upper 60 cm. A linear regression has been fit through the data in 4-16b with the 95 % confidence interval of the regression shown as dashed lines.

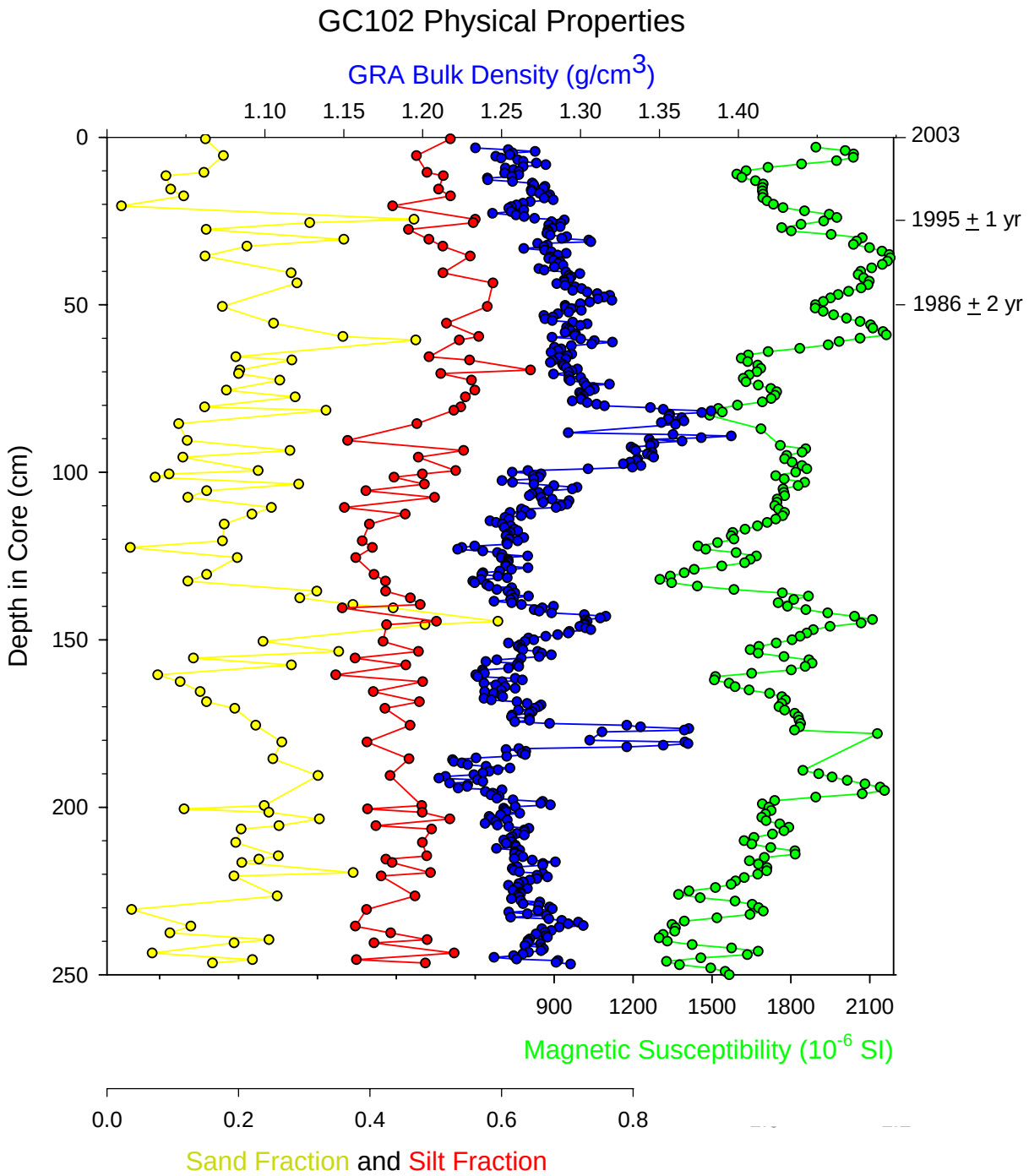

Figure 4-15. Physical properties of GC102.

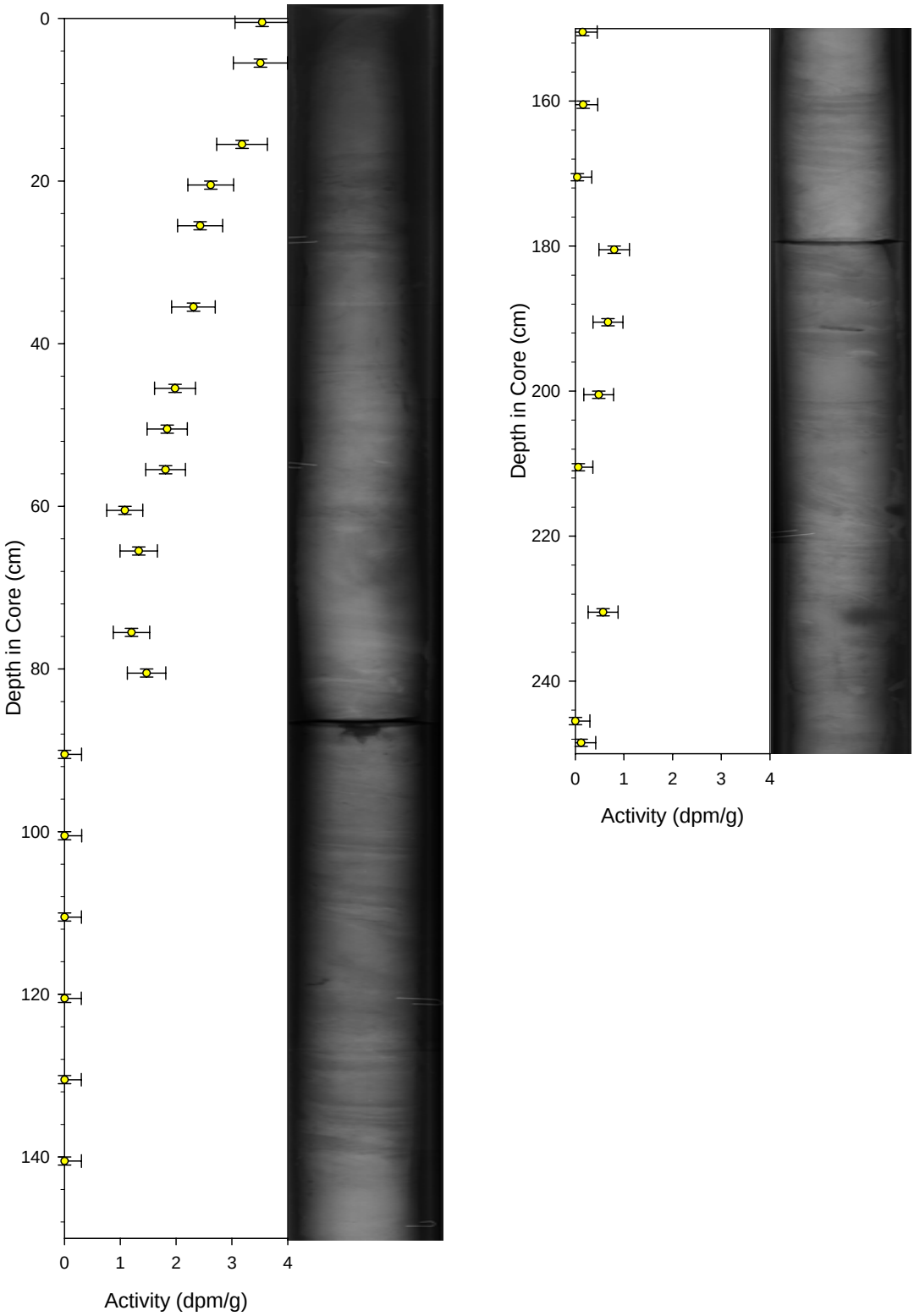

Figure 4-16. X-radiograph and ^{210}Pb data for GC102.

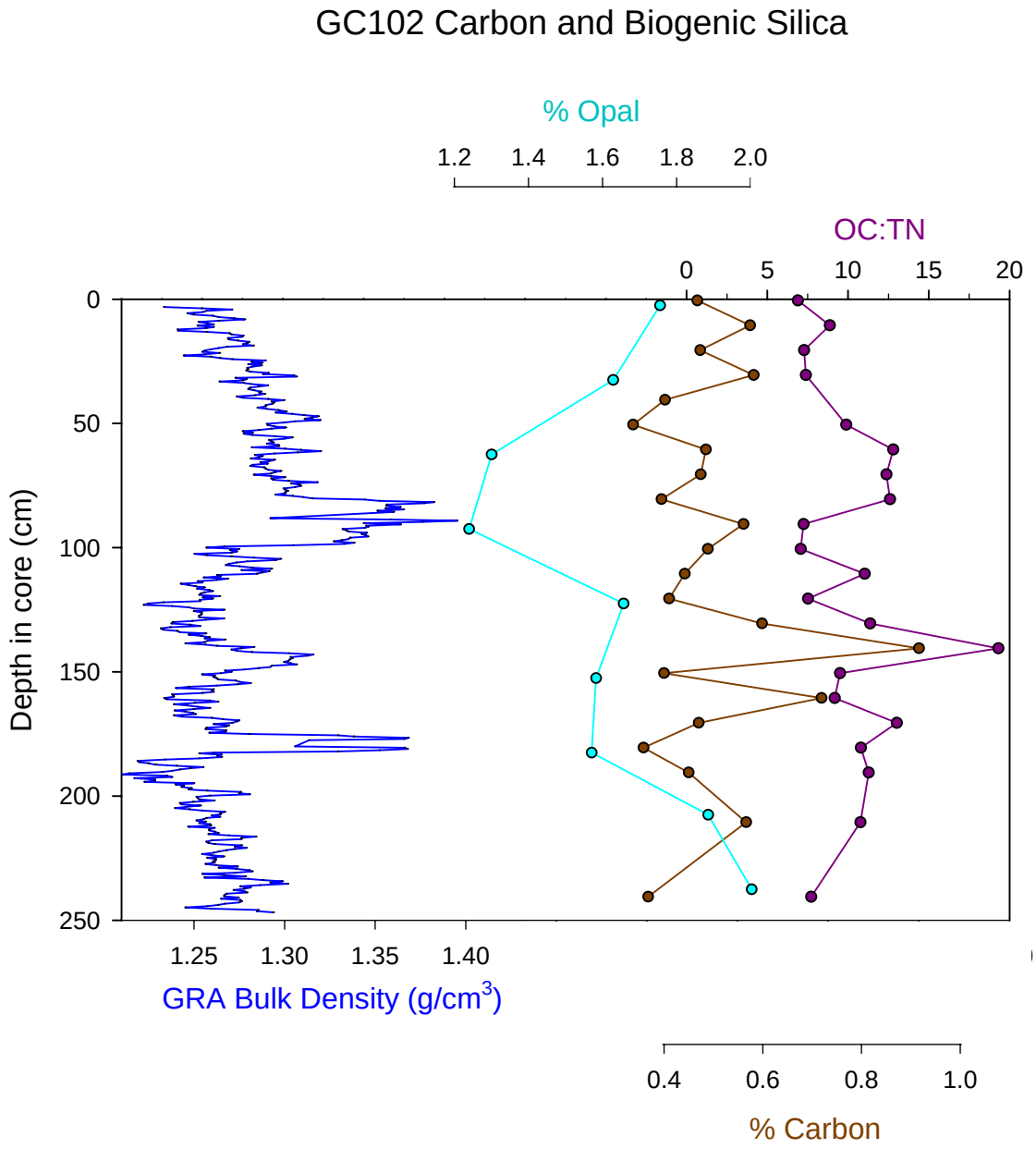

Figure 4-17. GC102 GRA bulk density, OC:TN, % carbon, and % biogenic silica.

CHAPTER 5
DISCUSSION

For reference, a table summarizing core locations, water depths, and sediment accumulation rates has been provided (Table 5-1).

Geochronology

Sediments accumulating at a steady rate display a ^{210}Pb activity profile that contains three distinct regions: a surface mixed layer of uniform activity, a zone of exponentially decreasing activities, and a lowermost zone of constant, low activity supported by the decay of ^{226}Ra (Nittrouer *et al.* 1979; Jaeger and Nittrouer 1998). None of the cores used in this study revealed a surface mixed layer of uniform ^{210}Pb activities. Jaeger and Nittrouer (submitted) found that the surface mixed layer for most GOA shelf strata was 5 – 7 cm thick. Because the cores were sampled for radioisotope analyses every 5 cm near their surface, the surface mixed layer likely went undetected because it occurred only in the upper 5 cm in each of the cores. Another possibility is that the gravity core blew off top sediment containing the surface mixed layer as it entered the substrate.

All three cores exhibit a region of exponentially decreasing ^{210}Pb activities from which a sedimentation rate was calculated using the method of Benninger *et al.* (1979) (Figures 4-2, 4-9, and 4-14). If an area that generally accumulates sediment at a steady rate undergoes occasional rapid sedimentation, event layers of irregular activity will be apparent in the radioisotope profile (Huh *et al*. 1990; Sugai *et al.* 1994; Jaeger and Nittrouer 1998). Event layers were distinguished in GC156 and GC102 as regions with

relatively homogenous ^{210}Pb activities, laminations in the x-radiograph, and in GC156 as regions with anomalous high values for mass percent silt, magnetic susceptibility, and GRA bulk density. An event layer measuring 15 – 20 cm in GC156 corresponds to the year 1964, the year of the extremely powerful Good Friday Earthquake (Figures 4-2, 4-3, and 4-4). Event layer type profiles were also prevalent throughout much of GC102 (Figure 4-14), including one at 90-170 cm that corresponds to ^{210}Pb and ^{137}Cs dates around 1964. The extensive laminations and homogenous ^{210}Pb profiles are evident of mixing and rapid deposition of sediments, and are likely the result of gravity flow deposits induced by the 1964 earthquake. There were no event layers evident in the radioisotope profiles of GCGAK4.

Only GCGAK4 reached supported ^{210}Pb levels. The 100-year average sediment accumulation rate derived by dividing the depth where supported levels of ^{210}Pb were reached (~4-5 half-lives, ~100 years) was consistent with the steady state sediment accumulation rate calculated using the method of Benninger *et al.* (1979) (Figure 4-9).

In order to check the accuracy of ^{210}Pb-derived sediment accumulation rates a simple model using the first appearance and peak in ^{137}Cs activities was additionally used to calculate sediment accumulation rates (Nittrouer *et al.* 1983; Smith and Comans 1996). The first appearance of ^{137}Cs is assumed to coincide with the onset of nuclear weapons testing in 1954, and the peak in ^{137}Cs is assumed to coincide with the peak in nuclear weapons testing in 1964. The peak in ^{137}Cs activity for GC156 occurs within the depth range of the 15 - 20 cm thick event layer present in the core (Figure 4-1). Setting all ages within the event layer to 1964 (the year corresponding to the peak in ^{137}Cs and the timing of the Good Friday Earthquake) a sedimentation rate of 3.2 cm y^{-1} was calculated. This

rate is identical to the sediment accumulation rate derived from ^{210}Pb and the first appearance of ^{137}Cs.

The peak in ^{137}Cs activity in GC102 occurs at 200 cm downcore within a region of steady sediment accumulation, evident by exponentially decreasing ^{210}Pb activities (Figure 4-14). Because the peak in ^{137}Cs does not coincide with the depth of the 1964 gravity flow deposit, it is possible that the true peak in ^{137}Cs activity was eroded during the gravity flow. Due to the magnitude of the gravity flow deposit and the likelihood that material was eroded below this interval, dating of GC102 below the gravity flow is problematic and not attempted in this study. For GCGAK4, peak ^{137}Cs activity occurs at the surface. This likely is a result of the redistribution of ^{137}Cs through bioturbation and is not a reflection of sediment accumulation (Figure 4-8) (Smith and Comans 1996).

GCGAK4 paleosecular variations in magnetite declination and inclination data were additionally used to develop an age model based on the global field model of Jackson *et al.* (2000) and observed data from Sitka, AK (Figure 4-10). ^{210}Pb was used to test the validity of this model for the past 100 years. The sediment accumulation rate based on the paleomagnetic model was a constant 0.33 cm y^{-1} for the past 70 years (0 – 21 cm), and increased to 0.70 cm y^{-1} over the 30 years prior (21 – 45 cm). A bulk sedimentation rate of 0.32 – 0.40 cm y^{-1} was calculated using the depth where ^{210}Pb goes to supported levels. A ^{210}Pb sediment accumulation rate of 0.29 $\pm$ 0.05 cm y^{-1} was derived using the method of Benninger *et al.* (1979). Both rates are consistent with the sediment accumulation rate derived from the paleomagnetic data for the past 70 years. Furthermore, a line fit through the last two points with excess ^{210}Pb (24 cm and 31 cm

core depth) has a steeper slope than the line fit through the data above these depths, suggesting a possible increase in sediment accumulation around 24 cm.

Lithology

Glacially derived sediments can be distinguished, in part, by a significant silt component dominated by the 10 – 30 μm size fraction (Andrews and Principato 2002), which coincides with the region where grains begin to behave non-cohesively and sorting of individual grains occurs (McCave *et al.* 1995). For this reason, textural statistics of the silt size fraction were used in this study to indicate the strength of sediment transport stresses acting to sort sediment along the GOA margin. GC156 mass percent silt showed a strong positive correlation with the mean silt grain size (Figure 4-5), suggesting that an increase in overall silt content coincides with an increase in average silt fraction particle diameter. Variability in the relative proportions of silt modes supports this. For example, in GC156 the depth intervals 178 – 179 cm and 182 – 183 cm correspond to a peak and trough, respectively, in mass percent silt and mean grain size. In both intervals there are prominent grain size modes at 2, 4, ~10, and ~20 μm (Figure 4-6). The modes at 2 and 4 μm remain nearly equal for both samples, but the 10 and 20 μm modes are distinctively larger in the 178 – 179 cm interval, which suggests that variability in mass percent silt is an indicator of variability in the 10 – 30 μm (i.e., sortable silt fraction) size range.

Nondestructive GRA bulk density measurements can be made at very high resolutions (< 1 cm) using a multi-sensor core logger and are useful in interpreting the causes of variations in the sediment record if the relationship between bulk density and other sediment properties (i.e., grain size, biogenic composition, mineral composition) are known (Weber *et al.* 1997; Rack *et al.* 1996). Previous studies have shown that

variability in bulk density in biogenically deficient sediments is dominantly controlled by grain size and sediment accumulation rate (Weber *et al.* 1997; Andrews *et al.* 2002). A decrease in grain size or an increase in sediment accumulation rate results in higher porosity and lower GRA bulk density. Conversely, an increase in grain size or a decrease in sediment accumulation rate results in lower porosity and higher GRA bulk density.

GRA bulk density and mass percent silt significantly correlate in all three cores used in this study (Table 4-1). Because the grain size distributions in GC156 and GCGAK4 are dominated by the mud fraction, the silt fraction represents the coarser end of the grain size spectrum in both of these cores. In effect, increasing mass percent silt significantly increases bulk density because it represents an overall coarsening in grain size. GC102 contains a large percentage of sand (~20 % on average), so its bulk density is influenced by the overall coarsening due to the input of sand as well as silt.

Bulk density values are often influenced by the amount of biogenic material present in samples (Weber *et al.* 1997; Rack *et al.* 1996). Diatomaceous material is the dominant biogenic component in fine-grained sediments on the GOA margin (Sharma 1979). A high resolution (every 1 cm) analysis of opal content in GCGAK4 was performed in order to evaluate the influence of biogenic material on GRA bulk density measurements. GCGAK4 contained the highest percentage opal (9 % on average) of all of the cores, but no significant correlation between variability in opal and GRA bulk density was found (Table 4-1). This suggests that the influence of biogenic material on GRA bulk density is minor in comparison to grain size.

In both GC156 and GC102 there are regions with very large peaks in mass percent silt, GRA bulk density, and magnetic susceptibility (Figures 4-3 and 4-15). These

regions correspond to homogenous ^{210}Pb activities and laminations in x-radiographs, indicating that they were likely deposited during single events, perhaps due to gravity flows. ^{210}Pb and ^{137}Cs-derived dates suggest that the section from 122.5 – 142.5 in GC156 was deposited in 1964, the year of the large Good Friday Earthquake (9.2 M_w) centered in northwestern PWS. The earthquake formed extensive tsunamis in the region. Uplift of 13 – 15 m off the southwest end of Montague Island and subsidence of up to 2.3 m in PWS was recorded (Stover and Coffman 1993). The section from 90 – 170 cm in GC102 is interpreted as a gravity flow deposit caused by the 1964 earthquake based on its homogenous ^{210}Pb profile, extensive laminae, and estimated ages based on ^{210}Pb and ^{137}Cs that roughly correspond to the year 1964. Similar deposits of the same age are found on the Copper River Delta (Jaeger and Nittrouer, submitted). Because the gravity flow deposit is so large in GC102, and because smaller flows are apparent in the x-radiographs of GC102, comparisons of sediment properties with climate time series data are difficult, and are not attempted in this study. For GC156, the comparably smaller section containing the gravity flow was subtracted out prior to comparing sediment properties and climate time series data.

Organic carbon was generally negatively correlated with GRA bulk density in the three cores (Figures 4-7, 4-12, and 4-17). Therefore, the concentration of organic carbon appears to be related to the amount of clay content in each of the cores. GC102 had the highest OC:TN of any of the cores, followed by GC156, then GCGAK4. The OC:TN for each of the cores reflects their relative proximity to a terrigenous sediment source (Meyers, 1997). GC102 likely received a significant portion of its sediment locally from

Montague Island, evident in the relatively large amount of sand and high OC:TN in the core.

JCGOA2 and GC156

JCGOA2 is a 15 m jumbo piston core recently collected by Jaeger in September of 2004. The GOA2 site is located on a sediment drift in PWS about 2 km east of Site 156 (Figure 3-1). A preliminary age model was developed for JCGOA2 for the past 100 years based a ^{210}Pb sediment accumulation rate of ~ 2 cm y^{-1} from a core collected at the edge of the slope between GC156 and JCGOA2 (Figure 3-1) by Jaeger (1998). JCGOA2 magnetic susceptibility and GRA bulk density correlate well with that of GC156 back to around 1960, but JCGOA2 GRA bulk density does not correlate with GC156 GRA bulk density prior to 1960 (Figure 5-1). However, GC156 magnetic susceptibility and JCGOA2 magnetic susceptibility do correlate prior to 1960. The overall similarity in physical properties (e.g., increasing GRA bulk density and magnetic susceptibility) between the two cores over roughly the same time interval indicates that the mechanisms controlling sediment delivery are generally uniform over this region of PWS.

Sediment Transport

Water Flow into Prince William Sound

Until recently, the conceptual model of water flow through PWS depicted simple inflow through HE and outflow through Montague Strait (Emery and Royer, 1987). This model was supported by drifter buoys from the shelf that entered but never exited PWS through HE (Royer and Emery 1987). In contrast, 11 acoustic Doppler current profiler (ADCP) transects within HE during 7 cruises from 1986 – 1990 revealed that both the north – south and east – west components of flow in HE underwent reversals in direction over a horizontal scale of 1 – 2 km (Niebauer *et al.* 1994). Also, the east – west

component of flow was generally of the same magnitude as the north – south component. Despite these complications, an analysis of flow through HE was performed using a single mooring of current meters placed at various depths throughout the water column from November 1977 to February 1979. The data indicated that flow into PWS was generally strong (> 25 cm s^{-1}) above 100 m water depth (Niebauer *et al*. 1994). Inflow at 200 m (near-bottom water) was strong from June to September 1978 with velocities generally greater or equal to 25 cm s^{-1}. Alternating inflow and outflow occurred at the bottom layer for the second half of September 1978 to February 1979 with velocities generally less than 25 cm s^{-1} in either direction. The net direction of flow during this period was westward (neither in or out of PWS). Niebauer *et al*. (1994) suggested that near-bottom current flow into PWS during summer was likely the result of weak upwelling. A relaxation in easterly winds during the summer creates small offshore Ekman transport that forces waters to a depth of 150 m out of PWS, allowing deeper, denser water to enter PWS. In fall and winter, downwelling currents drive surface waters into PWS, while bottom waters on the shelf are diverted from HE by outflowing bottom currents.

Bottom Currents

Feely *et al.* (1978) found that a plume of suspended sediment concentrations 5 m from the seafloor stretched from the Copper River Delta west into PWS in fall, winter, and spring. Wave orbital velocities are strong enough to resuspend silt-sized bottom sediment at water depths < 40 m throughout the year, and at a water depth of 60 m for most of the year (Figure 2-6) (Jaeger and Nittrouer, submitted). Water depths between the Copper River Delta and Hinchinbrook Island are less than 50 m within 15 km of the shoreline, so resuspension of bottom material due to waves likely occurs year round over

much of this region. Also, the resuspension of bottom material due to waves underestimates the total resuspension of material because tidal and current generated shear stresses, which have been shown to play a major role in resuspension of bottom material in the GOA (Feely *et al.* 1978), have not been taken into account. Tidal and wave orbital shear stresses work to resuspend material, but they are not able to move that material over long distances. In order to move sediment in the bottom benthic layer (BBL) over a long distance, a sustained current must be introduced. Downwelling currents generated in this region are likely moving west parallel to the shoreline as directed by Coriolis steering.

Suspended matter concentrations in the Copper River-PWS region were observed by using a transmissometer at various stations along the GOA shelf in the summer of 1994 by Jaeger (1998). A cross-section of the transect of stations from just west of the Copper River Delta to PWS revealed westward movement of suspended sediment near the seafloor (Figure 5-2). Suspended sediment moving from shallower regions of the Copper River Delta into the mid-water depths of deeper regions in PWS was evident. Although these data illustrate sediment movement only over a short time period in summer/fall, they support other observations that on occasion sediment is transported near the bed into PWS.

Sediment Flux into Prince William Sound

Jaeger and Nittrouer (1998) estimated the modern flux of sediment into PWS to be approximately 15×10^6 tons y^{-1} based on ^{210}Pb sediment accumulation rates and sediment volumes derived from seismic reflection surveys. Sediment being deposited in PWS is derived from settling of particles from the surface layer plume (upper 50 m water depth) and by movement of material along the BBL. Suspended sediment concentrations

measured by Feely *et al.* (1978) in the surface plume between the Copper River Delta and Hinchinbrook Island were generally around 1 - 2 mg L^{-1}, which is supported by additional suspended sediment concentration measurements in the summer of 1994 by Jaeger (1998). A simple model to calculate sediment flux can be created using the sediment inventory for the 50 m surface layer and the velocity of the surface layer, which is assumed to be equal to the velocity of the ACC (15 – 30 cm s^{-1} in the area; Weingartner personal communication). Discharge for the Copper River is highest in July – September, while in other months of the year it is generally less than half the average of these three months. Therefore, flux of sediment in the surface plume was determined over a three month summer period. The estimated sediment flux to PWS from the surface plume is approximately 2 x 10^6 tons y^{-1}, assuming an ACC velocity of 20 cm s^{-1} and a sediment concentration of 2.0 mg L^{-1}.

For the BBL plume a period of four months of sediment flux is assumed because only the months June to September are dominated by deep water flow into PWS (Niebauer *et al.*1994). Because no BBL (< 1 m from the seafloor) sediment concentration measurements are available for this study area, estimates were made based on data from the Northern California Shelf (Ogston *et al.* 2004), which has a similar wind, wave, and current regime to the coastal GOA. A similar estimate of sediment transport was made for near-bed flow in the BBL. Using a BBL concentration of 500 mg L^{-1} (at 1 m above the seafloor) and a bottom current velocity of 20 cm s^{-1} (estimated from Feely *et al.* 1978; Ogston *et al.* 2004), the estimated near-bed sediment flux to PWS is approximately 15 x 10^6 tons y^{-1}, which is equal to the value calculated by Jaeger *et al.* (1998), which was derived from seismic reflection profiles and ^{210}Pb sediment

accumulation rates from cores collected in PWS. The estimates of sediment transport made here emphasize the likely dominant contribution of sediment carried near the bed to distal depocenters of the Copper River.

Spectral Analysis

Spectral analysis was performed using Redfit (Schulz and Mudelsee, in press) on the time series of GC156 GRA bulk density, magnetic susceptibility, and mass percent silt (Figure 5-3, 5-4, and 5-5). Spectral peaks above the 80% confidence level appear at 3, 6, 23, and 69 years for GRA bulk density, at 4, 7, and 12 years for magnetic susceptibility, and at 5, 33, and 67 years for mass percent silt. The 12 to 23-year peaks correspond to PDO-length periodicities (Mantua and Hare 2002). The 3 to 7 year peaks correspond to the frequency of ENSO events. The peaks of 33 and ~70 years are not considered because the sediment record at site 156 only extends back 70 years, and not enough cycles have occurred for the peaks to be significant. For comparison, spectral analysis on GC156 bulk density was also performed using the Blackman-Tukey method. Peaks of ~4 years were recognized using this method, which agrees with the ENSO-like periodicities found using Redfit (Figure 5-6).

The GC156 record of silt accumulation (GRA bulk density * sediment accumulation rate * mass percent silt) (1933 - present) was compared to both PDO and ENSO indexes. The PDO Index was developed by Hare (1996) and Zhang (1997) and is based on sea surface temperature (SST) anomalies above 20° N latitude in the Pacific Ocean. Both the GC156 silt accumulation record and the PDO Index show roughly an overall increase in values from ~1950 to ~1995 with a subsequent decrease in values (Figure 5-7). However, the records appear to diverge prior to 1950. Moore *et al.* (2002) found similar results in the snow accumulation record of an ice core taken from Mt.

Logan (Figure 2-1 for location). The ice core record correlated with the PDO Index during the period 1948 – 2000, but not prior to this period.

Increased temperatures, decreased salinities, and increased strength in the ACC have been connected to ENSO events (Royer and Weingartner 1999). Spectral analyses of both GCGAK4 and GC156 reveal significant peaks with ENSO periodicities. In addition, a high-resolution record of GC156 silt accumulation has been compared with the Multivariate ENSO Index (MEI) (Figure 5-8). This index is calculated using the principal components of the six main observed variables in the tropical Pacific: sea-level pressure (SLP), zonal (U) and meridional (V) winds, sea surface temperature, surface air temperature, and fraction of the sky containing clouds. The two data sets are positively correlated ($r^2 = 0.2$) over the period for which the MEI is calculated (1950 – present), which is statistically significant. A general increase in the values of the MEI, the PDO, and silt accumulation in GC156 occurs over this time period.

GC156 Sediment Properties, Upwelling, Freshwater Discharge, and Precipitation

Several factors appear to have a significant influence on sedimentary properties in core GC156. Cross-correlation analyses revealed that annual precipitation as measured at meteorological stations in Yakutat and Cordova showed a significant positive correlation with mass percent silt ($r^2 = 0.2$) and magnetic susceptibility ($r^2 = 0.2$). Furthermore, winter and summer precipitation records from these stations significantly correlated with ~40 year records of freshwater discharge in spring for the Copper River; spring, summer, and fall for Power Creek (near Cordova); and spring and fall for the Kenai River. The spring discharge record of the Copper River showed a negative correlation ($r^2 = -0.3$) with the annual snow to precipitation ratio (cm's of snow/cm's of total precipitation; an index of years with more snow) at both Yakutat and Cordova, which suggests that

increased relative rainfall results in increased freshwater discharge. There were no significant **annual** correlations found directly between freshwater discharge from the three rivers and mass percent silt and magnetic susceptibility. However, such a perfect one-to-one correlation was not expected given an apparent control on sediment transport to the site by near-bed flow. Inter-decadal trends in mass percent silt and magnetic susceptibility appear to match well with records of Copper River discharge (spring and summer) and annual precipitation records (Figure 5-9 and 5-10). A general trend of increasing values from ~1950 onward, followed by a decrease in values around 1992 occurs in each of these records. This same trend is seen in the discharge records of rivers in the region, particularly in the spring (Figure 5-10). There are also numerous annual and inter-annual highs and lows in sediment properties, precipitation, and freshwater discharge that correlate (e.g., 1948, 1950, 1952, 1960, 1962, 1966-1970, 1973, 1981, 1987, 1992, and 1996; Figure 5-9). The PFEL record of upwelling does not appear to contain a inter-decadal trend, but annual to inter-annual highs and lows in upwelling, mass percent silt, and magnetic susceptibility do appear to correlate in some instances with upwelling records (e.g., 1948, 1950, 1952, 1961, 1966, 1975, 1978, 1980-1984, 1987-1988, 1990, 1993, and 1996; Figure 5-9). Due to the homogenization effects of bioturbation and errors from sampling resolution, these annual to inter-annual correlations are tentatively considered.

The principle components (PC) of GC156 mass percent silt and magnetic susceptibility were calculated using Analyseries (Figure 5-11). The first PC of mass percent silt, magnetic susceptibility, and GRA bulk density correspond well to the overall increase in regional spring river discharge (Figures 5-10 and 5-11) from 1950 – 1990,

further validating the interpretation that fluvial discharge is the primary control of sediment properties at Site 156. Peaks in the second PC of magnetic susceptibility match well with the timing of El Niño events, which is expected because ENSO events have been correlated with precipitation and freshwater discharge records along the coast of southern Alaska (Weingartner *et al.* 2002; Stabeno *et al.* 2004).

Annual to inter-annual variability in mass percent silt and magnetic susceptibility appears to be the result of complex interactions between fluvial discharge and upwelling. For example, peaks in mass percent silt generally correspond to peaks in precipitation and discharge, but for the year 1983 mass percent silt is relatively high, while precipitation, spring Copper River discharge, and summer Copper River discharge are low. During this year the summer upwelling was high and January upwelling was low (i.e., increased downwelling), suggesting increased flow into PWS during summer and stronger downwelling currents on the shelf in winter. The inverse was true for 1955. In that year, an increase in spring and summer Copper River discharge corresponded to an increase in mass percent silt, relatively weak summer upwelling, and high January upwelling.

Longer-term Climate Controls on Shelf Strata Properties

Calkin *et al.* (2001) recognized four major glacial advances (A.D. 1250, 1450, 1650, and 1850) in southern Alaska during the LIA using their Glacier Expansion Index (GEI). Blackman-Tuckey spectral analysis of the GEI time series yielded peaks at 65, 104, and 170 – 210 years (Wiles *et al.* 2004). The 210-year peak corresponded to the timing of the deVries mode of solar variability, which appears in solar irradiance records derived from ^{14}C preserved in tree rings.

Two major glacial advances (A.D. 1650 and 1850) occurred over the period that GCGAK4 extends (Figure 2-7). Bulk density, magnetic susceptibility, and mass percent

silt increased significantly during these glacial advances (Figure 5-12). Solar irradiance data from Bard *et al.* (2000) show a general coherence with variability in physical and magnetic properties of GCGAK4 and with glacial activity. Relative highs in solar irradiance correspond to retreating glaciers and lower values in GCGAK4 physical and magnetic properties. Relative lows in solar irradiance correspond to subsequent glacial advances and higher values of physical and magnetic properties.

Spectral analysis of GCGAK4 bulk density using Redfit revealed peaks above the 95% confidence level at 167, 33, 27, 24, 19, 15, 14, 10, 8, and 7 years (Figure 5-13). Given the imprecision of the age model, which was based on subjective peak matching of declination and inclination records of GCGAK4, the Sitka, AK observatory record, and the model of Jackson *et al.* (2003), many of these peaks may actually be of the same period. The 167-year peak is similar to the periodicity of the 170 – 210 year peak that Wiles (2004) attributed to variability in solar irradiation, but because only two cycles at this periodicity occur in the GCGAK4 record the peak is not significant. The 14 – 33 year peaks correspond to PDO-length periodicities, while the 7 – 8 year peaks correspond to the timing of ENSO events. A Blackman-Tukey spectral analysis of GCGAK4 reveals peaks with 7, 20, and 26-year periods, which is similar to the results of the spectral analysis using Redfit (Figure 5-14).

There is a maximum oscillation frequency that can be achieved when analyzing discrete samples. This maximum frequency is called the Nyquist frequency, and is equal to 1/(2 x sample interval) (Weedon 2003). GCGAK4, with a sampling interval of 1 cm, has a Nyquist frequency of 0.5 cycles cm^{-1}. Because the sediment accumulation rate varies from around 0.33 cm y^{-1} to 1 cm y^{-1} in GCGAK4, the Nyquist frequency represents

a period ranging from 2 – 6 years. Therefore, all of the peaks represented as significant in the spectral analysis are valid because they have a longer period, or lower frequency, than the Nyquist frequency. For GC156 the maximum sampling interval was 5 cm, which applies to a few regions of the silt record. The Nyquist frequency for the GC156 silt record is 0.1 cycles cm^{-1}. With a sediment accumulation rate of 3.2 cm y^{-1}, this is equivalent to a period of 3.1 years, which negates the validity of the 3 year peak found in the spectral analysis of the GC156 mass percent silt record (Figure 5-5). Because GC156 GRA bulk density and magnetic susceptibility were sampled at higher frequencies (0.5 cm and 1 cm, respectively), all of the significant peaks recognized in the spectral analyses of these records is acceptable.

Table 5-1. Summary of core information. Refer to Figure 2-2 for map view of core locations.

Core	Location	Water Depth	Sed. Rate
GC156	Prince William Sound, Proximal to Copper River	415 m	3.2 cm/yr
GC102	GOA Shelf, Proximal to Copper River	250 m	3.0 cm/yr (upper 60 cm)
GCGAK4	GOA Shelf, Distal to Copper River	195 m	< 1 cm/yr

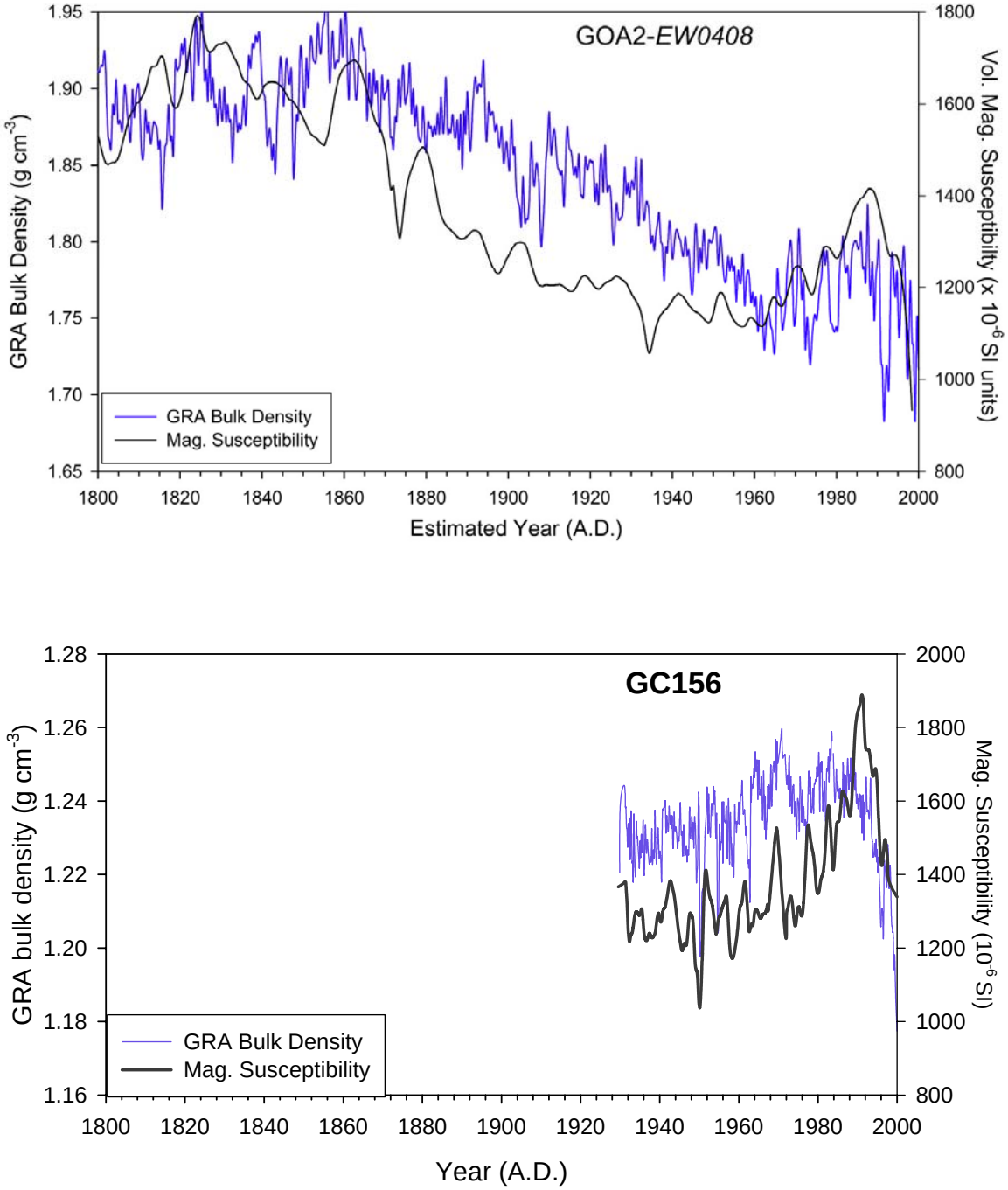

Figure 5-1. Sediment properties for GC156 and JCGOA2. Sediment properties of the cores match well back to 1960. The discrepancy between the bulk density records before 1960 may be an artifact of the poor age constraint on JCGOA2, or it may reflect a real difference in processes affecting bulk density at both sites.

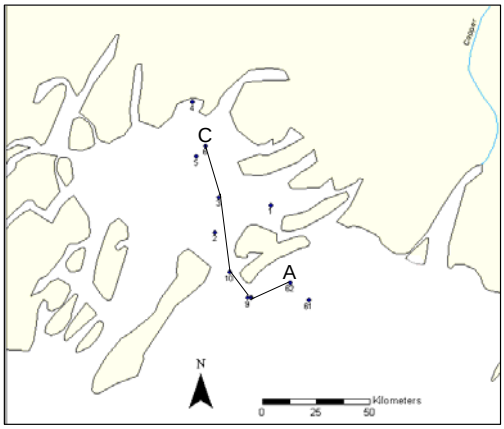

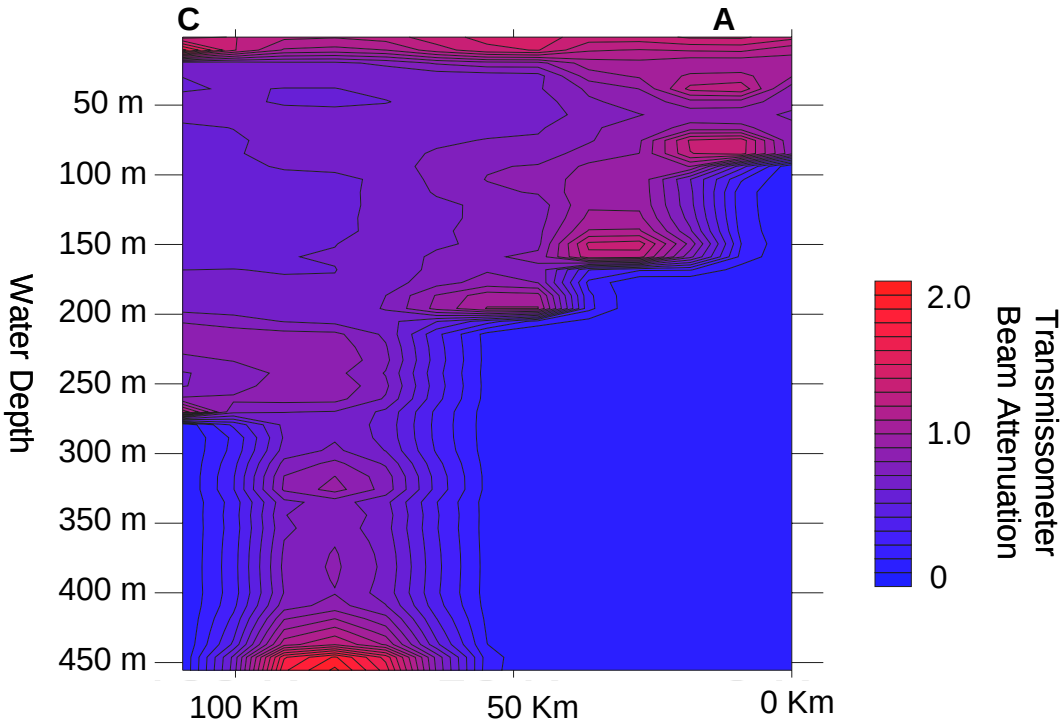

Figure 5-2. Transmissometer beam attenuation coefficients (BAC) (Jaeger, 1998a) for transect into PWS. The BAC is a measure of suspended matter concentration in the water column. Higher BAC values indicate higher sediment concentrations. Note the nephaloid layers at 100, 150, 200, and 250 m water depth that correspond to movement of BBL material into open water. This survey was performed in the summer of 1994.

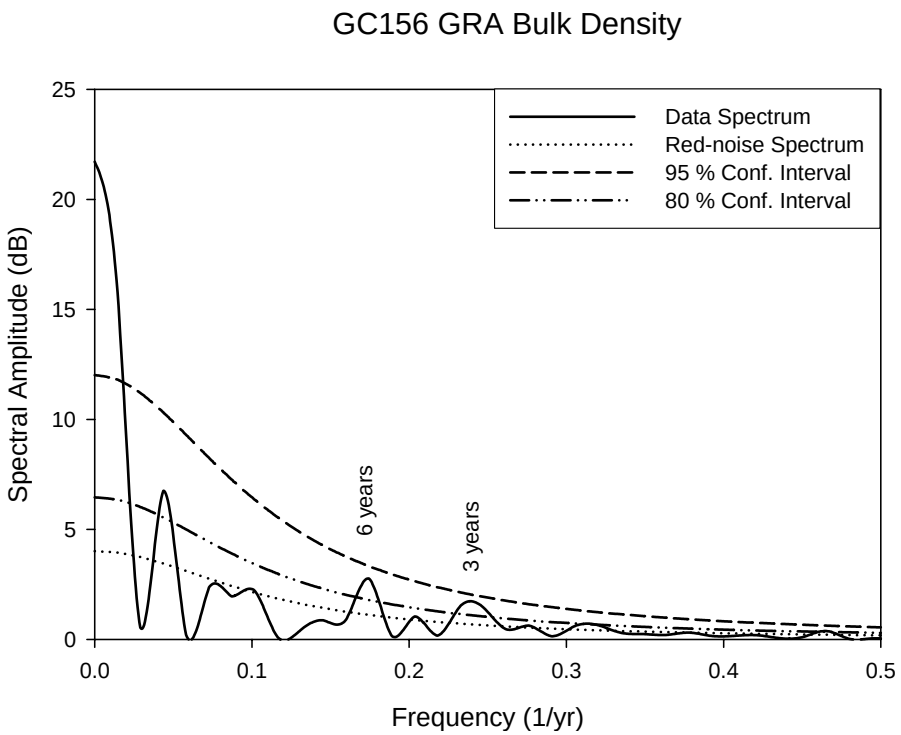

Figure 5-3. Redfit spectral analysis of GC156 GRA bulk density.

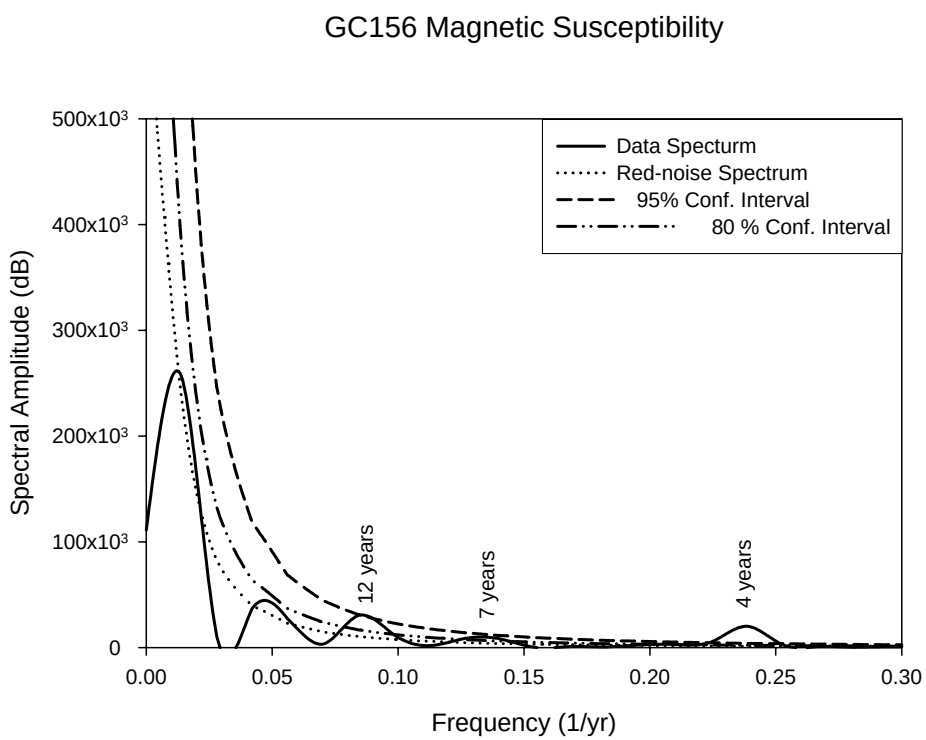

Figure 5-4. Redfit spectral analysis of GC156 magnetic susceptibility.

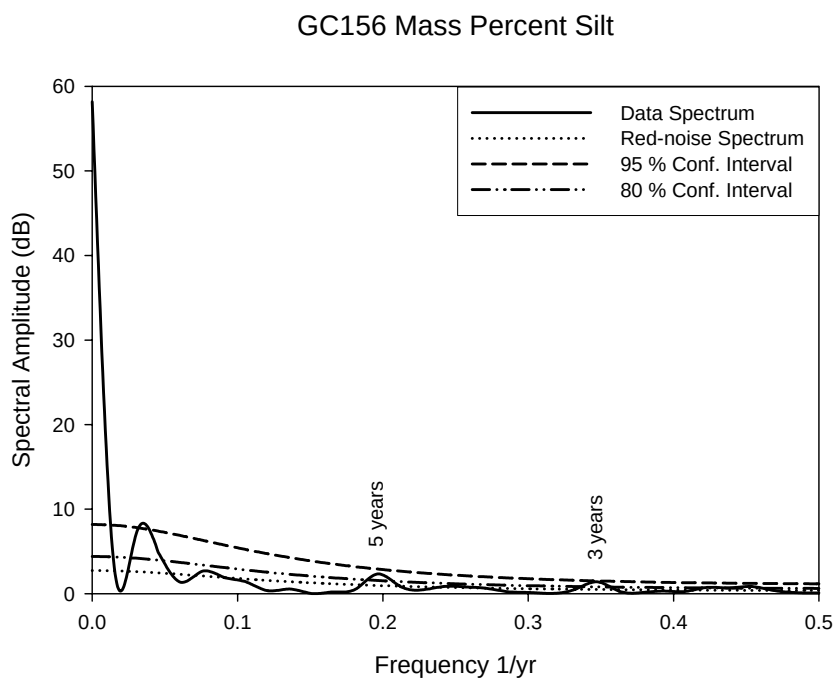

Figure 5-5. Redfit spectral analysis of GC156 mass percent silt.

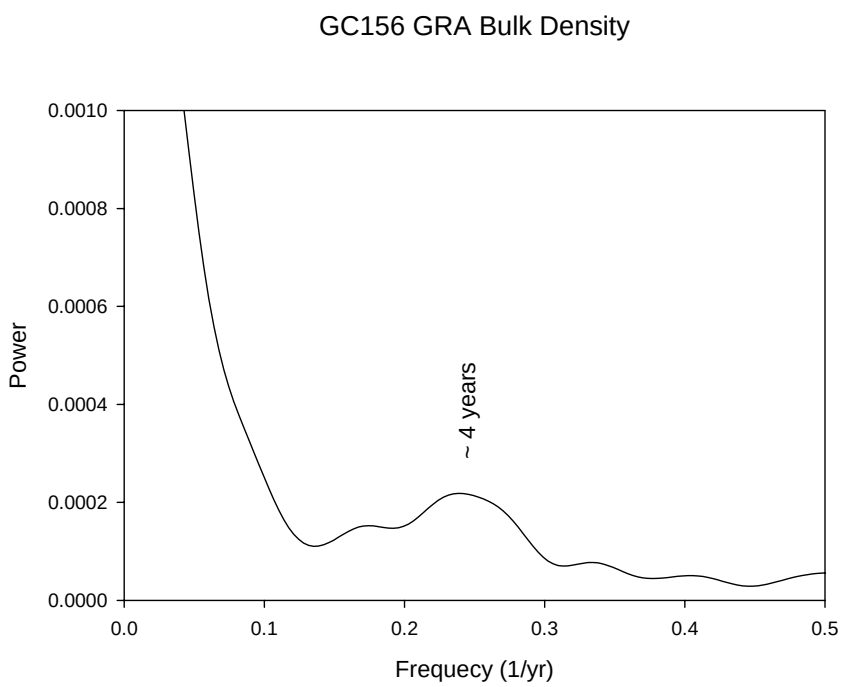

Figure 5-6. Blackman-Tukey spectral analysis of GC156 GRA bulk density.

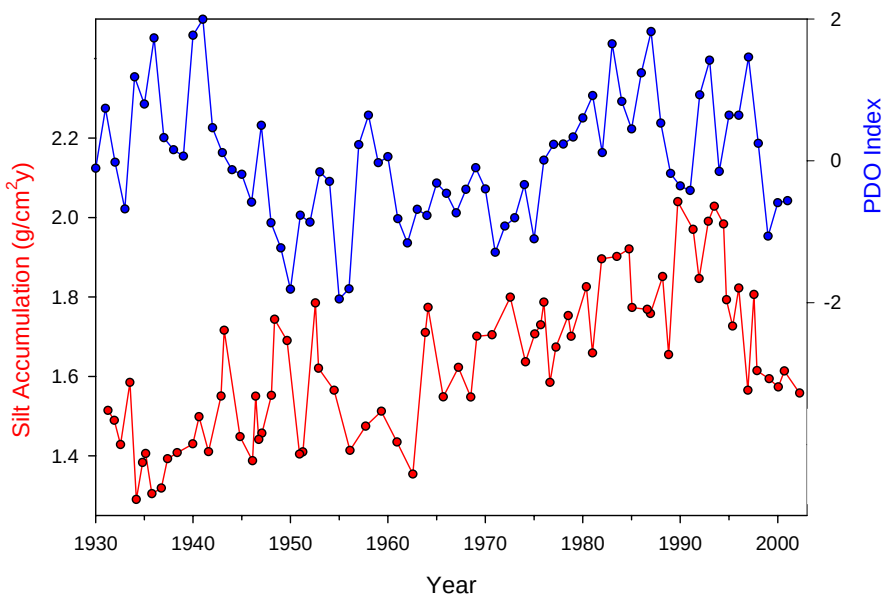

Figure 5-7. GC156 silt accumulation and the PDO Index. The index was developed by Hare (1996) and Zhang (1996) and is based on SST anomalies north of 20 N latitude in the Pacific.

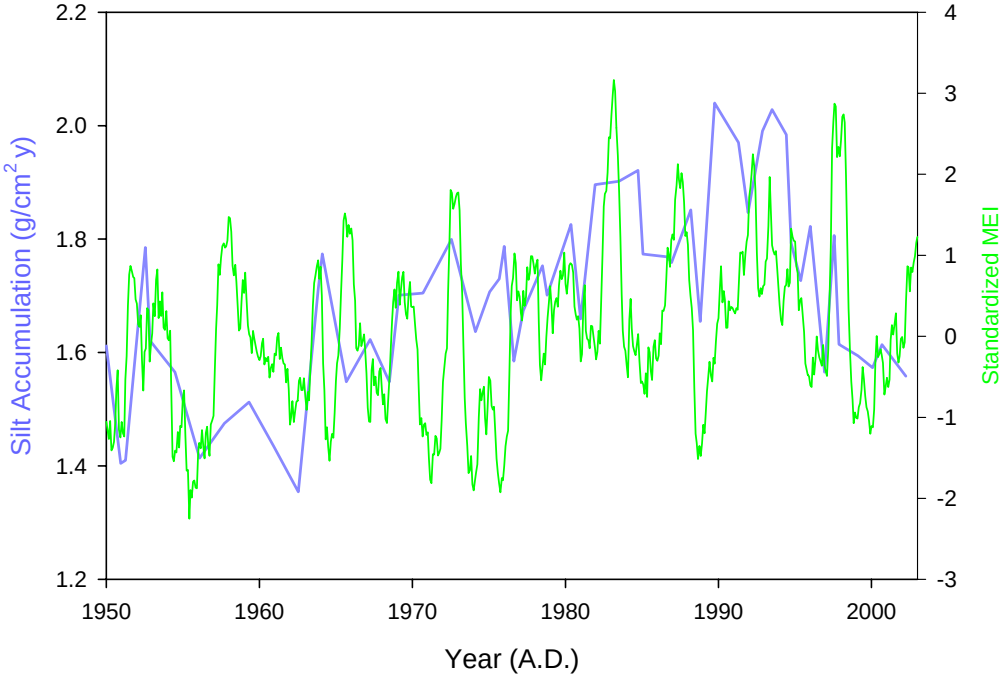

Figure 5-8. GC156 silt accumulation and the standardized MEI.

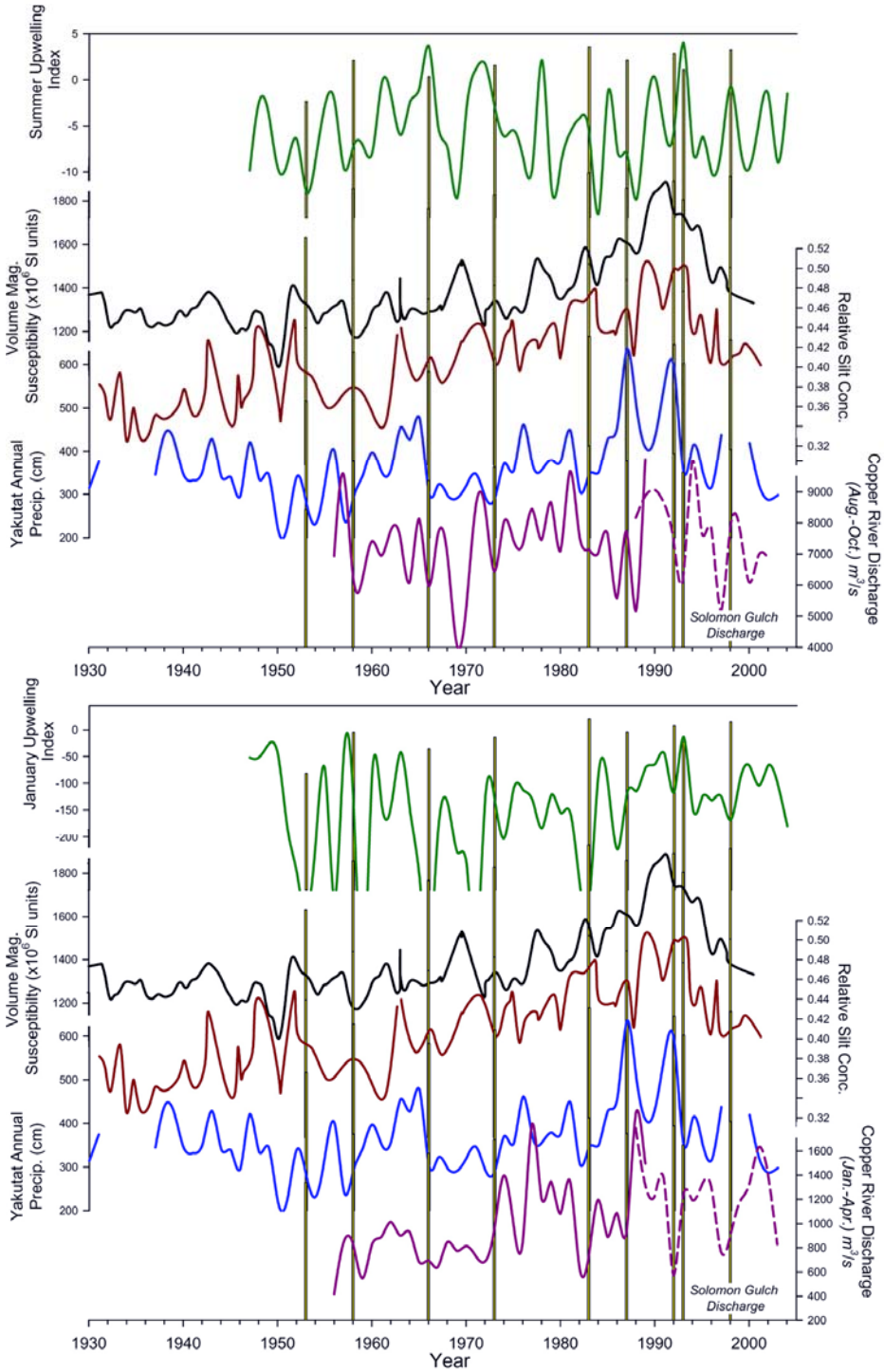

Figure 5-9. GC156 sediment properties, upwelling, and river discharge. The yellow vertical lines represent ENSO events. The discharge record of Solomon Gulch, located near Valdez, AK was matched qualitatively to data from the Copper River to examine discharge trends beyond 1990.

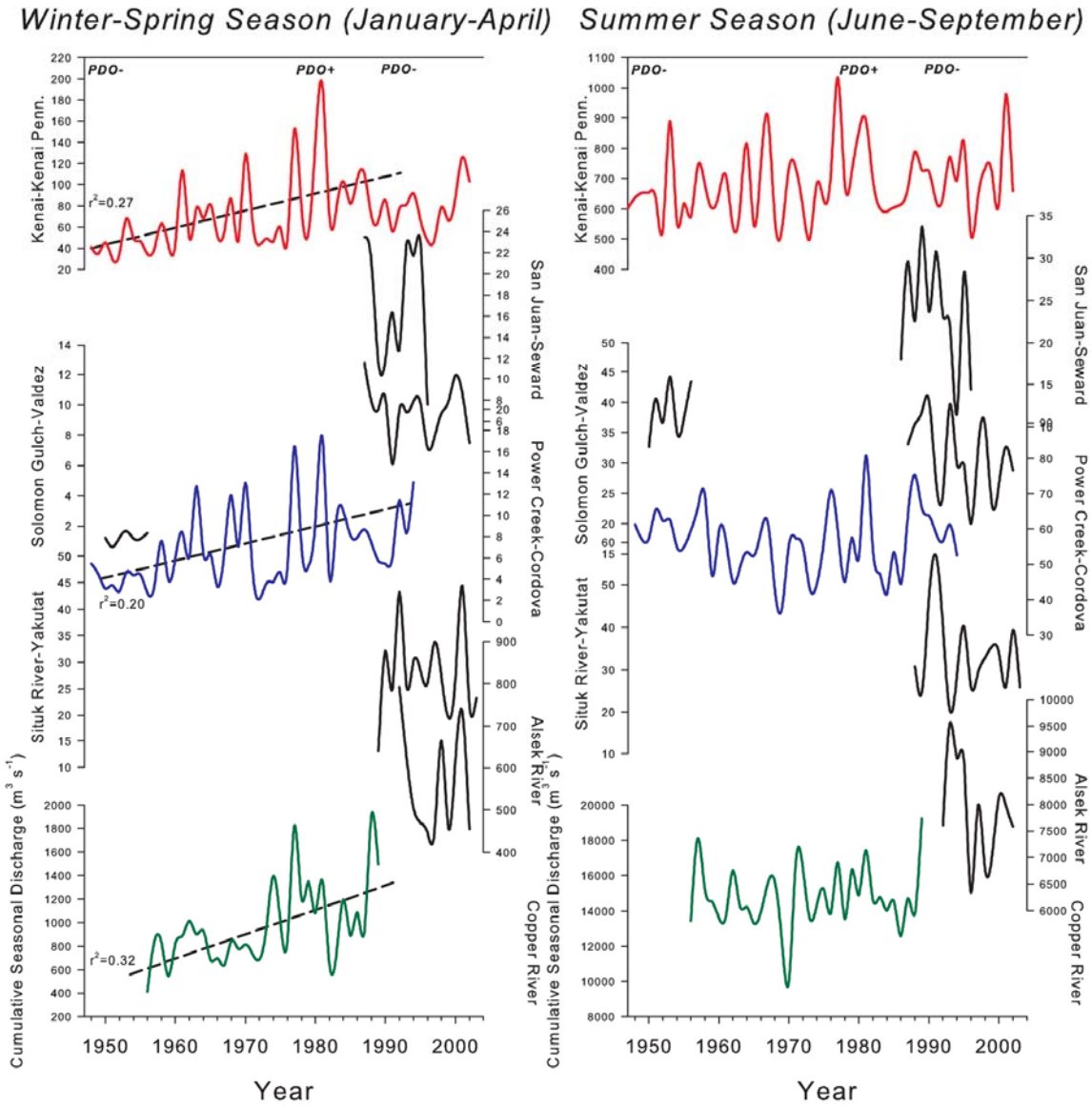

Figure 5-10. Discharge records of coastal rivers in southern Alaska. The winter-spring discharge records show a long-term increasing trend.

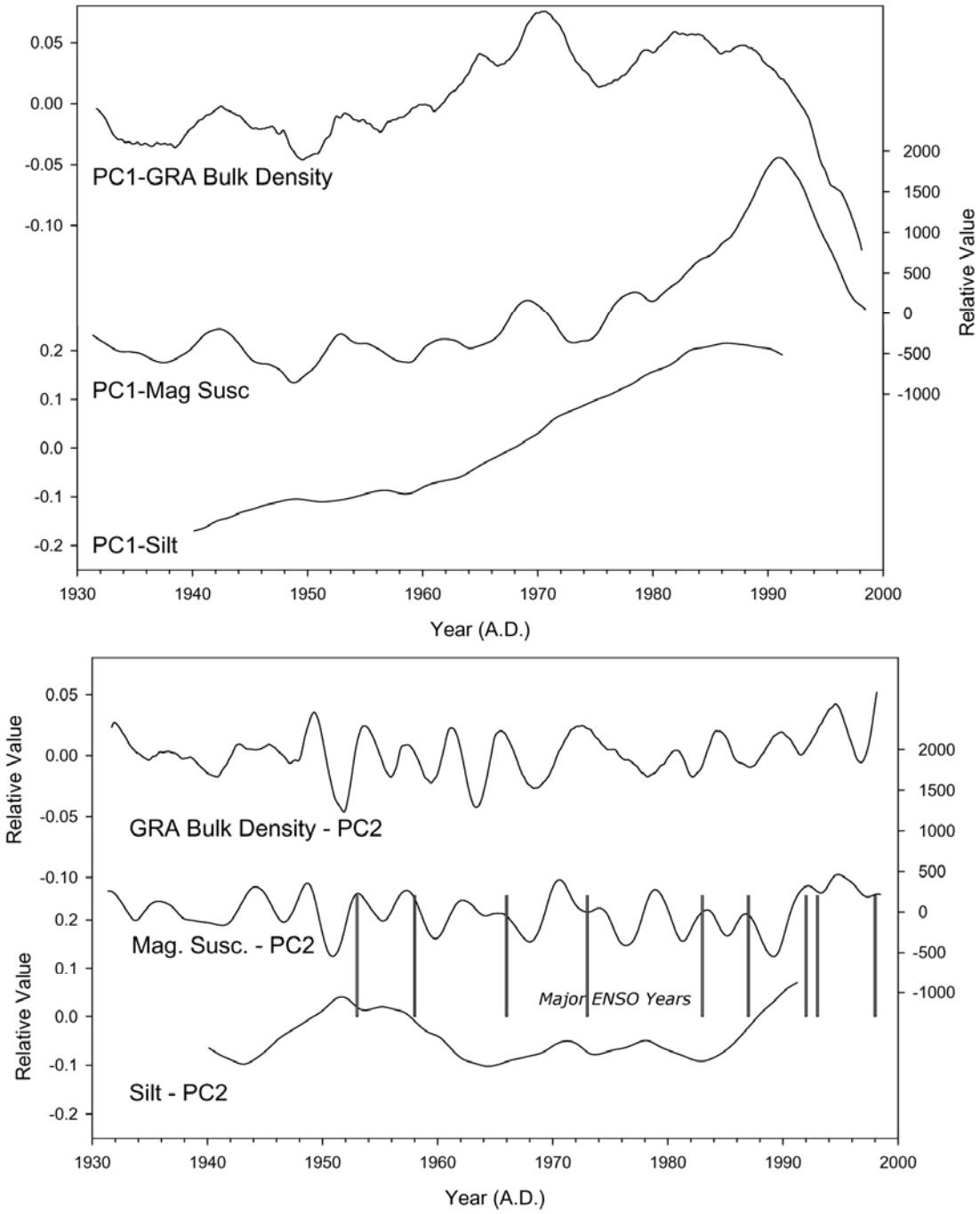

Figure 5-11. Principle components of GC156 sediment properties. The first principle component of mass percent silt, magnetic susceptibility, and GRA bulk density correspond to the overall increase in river discharge (Figure 5-5) over the same time periods. Peaks in the second principle component of magnetic susceptibility matches well with El Niño years.

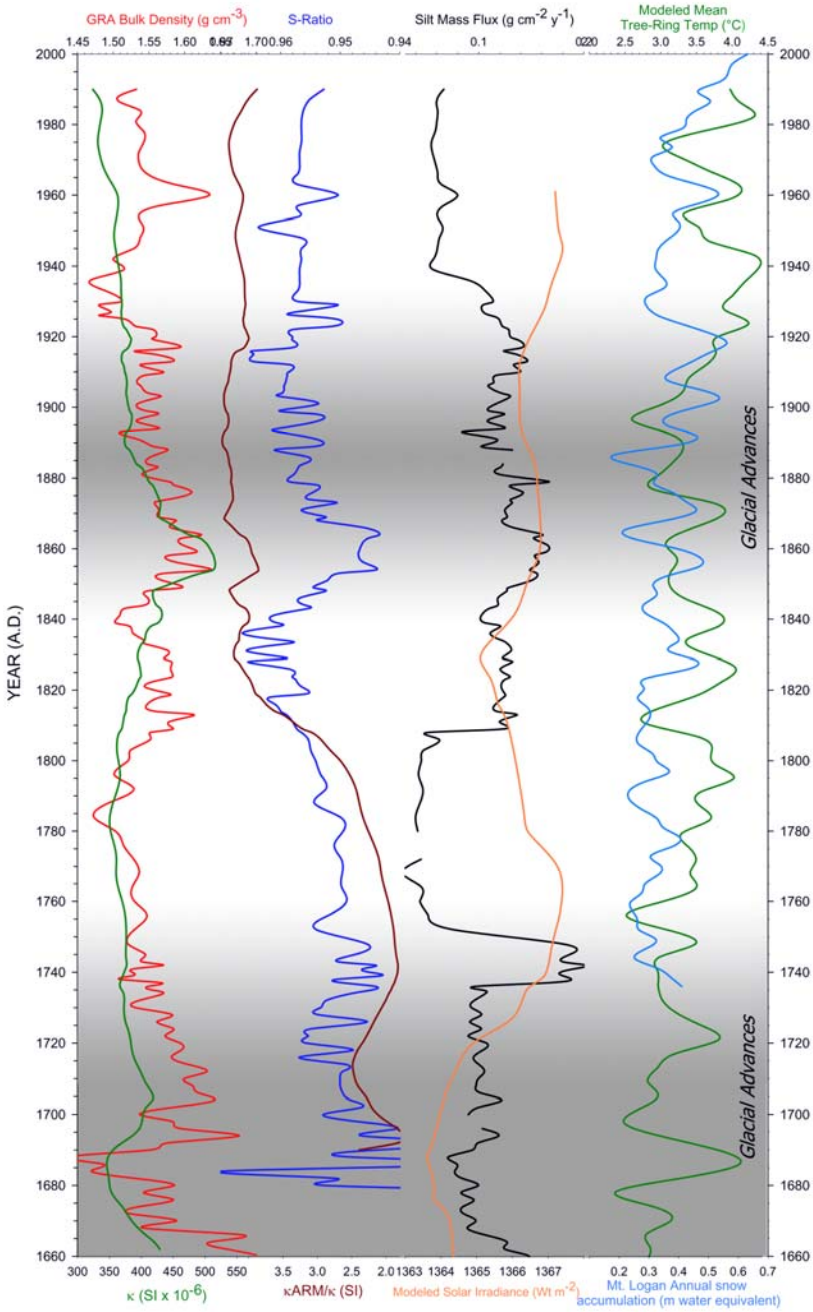

Figure 5-12. GCGAK4 sediment properties and regional climate indices. The magnetic susceptibility, k, compared with the proxy for magnetic grain size: the ratio of ARM to susceptibility (kARM/k). Smaller numbers correspond to increased grain size. S-Ratio can be used to estimate the magnetic mineralogy (magnetite vs. hematite). Also note that small increases in temperature and high-altitude precipitation (~1960 A.D.) are reflected in sedimentary record, suggesting that sediments are very sensitive records of terrestrial climate change. Solar data from Bard et al. (2000), Mt. Logan data from Moore et al., (2002), and tree-ring data from Wiles et al. (1998).

GCGAK4 GRA Bulk Density

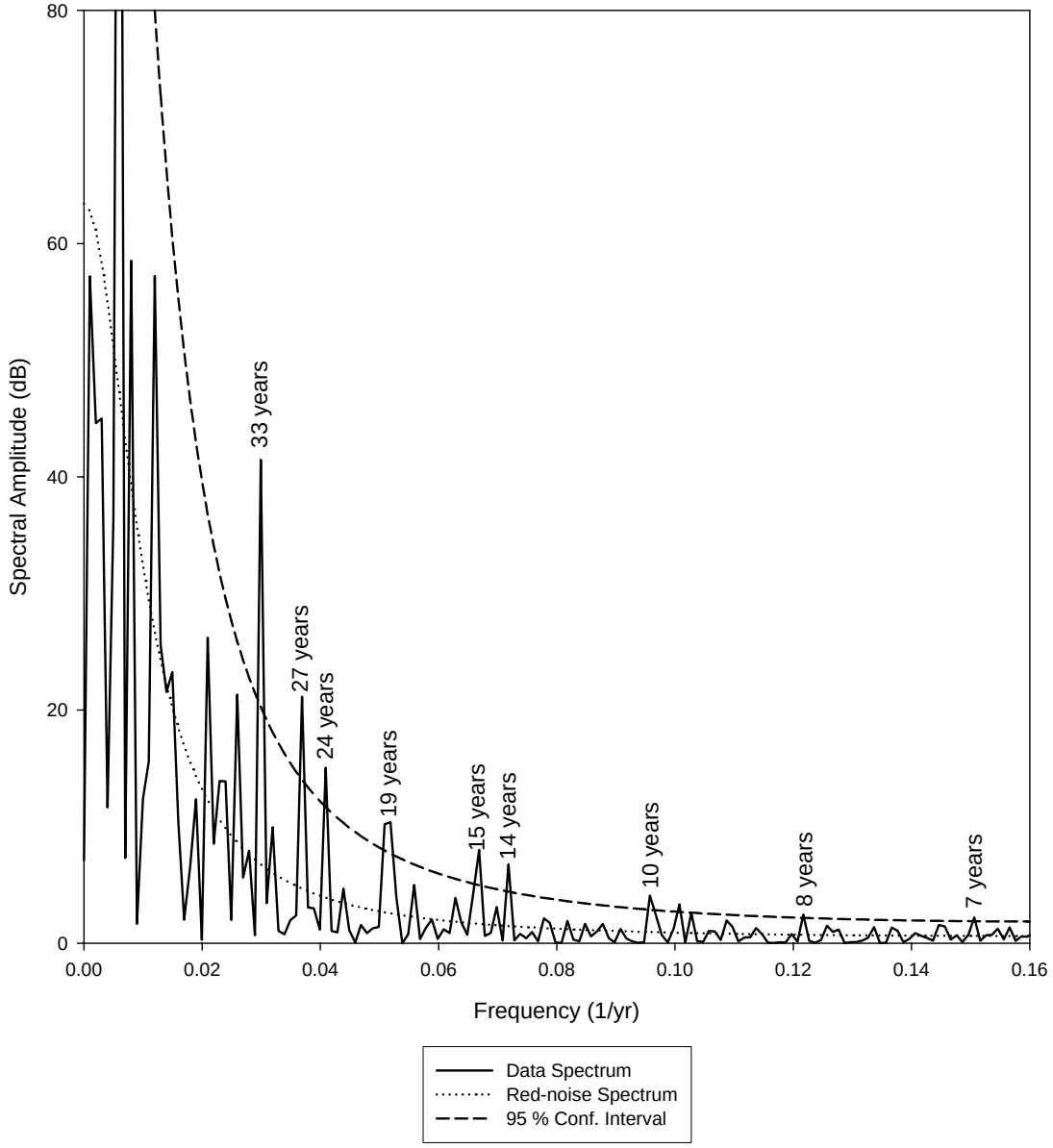

Figure 5-13. Redfit spectral analysis of GCGAK4.

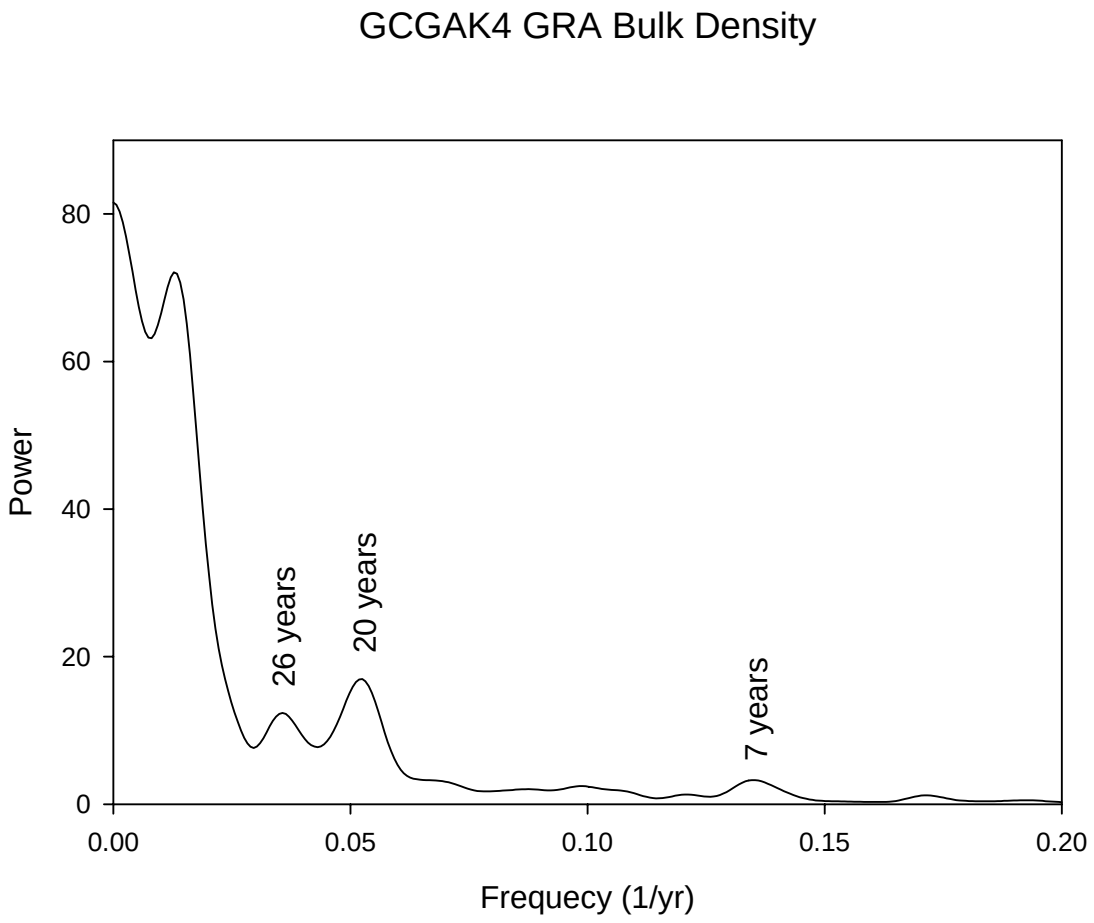

Figure 5-14. Blackman-Tukey spectral analysis of GCGAK4.

CHAPTER 6
CONCLUSIONS

One of the initial hypotheses of this study was that increased precipitation and freshwater discharge along the GOA margin would result in a faster flowing ACC and wider dispersal of fluvial-derived sediment. Calculations of the relative contributions to the overall sediment flux into PWS reveal that the surface plume component of transport is an order of magnitude less than the near-bed component. Therefore, it is likely that bottom currents, not the ACC, are responsible for transporting the majority of sediments from the Copper River to PWS. However, decadal-scale trends in mass percent silt, magnetic susceptibility, and bulk density do correspond to similar trends in freshwater discharge and precipitation. Increased freshwater discharge, due to increased precipitation, particularly rainfall, appears to supply coarser sediment to the continental shelf, which is then transported to PWS by downwelling-driven westward flowing bottom currents (Figures 6-1 and 6-2). Given near-bed speeds of possibly 10-20 cm s^{-1} (e.g., Ogston *et al.* 2004), the sediment transported near the bed could make the transit to HE (~100 km) in 10 – 20 days. Inter-annual variability in the sortable silt population (10 - 30 μm, Figure 4-6) supports the conclusion that resuspension and near-bed transport are the most likely controls on higher-frequency changes in physical properties and lithology, although ENSO-induced changes in precipitation and runoff may play a possibly equal role.

The second initial hypothesis was that stronger downwelling conditions would transport coarser sediment to PWS. Niebauer *et al.* (1994) showed that bottom inflow

dominates in summer at HE, while winter bottom currents at HE are highly variable, moving both in and out of PWS. Bottom currents that force material **into** PWS are closely tied to summer upwelling or weak downwelling conditions (Figures 6-3 and 6-4). Mass percent silt, magnetic susceptibility, and bulk density of deposits in PWS appear to be influenced by the strength of these bottom currents in particular. However, there are no decadal to inter-decadal trends in winter downwelling or summer upwelling, which indicates that has been no net increase in the strength of bottom currents over these time periods. Therefore, over decadal to inter-decadal timescales runoff appears to be the dominant influence on long-term variability in the sediment record at Site 156, and is possibly the dominant influence throughout the central basin of PWS.

The last hypothesis regarded the input of sediment to the continental shelf during periods of altered precipitation and runoff associated with glacial activity in the LIA. Mass percent silt, magnetic susceptibility, and GRA bulk density increased during periods of glacial advance and decreased during periods of glacial retreat. During periods of increased glacial advance coarser material appears to have been transported to more distal locations on the continental shelf. This suggests that higher runoff and glacial advance are linked, with both possibly due to increased precipitation.

Central to the ongoing NSF Source-to-Sink initiative is an effort to understand the mechanisms that alter the magnitude, grain size, and delivery rate of sediments as they are transported to sediment sinks. The conclusions of this study emphasize the importance of decadal to centennial climate variability, particularly in fluvial discharge and precipitation, on the formation of continental shelf strata. Currently, a broader study, both spatially and temporally, is being performed on the Gulf of Alaska margin.

Extensive coring (including JCGOA2) and seismic reflection surveys of the shelf were conducted in 2004. This ongoing study will build on the observations from GC156, GC102, and GCGAK4 in order to develop a clearer picture of the influences to shelf-wide strata formation in the northern Gulf of Alaska.

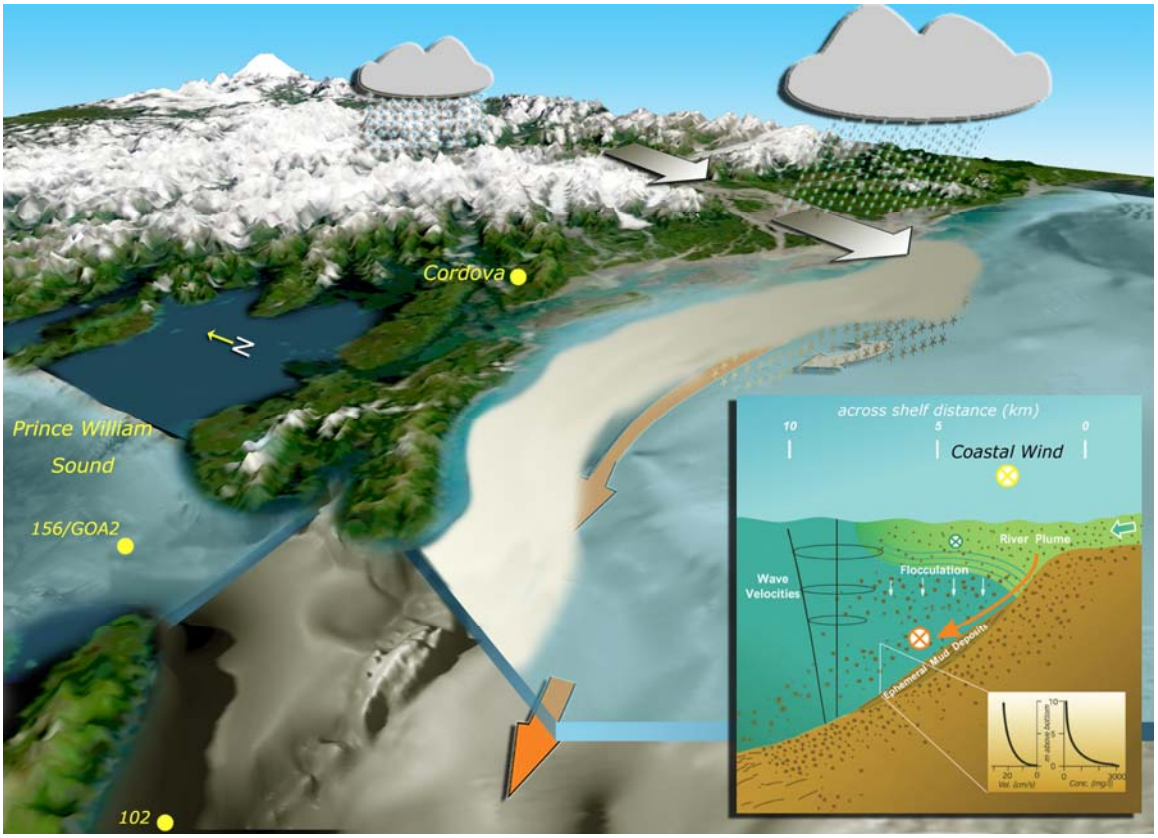

Figure 6-1. Model of high precipitation on the GOA margin. During periods of increased precipitation, coarser sediment is deposited on the GOA shelf and transported along-shelf by downwelling currents and the ACC. The ACC becomes stronger during periods of increased freshwater discharge. Inset figure after Geyer and Traykofsky (2002).

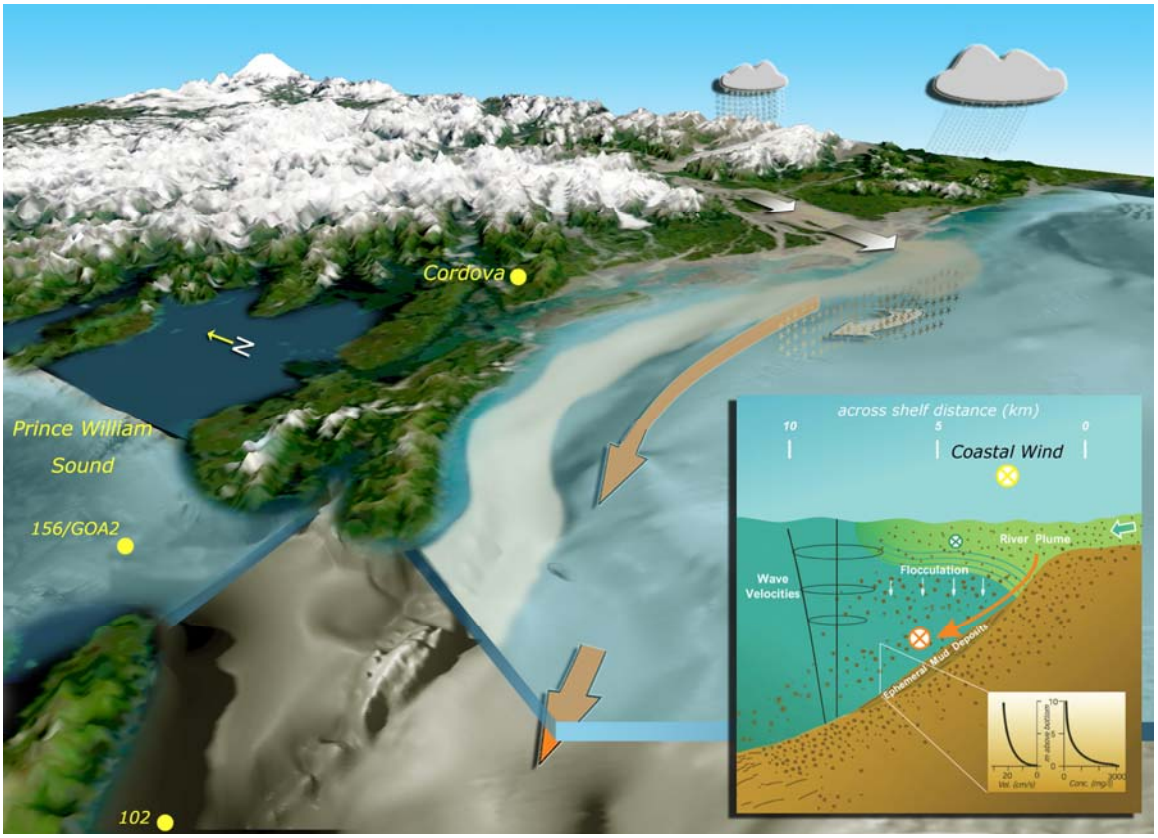

Figure 6-2. Model of low precipitation on the GOA margin. During periods of decreased precipitation, finer sediment is deposited on the GOA shelf and transported along-shelf by downwelling currents and the ACC. The ACC becomes weaker during periods of increased freshwater discharge.

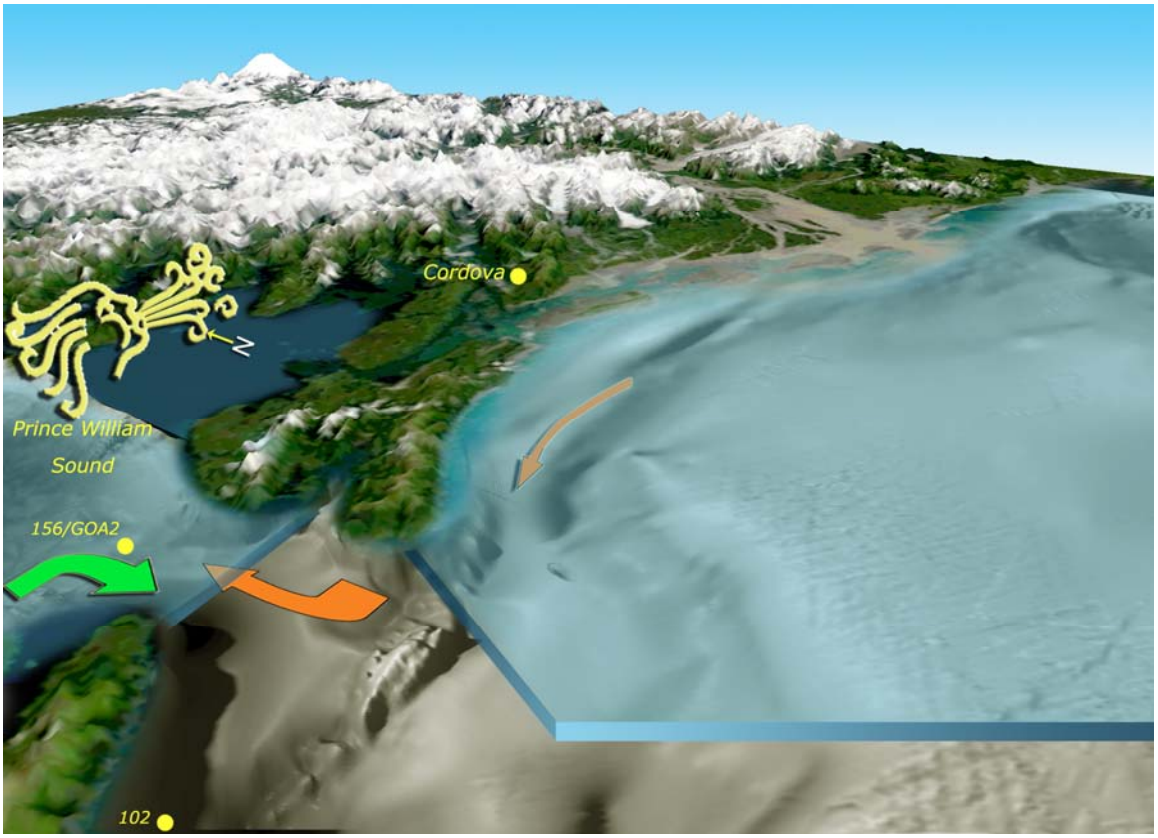

Figure 6-3. Model of summer upwelling conditions. During periods of upwelling and weak downwelling, surface flow is directed out of PWS and BBL flow is directed into PWS (Niebauer *et al.* 1994). Winds during these periods are generally weak, and often have a significant westerly component.

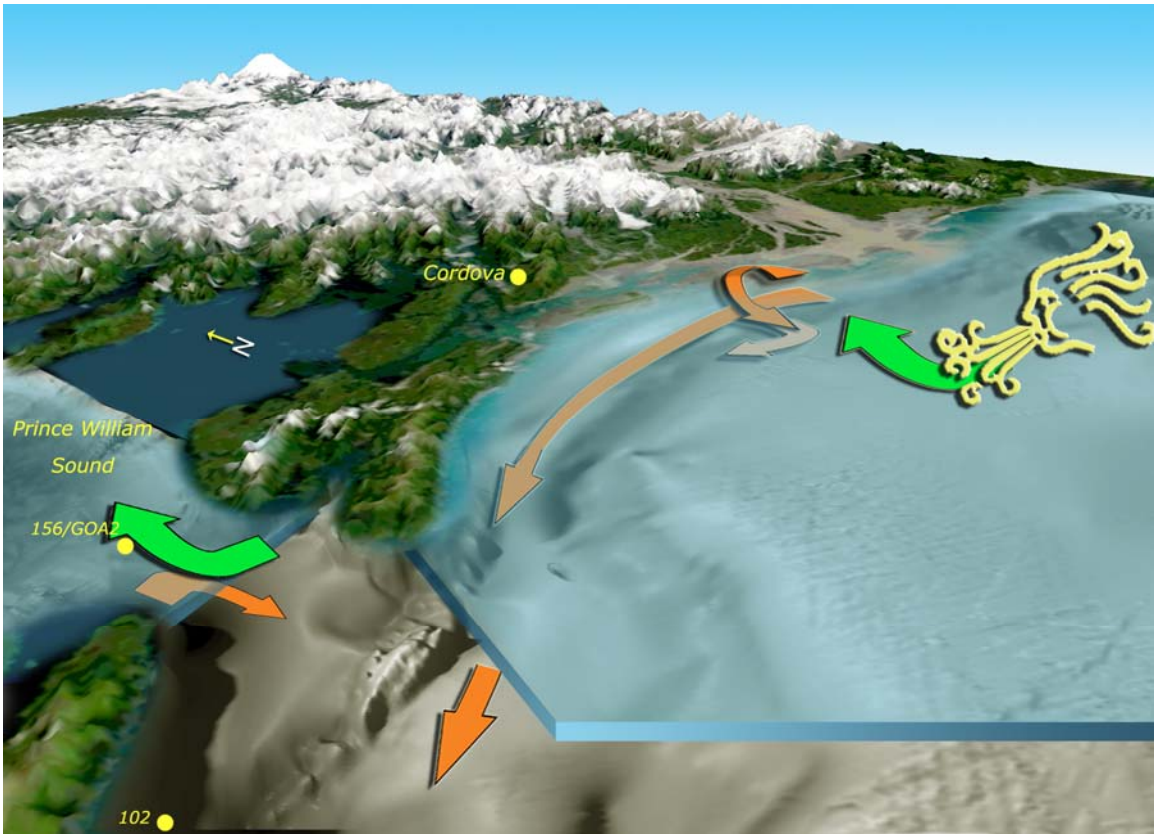

Figure 6-4. Model of downwelling conditions. During periods of downwelling, surface flow is directed into of PWS and BBL flow is directed out PWS (Niebauer *et al.* 1994). Easterly winds during these periods are generally strong.

LIST OF REFERENCES

Ager, T. M. (1983) Holocene vegetation history of Alaska, In: H. E. Wright Jr (ed.), *Late Quaternary Environments of the United States Volume 2, the Holocene*, University of Minnesota Press, Minneapolis, 128-140

Andrews, J., Kihl, R., Kristjansdottir, G., Smith, L., Helgadottir, G., Geirsdottir, A., and Jennings, A. (2002) Holocene sediment properties of the East Greenland and Iceland continental shelves bordering Denmark Strait (64-68°N), North Atlantic, *Sedimentology*, **49**, 5-24

Appleby, P.G. and Oldfield, F. (1992) Application of lead-210 to sedimentation studies, In: M. Ivanovich and R. S. Harmon (ed.), *Uranium-Series Disequalibrium: Applications to Earth, Marine, and Environmental Sciences*, Clarendon Press, Oxford, 731-778

Barclay, D. J. (1998) Tree-ring and glacial records of Holocene climate change, northern Gulf of Alaska region, Ph.D. dissertation, State University of New York at Buffalo, 232 pp.

Bard, E., Raisbeck G, Yiou F, and Jouzel J. (2000) Solar irradiance during the last 1200 yr based on cosmogenic nuclides, *TELLUS B*, **52** (3), 985-992.

Benninger, L. K., Aller, R. C., Cochran, J. K., and Turekian, K. K. (1979) Effects of biological sediment mixing on the Pb-210 chronology and trace meal distribution in a Long Island Sound sediment core, *Earth and Planetary Letters*, **43**, 241-259

Brabets, T. P. (1997) Geomorphology of the lower Copper River, Alaska, Alaska Department of Transportation and Public Facilities Report, Anchorage, AK

Bulfinch, D. L. and Ledbetter, M. T. (1984) Deep western boundary undercurrent delineated by sediment texture at base of North American continental rise, *Geological Marine Letters*, **3**, 31-36

Calkin, P. E., (1988) Holocene glaciation of Alaska (and adjoining Yukon Territory, Canada), *Quaternary Science Reviews*, **7**, 159-184

Calkin, P. E., Wiles, G. C., and Barclay, D. J. (2001) Holocene coastal glaciation of Alaska, *Quaternary Science Reviews*, **20**, 449-461

Carlson, P. R., (1989) Seismic reflection characteristics of glacial and glacimarine sediment in the Gulf of Alaska and adjacent fjords, *Marine Geology*, **85** (2-4), 391-416

Carlson, P. R. and Karl, H. A. (1982) *High-resolution seismic reflection profiles; Navarin Basin Province, northern Bering Sea: U.S. Geological Survey Open-File Report,* **82**, 6 pp.

Carpenter, R., Peterson, M. L., and Bennett, J. T. (1982) ^{210}Pb derived sediment accumulation and mixing rates for the Washington continental slope, *Marine Geology*, **48**, 135-164

Carrick, S. (1992) Copper River Highway environmental impact studies: hydrologic aspects, State of Alaska, Department of Natural Resources, Division of Geological and Geophysical Surveys, Fairbanks, Alaska

Driscoll, M. L., Tucholke, B. E., and McCave, I. N. (1985) Seafloor zonation in sediment texture on the Nova Scotian lower continental rise, *Marine Geology*, **66**, 25-41

Emery, W. J., Royer, T. C., and Reynolds, R. W. (1985) The anomalous tracks of North Pacific drifting buoys 1981 to 1983, *Deep Sea Research*, **32**, 315-347

Feely, R. A., Baker, E. T., Schumacher, J. D., Massoth, G. J, and Landing, W. M. (1978) Processes affecting the distribution and transport of suspended matter in the northeast Gulf of Alaska, *Deep-Sea Research*, **26A**, 445-464

Gilhousen, D. B., Quayle, R. G., Baldwin, R. G., Karl, T. R., and Brines, R. O. (1983) Climatic summaries for NOAA data buoys, National Climatic Data Center, National Weather Center, NOAA Data Buoy Center, NSTL Station, MS

Hallet, B., Hunter, L., and Bogen, J. (1996) Rates of erosion and sediment evacuation by glaciers: A review of field data and their implications. *Global and Planet*, **12**, 213-235

Hampton, M. A., Carlson, P. R., Lee, H. J., and Feely, R. A. (1986) Geomorphology, sediment, and sedimentary processes, In: D. W. Hood and S. T. Zimmerman (ed.), *The Gulf of Alaska, Physica, Environment and Biological Resources*, U.S. Department of Commerce, Anchorage, 93-143

Hare, S. R (1996) Low frequency climate variability and salmon production, P.h.D. dissertation, University of Washington, Seattle

Haug, G. H, Ganopolski, A., Sigman, D. M., Rosell-Mele, A., Swann, G. E. A., Tiedemann, R., Jaccard, S. L., Bollmann, J., Masiln, M. A., Leng, M. J., and Eglinton, G. (2005) North Pacific seasonality and the glaciation of North America 2.7 million years ago, *Nature*, **433**, 821-825

Heusser, C. J. (1995) Late Quaternary vegetation response to climatic-glacial forcing in North Pacific America, *Physical Geography*, **16**, 118-149

Huh, C. A., Small, L. F., Niemnil, S. F., Finney, B. P., Hickey, B. M., Kachel, N. B., Gorsline, D. S., and Williams, P. M. (1990) Sedimentation dynamics in the Santa Monica-San Pedro Basin off Los Angeles, radiochemical, sediment trap and transmissometer studies, *Continental Shelf Research*, **10**, 137-164

Humphrey, N. F. and Raymond, C. F. (1994) Hydrology erosion and sediment production in a surging glacier, *Journal of Glaciology*, **136** (40), 539-552

Inman, D. L. (1949) Sorting of sediments in the light of fluid mechanics, *Journal of Sedimentary Petrology*, **19**, 51-70

Jackson, A., Jonkers, A. R. T., and Walker, M. R. (2000) Four centuries of geomagnetic secular variation from historical records, *Philosophical Transactions – Royal Society. Mathmatical, Physical and Engineering Sciences*, **358**, 1768, 957-990

Jaeger, J. M. (1998) Sediment accumulation along a glacially impacted, mountainous coastline, south-central Alaska, P.h.D. dissertation, State University of New York at Stony Brook, 296 pp.

Jaeger, J. M. (2002) Developing high-resolution chronologies in glacimarine sediments; examples from southeastern Alaska, *Geological Society Special Publications*, **203**, 195-213

Jaeger, J. M. and Nittrouer, C. (1998) Modern sedimentary processes on a glacially impacted mountainous coastline: Northeast Gulf of Alaska. *Basin Research*, **10**, 155-173

Jaeger, J. M. and Nittrouer, C. (submitted) The formation of sedimentary lithofacies on the Gulf of Alaska continental shelf, *Continental Shelf Research*

Jaeger, J. M., Vienne, W., Hildick, A., Stoner, J. (2004) Sediment proxies of Quaternary glacial dynamics in the Gulf of Alaska region, *Eos Transaction*, AGU **85** (47), Fall Meeting, Abstract H51A-1098

Ledbetter, M. T. and Klaus, A. (1987) Influence of bottom currents on sediment texture and sea-floor morphology in the Argentine Basin, in: Geology and Geochemistry of Abyssal Plains, Weaver, P. P. and Thomson, J. (ed.), *Geological Society of London Special Publication*, **31**, 23-31

Luckman, B. H. (1986) Reconstruction of Little Ice Age events in the Canadian Rocky Mountains, *Geographic Physique et Quarternaire*, **40**, 17-28

Luckman, B. H. (1995) Calendar-dated, early “Little Ice Age” glacier advance at Robson Glacier, British Columbia, Canada, *The Holocene*, **5**, 149-159

Mantua, N. J. and Hare, S. R. (2002) The Pacific Decadal Oscillation, *Journal of Oceanography*, **58**, 35-44

Mayo, L. R., March, R. S. (1990) Air temperature and precipitation at Wolverine Glacier, Alaska; glacier growth in a warmer, wetter climate, *Annals of Glaciology*, **14**, 191-194

McCave, I. N., Manighetti, B., Robinson, S. G. (1995) Sortable silt and fine sediment size/composition slicing: parameters for palaeocurrent speed and palaeoceanography, *Paleoceanography*, **10** (3), 593-610

Meigs, A. and Sauber, J. (2000) Southern Alaska as an example of the long-term consequences of mountain building under the influence of glaciers, *Quaternary Science Reviews*, **19** (14-15), 1543-1562

Meyers, P. A. (1997) Organic geochemical proxies of paleoceanographic, paleolimnologic, and paleoclimatic processes, *Organic Geochemistry*, **27**, 213-250

Milliman, J. D. and Meade, R. H. (1983) World-wide delivery of river sediment to the oceans, *Journal of Geology*, **91** (1), 1-21

Molnia, B. F., and Carlson, P. R. (1978) Surface sedimentary units of northern Gulf of Alaska continental shelf, *AAPG Bulletin*, **62** (4), 633-643

Molnia, B. F. and Hein, J. R. (1982) Clay mineralogy of a glacially dominated, subarctic continental shelf: Northeastern Gulf of Alaska, *Journal of Sedimentary Petrology*, **52** (2), 515-527

Moore, G. W. K., Holdsworth, G., and Alverson, K. (2002) Climate change in the North Pacific region over the past three centuries, *Nature* (London), **420**, 401-403

Niebauer, H. J., Royer, T. C., and Weingartner, T. J. (1994) Circulation of Prince William Sound, Alaska, *Journal of Geophysical Research*, **99** (C7), 14113-14126

Nishenko and Jacob (1990) Seismic potential of the Queen Charlotte-Alaska-Aleutian seismic zone, *Journal of Geophysical Research, B, Solid Earth and Planets*, **95** (3), 2511-2532

Nittrouer, C. A., Demaster, D. J., Mckee, B. A., Cutshall, N. H., and Arsen, I. L. (1983) The effect of sediment mixing on ^{210}Pb accumulation rates for the Washington continental shelf, *Marine Geology*, **54**, 201-221

Nittrouer, C. A., Sternberg, R. W., Carpenter, R., and Bennett, J. T. (1979) The use of Pb-210 geochronology as a sedimentological tool: application to the Washington continental shelf, *Marine Geology*, **31** (3-4), 297-316

Ogston, A. S., Guerra, J. V., and Sternberg, R. W. (2004) Interannual variability of nearbed sediment flux on the Eel River Shelf, Northern California, *Continental Shelf Research*, **24** (1), 117-136

Pewe, T. L (1975) *Quaternary Geology of Alaska*, United States Government Printing Office, Washington D.C.

Plafker, G. (1987) Regional geology and petroleum potential of the northern Gulf of Alaska continental margin, *Circum-Pacific Council for Energy and Mineral Resources, Earth Science Series*, **6**, 229-268

Plafker, G., Moore, M. J., and Winkler, G. R. (1994) Geology of the southern Alaska margin, In: G. Plafker and H. Berg (ed.), *The Geology of Alaska*, 389-449

Porter, S. C. (1986) Pattern and forcing of Northern Hemisphere glacier variations during the last millennium, *Quaternary Research*, **26**, 27-48

Powell, R. D. and Molnia, B. F. (1989) Glacimarine sedimentary processes, facies and morphology of the South-Southeast Alaska shelf and fjords. *Marine Geology*, **85**, 359-390

Rack , F. R., Bloemendal, J., Wolf-Welling, T. C. W., O'Connell, S., Cremer, M., Winkler, A., Thiede, J., Black, K., and Hood, J. (1996) Development of physical properties relationships, interhole composite depth profiles, and sedimentologic ground truthing of multi-sensor core measurements: A synthesis of results, *Proceedings of the Ocean Drilling Program, Scientific Results*, **151**

Rasmussen, E. M., and Wallace, J. M. (1983) Meteorological aspects of the El Niño/Southern Oscillation, *Science*, **222**, 1195-1202

Robinson, S. G. and McCave, I. N. (1994) Orbital forcing of bottom-current enhanced sedimentation on Feni Drift, NE Atlantic, during the mid-Pleistocene, *Paleoceanography*, **9**, 943-972

Royer, T. C. (1981) Baroclinic transport in the Gulf of Alaska, part II, freshwater driven coastal current. *Journal of Marine Research*, **39**, 251-252

Royer, T. C. (1982) Coastal freshwater discharge in the Northeast Pacific, *Journal of Geophysical Research*, **87** (C3), 2017-2021

Royer, T. C., Hansen, D. V., and Pashinski, D. J. (1979) Coastal flow in the northern Gulf of Alaska as observed by dynamic topography and satellite-tracked drogued drift buoys, *Journal of Physical Oceanography*, **9**, 785-801

Royer, T. C. and Weingartner, T. (1999) Coastal hydrographic responses in the northern Gulf of Alaska to the 1997-1998 ENSO event, Proceedings of the 1998 Science Board Symposium on the Impacts of the 1997/98 El Nino Event on the North Pacific Ocean and its Marginal Seas, PICES Scientific Report no. 10, 89-92

Ruby, C. H. and Hayes, M. O. (1994) Barriers of Pacific Alaska, In: R. A. Davis (ed.) *Geology of Holocene barrier island systems*, 395 - 433

Schulz, M., and Mudelsee, M. (in press) REDFIT: Estimating red-noise spectra directly from unevenly spaced paleoclimatic time series, *Computers and Geosciences*

Schumacher, J. D., Stabeno, P. J., and Roach, A. T. (1989) Volume transport in the Alaska Coastal Current, *Continental Shelf Research*, **9** (12), 1071-1083

Sharma, G. D. (1979) *The Alaskan Shelf: Hydrographic, Sedimentary, and Geochemical Environment*, Springer-Verlog, New York

Smith, J.T. and Comans, R.N. (1996) Modeling the diffusive transport and remobilization of ^{137}Cs in sediments: The effects of sorption kinetics and reversibility, *Geochemica et Cosmochimica Acta*, **60**, 995 -100

Somerfield, C. K., Drake, D. E., and Wheatcroft, R. A. (2002) Shelf record of climatic changes in flood magnitude and frequency, north-coastal California, *Geology*, **30** (5), 395-398

Stabeno, P.J., Bond, N.A., Hermann, A.J., Kachel, N.B., Mordy, C.W., and Overland, J.E. (2004) Meteorology and oceanography of the Northern Gulf of Alaska, *Continental Shelf Research*, **24**, 859-897

Sugai, S. F., Alperin, M. J., and Reeburgh, W. S. (1994) Episodic deposition and Cs-137 immobility in Skan Bay sediments: A ten year Pb-210 and Cs-137 time series, *Marine Geology*, **116** (3-4), 351-372

Thomas, R.G., Guyodo, Y., and Channell, J.E.T. (2003) U channel track for susceptibility measurements, *Geochemistry Geophysics Geosystems*, **4** (6), 6 pp.

Weber, M.E., Niessen, F., Kuhn, G., and Wiedicke, M. (1997) Calibration and application of marine sedimentary physical properties using a multi-sensor core logger, *Marine Geology*, **136**, 151-172

Weedon, G. P. (2003) Time-series analysis and cyclostratigraphy: examining stratigraphic records of environmental cycles, Cambridge University Press, New York, 274 pp.

Weingartner, T., Coyle, K., Finney, B., Hopcroft, R., Whitledge, T., Brodeur, R., Dagg, M., Farley, E., Haidvogel, D., Haldorson, L., Hermann, A., Hinckley, S., Napp, J, Stabeno, P., Kline, T., Lee, C., Lessard, E., Royer, T., and Strom, S. (2002) *The Northeast Pacific GLOBEC Program: Coastal Gulf of Alaska: Oceanography*, **15**, 10-35

Weingartner, T., Danielson, S., and Royer, T. (in preparation) Seasonal and interannual variability in freshwater content and transport in the Alaska Coastal Current

Wheatcroft, R. A., Wiberg, P. L., Alexander, C. R., Bentley, S. J., Drake, D. E., Harris, C. K., and Ogston, A. S. (in preparation) Depositional alteration and preservation of strata, in: STATAFORM

Wheatcroft, R. A. and Drake, D. E. (2003) Post-depositional alteration and preservation of sedimentary event layers on continental margins, the role of episodic sedimentation, *Marine Geology*, **199**, 123-137

Wiles, G. C., D'Arrigo, R. D., Villalba, R., Barclay, D. J., and Calkin, P. E. (2004) Alaskan temperature change over the past millennium: Solar forcing modulated by the arctic and pacific decadal oscillations, *Abstracts for the 34th annual International Arctic Workshop*

Wilson, J. and Overland, J. (1986) Meteorology, In: Hood and Zimmerman (ed.), *The Gulf of Alaska, physical environment and biological resources*, Alaska Office, Ocean Assessments Division, National Oceanic and Atmospheric Administration, U.S. Department of Commerce, 31-53

Zhang, Y., Wallace, J. M., and Battisti, D. S. (1997) ENSO-like interdecadal variability, *Journal of Climate*, **10**, 1004-1020

BIOGRAPHICAL SKETCH

William Vienne grew up in the small town of Natchitoches, Louisiana. He received a B.S. in geology from Louisiana State University in 2002 and an M.S. in geology from the University of Florida in 2005. He has participated in research projects on the chenier plain coast of southwest Louisiana, in Mississippi Sound, in the Gulf of Alaska, and in coastal Florida.